



UNIVERSIDADE DA BEIRA INTERIOR
Engenharia

Longitudinal Flight Control with a Variable Span Morphing Wing

Tiago Nunes Sanches

Dissertação para obtenção do Grau de Mestre em
Engenharia Aeronáutica
(2º ciclo de estudos)

Orientador: Professor Doutor Kouamana Bousson
Co-orientador: Professor Doutor Pedro Gamboa

Covilhã, Outubro de 2012

Blank Page

Dedicatory

I dedicate this work to my close family that always believed in me and always supported my causes. Father, Mother and Sister, to all of you, a major and sincere Thank You.

Tiago Sanches

Blank Page

Agradecimentos

Em primeiro lugar, gostaria de agradecer à minha família, principalmente aos meus pais e à minha irmã por sempre terem acreditado nas minhas capacidades. Sem eles e o seu contínuo apoio e orientação, eu nunca teria chegado tão longe.

Em segundo lugar, tenho de agradecer ao meu orientador, Professor Kouamana Bousson, por toda a ajuda e esclarecimentos prestados ao longo do curso. Sem ele, o trabalho aqui apresentado não teria sido possível.

Também quero agradecer a todas as pessoas envolvidas nos sucessivos desenvolvimentos do projeto *OLHARAPO* e a sua Asa Telescópica (VSMW). Gostaria, nomeadamente, de referir o Professor Pedro Gamboa, pela supervisão de ambos os projetos, e os meus colegas e amigos João Mestrinho, João Felício e Filipe Tavares que trabalharam no referido projeto da Asa Telescópica. Só a sua dedicação a estes projetos permitiu a possibilidade da elaboração do presente trabalho.

Por último, quero agradecer a todos os meus amigos pelo seu apoio e amizade ao longo destes últimos anos. Sem eles, tudo teria sido bem mais difícil.

Blank Page

Acknowledgements

First and foremost, I would like to give thanks to all my family, most especially to my parents and sister who have always believed in my abilities and aspirations, and without them and their continuous support and guidance I would never have gotten this far.

Secondly, I have to thank my supervisor, Prof. Kouamana Bousson, for the help and enlightenment provided along the course. This work presented here would not have been possible without him.

I also have to thank to all the people involved in the *OLHARAPO*'s VSMW Project as well as those involved in the continued iterations of the *OLHARAPO*'s Project itself. Namely, I would like to refer to Prof. Pedro Gamboa for his supervision of these projects, and to my colleagues and friends João Mestrinho, João Felício e Filipe Tavares that worked on the VSMW project. Their dedication to these projects was that what enabled the possibility of the present work.

Lastly, I want to thank all my friends for their support and friendship over these past years. Without them, things would have been much more difficult.

Blank Page

Preface

Following on the work developed by my colleague and friend Filipe Tavares entitled “Roll Motion Control of a Dissymmetrical Wingspan Aircraft”[3], the present work aims to deliver a robust controller with regard to the longitudinal stabilization of an aircraft equipped with a variable-span (telescopic) wing, by furthering the prospects of the less developed parts of the longitudinal stability controller while attempting to rectify some minor issues of his work due to the preliminary XFLR5’s data used as the only one available at the time. As such, and this being a job that involves a direct integration with the work already done that addressed this same subject, it would be counterproductive to completely rewrite from scratch all the theoretical foundations and followed models of controller’s architecture, such as would be in the case of updating an aircraft’s maintenance manual. At the same time, and unlike what happens on the given example, it is not feasible to redirect the reader to a previous chapter that is on a different document to which the reader may not have access at all. Thus, even for the sake of consistency, and since we’re dealing with work done under the supervision of the same supervisor from the same department at the same university, it was established both the practical (programming) and written work (the present document) would strictly follow the same line of work presented by its predecessor. Therefore, it should not be surprising to notice the strong similarities between the two documents, especially with regard to the chapters concerning the theoretical concepts and the fundamentals behind this work. Therefore, following on the line of work established by that previous work, from now on referred to as RMCDWA [3] for convenience, and having been given access to more recent data (namely the longitudinal stability derivatives) obtained with the help of the XFLR5® [35] software, it was possible to start scripting the programming lines of the MATLAB® [33] file that incorporates the controller. Once again, two different controller methods were tested: LQR and *Batz-Kleinman* controller. Sinusoidal and random pitch variation simulations were also conducted in order to prove the working concept of the controller mechanism of such complex controller program structure.

Note: The present document’s sections in Portuguese are written in accordance with the new orthographic agreement for the Portuguese Language. (*Nota: As secções em Português do presente documento encontram-se escritas ao abrigo do novo Acordo Ortográfico da Língua Portuguesa*).

Blank Page

Resumo

O presente trabalho consiste na projeção, programação e teste de um controlador de voo longitudinal destinado a uma aeronave não-tripulada equipada com um sistema de variação dissimétrica da envergadura das asas (conhecido como VSMW, asa dissimétrica ou asa telescópica). Este trabalho tem como principal objetivo desenvolver um controlador capaz de assegurar a estabilidade longitudinal da aeronave em voo nivelado a velocidade de cruzeiro, contudo, este foi também projetado para providenciar essa mesma estabilidade noutras fases de voo tais como a aterragem ou a descolagem. O algoritmo de estabilização baseia-se nas mais sofisticadas técnicas de controlo de voo atualmente disponíveis, mais concretamente LQR e *Batz-Kleinman*, para estabilizar a aeronave na atitude pretendida aquando da ocorrência de quaisquer pequenas perturbações atmosféricas que afetem a aeronave durante o voo. A aeronave a que se destina trata-se de um protótipo designado de *Olharapo* equipado com uma asa telescópica que permite ajustar a envergadura total das asas de acordo com a velocidade de voo. No entanto, o conceito modular da estrutura do programa permite que o controlador possa ser utilizado para diferentes configurações da mesma aeronave, ou até mesmo com uma aeronave totalmente diferente. Tanto o desenvolvimento como as simulações e testes do algoritmo foram efetuados com recurso ao *software* MATLAB®, tendo as necessárias derivadas de estabilidade e controlo iniciais sido providenciadas pelo *software* XFLR5®. As equações de voo foram devidamente adaptadas para permitirem uma compatibilização com o sistema da asa telescópica e a sua integração nos métodos de controlo LQR e *Batz-Kleinman*. As qualidades de voo da aeronave foram devidamente definidas e impostas ao controlador para garantir a afinação da matriz de ponderação para valores ótimos. Por fim, o algoritmo foi sujeito a três tipos de testes e simulações: Simulação Clássica por meio de Imposição de Perturbações Atmosféricas, Teste de Resposta a uma Variação Sinusoidal do Ângulo de Arfagem, e Teste de Reposta a uma Variação Aleatória do Ângulo de Arfagem.

Palavras-chave

Aeronave, Piloto-Automático, Controlador *Batz-Kleinman*, Estabilização de Voo, Regulador Quadrático Linear, Dinâmica de Voo Longitudinal, LQR, Tecnologia *Morphing*, Controlador Robusto, UAV, Asa de envergadura variável, Geometria Variável.

Blank Page

Abstract

The present study focuses on the design of a longitudinal flight controller for an unmanned aircraft equipped with dissymmetric variable-span system (VSMW or Variable-Span Morphing Wing). Its primary role consists in the longitudinal flight stabilization of the aeroplane while in levelled cruise flight, although, it was designed to offer longitudinal flight stabilization for other flight phases as well, such as e.g. take-off and landing. The stabilization algorithm relies on the most up-to-date developments in the state-of-the-art LQR and *Batz-Kleinman* controller techniques to stabilize the aircraft on its intended longitudinal attitude upon any small atmospheric disturbances inflicted. It was designed for the experimental UAV prototype *Olharapo* equipped with the VSMW, so it can automatically adjust the VSMW overall wingspan in accordance with the flight speed and stabilize the aircraft in the desired attitude, although, its modular concept allows it to be used for different configurations of the aircraft or even for a different aircraft. The development, simulation and testing of the algorithm were done using the MATLAB[®] software and the aircraft's stability and control derivatives previously obtained using the XFLR5[®] software. Minor adaptations of the flight dynamics equations were performed to allow the compatibilization with the VSMW. The required implementation of imposed flight qualities was also performed to ensure proper scaling the controller weight matrix for optimal values. Finally, the algorithm was tested using three different methods: Classic Disturbances Simulation, Sinusoidal Pitch Variation Test Response and Random Pitch Variation Test Response.

Keywords

Aircraft, Autopilot, *Batz-Kleinman* Controller, Flight Stabilization, Linear Quadratic Regulator, Longitudinal Flight Dynamics, LQR, Morphing Technology, Robust Controller, UAV, Variable-Span Wing, Variable Geometry.

Blank Page

Index

List of Figures	xix
List of Tables	xxv
List of Graphics	xxvii
Nomenclature	xxix
Glossary	xxxiii
Chapter 1	1
Introduction	1
1.1 Morphing Technologies in Aviation	4
1.2 Dissertation's Objectives	5
Chapter 2	9
Theoretical Concepts of Flight Dynamics and Mechanics	9
2.1 Flight Dynamics Theory	9
2.1.1 Longitudinal Flight Dynamics	14
2.2 Stability and Control Derivatives	18
2.3 Flight Stability	18
2.3.1 Longitudinal Flight Static Stability	19
2.4 Flight Modes (Handling Qualities)	22
2.4.1 <i>Cooper-Harper</i> Scale	22
2.4.2 Longitudinal Flight Modes	22
2.5 System Linearization	25
2.5.1 Generalized <i>Taylor's</i> Theorem	26
2.5.2 <i>Butcher's</i> Algorithm	28
2.6 LQR Controller	28
2.7 <i>Batz-Kleinman</i> Controller	33
2.8 Block Diagram of a Control System	33
Chapter 3	37
VSMW (Variable-Span Morphing Wing)	37
3.1 UAV <i>Olharapo</i>	37
3.2 <i>Olharapo's</i> Dissymmetrical Telescopic Wing	38
3.3 UAV Specifications	40
Chapter 4	49
Simulation and Tests	49
4.1 Imposed Flight Qualities	49
4.2 Classical Control Method (Disturbances Response)	52
4.3 Simulation Results	56
4.3.1 Altitude Hold Mode	57

4.3.2	Pitch Attitude Hold Mode	59
4.3.3	Climb or Descent/Dive Hold Mode	61
4.3.4	Landing Mode	64
4.3.5	Take-Off Mode	67
4.3.6	TFTA Mode	67
4.3.7	Dissymmetrical Wing Mode	67
4.4	Pitch Angle Sinusoidal Variation Test Response	70
4.5	Random Pitch Angle Variation Test Response	77
Chapter 5		81
Conclusions		81
Bibliography		85
Appendix		91
Annex A	UAV <i>Olharapo</i> Drawings	91
Annex B	UAV <i>Olharapo</i> Specifications	93
Annex C	Handling Qualities Data	97
Annex D	Simulation's Full Output Data Example	103
Annex E	Paper	109

Blank Page

Blank Page

List of Figures

Chapter 1

Figure 1.1 – Schematic of the B-24 “Liberator”.	2
Figure 1.2 – Sketch of an aeroplane’s classical control system.	3
Figure 1.3 – Diagram of a classical linkage between the controller stick (input) and the elevator (output).	3
Figure 1.4 – Variable geometry wing’s configurations. From left to right: Variable Sweep Wing; Telescopic Wing; Extendable Wing; and Folding Wing.	5

Chapter 2

Figure 2.1 – a) Earth and body (aircraft) axis Systems; b) Forces, moments, angles and angular velocities acting on an aircraft.	10
Figure 2.2 – General classic control surfaces and respective positive deflections.	10
Figure 2.3 – Forces and angles concerning the longitudinal flight plane analysis.	14
Figure 2.4 – Relation between the angle of attack (α) and the path angle (γ) in perturbed flight.	15
Figure 2.5 – Pressure distribution along the tail’s horizontal empennage and elevator and its change due to elevator defection.	16
Figure 2.6 – Effect of the elevator deflection on the tail’s angle of attack.	17
Figure 2.7 – Forces and moments actuating on an aircraft in levelled flight.	17
Figure 2.8 – Sketches illustrating various conditions of static stability (left) and examples of stable and unstable dynamic motions (right).	19
Figure 2.9 – (Left) Stable and unstable static stability with regard to the relation between the pitch moment coefficient ($C_M = C_m$) and the angle of attack (α); (Right) Static stability with regard to the relation between the pitch moment coefficient relative to the centre of gravity ($C_{m_{c.g.}}$) and the lift coefficient (C_L).	20
Figure 2.10 – Example of an aeroplane change in altitude and attitude in a pughoid mode oscillation trough time. The pughoid period is generally between 20 and 100 seconds.	23
Figure 2.11 – Short Period movement characterization.	25
Figure 2.12 – A F-35B performing a vertical take-off and landing test (left); and a Mig-29 performing the <i>Pugachev’s Cobra</i> Manoeuvre (right).	29

Figure 2.13 – General block diagram of an AFCS.	34
Figure 2.14 – Closed loop state regulator with optimal feedback.	34
Figure 2.15 – Actuator's control system scheme.	35

Chapter 3

Figure 3.1 – <i>Olharapo</i> light UAV prototype featuring its standard wing configuration.	37
Figure 3.2 – CAD Drawing (left) and the actual actuation system (right).	38
Figure 3.3 – VSMW mechanical system.	39
Figure 3.4 – <i>Olharapo</i> UAV prototype equipped with the VSMW: (a) fully retracted wing; and (b) fully extended wing.	39
Figure 3.5 – (a) Drag variation with flight speed; (b) Drag reduction with the VSMW relatively to the original standard wing; (c) Wingspan variation with flight speed; (d) Angle of Attack variation with flight speed.	40
Figure 3.6 – Dissymmetrical Wing Variation (δ_y).	44

Chapter 4

Figure 4.1 – Short-Period parameters definition based on pilot opinions.	51
Figure 4.2 – Diagram of the general path scheme of the simulation code.	53
Figure 4.3 – (AHM) Classic disturbance simulation response for the Altitude Hold Mode with LQR for disturbances case 2 (x_2).	58
Figure 4.4 – (AHM) Classic disturbance simulation response for the Altitude Hold Mode with the <i>Batz-Kleinman</i> controller for disturbances case 2 (x_2).	58
Figure 4.5 – (AHM) Comparison between the simulation responses for the Altitude Hold Mode of both methods with x_2 .	58
Figure 4.6 – (AHM) Detailed comparison between the longitudinal responses for both methods of the Altitude Hold Mode with x_2 .	58
Figure 4.7 – (AHM) Complementary longitudinal parameters response results with x_2 .	59
Figure 4.8 – (PAH) Classic disturbance simulation response with LQR for disturbances case 2 (x_2).	60
Figure 4.9 – (PAH) Classic disturbance simulation response with the <i>Batz-Kleinman</i> controller for disturbances case 2 (x_2).	60

Figure 4.10 – (PAH) Comparison between the simulation responses of both methods with x_2 .	61
Figure 4.11 – (PAH) Detailed comparison between the longitudinal responses for both methods with x_2 .	61
Figure 4.12 – (PAH) Detailed comparison between the vertical velocity, pitch rate and elevator responses for both methods with x_2 .	61
Figure 4.13 – (CDDRH) Classic disturbance simulation response with LQR for disturbances case 2 (x_2).	63
Figure 4.14 – (CDDRH) Classic disturbance simulation response with the <i>Batz-Kleinman</i> controller for disturbances case 2 (x_2).	63
Figure 4.15 – (CDDRH) Comparison between the simulation responses of both methods with x_2 .	63
Figure 4.16 – (CDDRH) Detailed comparison between the longitudinal parameters responses for both methods with x_2 .	64
Figure 4.17 – (CDDRH) Detailed comparison between the vertical velocity, pitch rate and elevator responses for both methods with x_2 .	64
Figure 4.18 – (LM) Classic disturbance simulation response with LQR for disturbances case 2 (x_2).	66
Figure 4.19 – (LM) Classic disturbance simulation response with the <i>Batz-Kleinman</i> controller for disturbances case 2 (x_2).	66
Figure 4.20 – (LM) Comparison between the simulation responses of both methods with x_2 .	66
Figure 4.21 – (LM) Detailed comparison between the longitudinal parameters responses for both methods with x_2 .	66
Figure 4.22 – (LM) – Detailed comparison between the vertical velocity, pitch rate and elevator responses for both methods with x_2 .	67
Figure 4.23 – (DWM) – Classic disturbance simulation response with LQR for disturbances case 2 (x_2).	68
Figure 4.24 – (DWM) Classic disturbance simulation response with the <i>Batz-Kleinman</i> controller for disturbances case 2 (x_2).	68
Figure 4.25 – (DWM) Comparison between the simulation responses of both methods with x_2 .	69
Figure 4.26 – (DWM) – Detailed comparison between the longitudinal parameters responses for both methods with x_2 .	69
Figure 4.27 – LQR simulation for a sinusoidal variation of the pitch angle for y_1 .	71

Figure 4.28 – <i>Batz-Kleinman</i> simulation for a sinusoidal variation of the pitch angle for y_1 .	72
Figure 4.29 – Detailed pitch control and state variables comparison between the two methods for a sinusoidal variation of the pitch angle for y_1 .	72
Figure 4.30 – Single variable response comparison between LQR and <i>Batz-Kleinman</i> controller methods for a sinusoidal variation of the pitch angle for y_1 .	73
Figure 4.31 – LQR simulation for a sinusoidal variation of the pitch angle for y_2 .	73
Figure 4.32 – <i>Batz-Kleinman</i> simulation for a sinusoidal variation of the pitch angle for y_2 .	73
Figure 4.33 – Detailed pitch control and state variables comparison between the two methods for a sinusoidal variation of the pitch angle for y_2 .	74
Figure 4.34 – Single variable response comparison between LQR and <i>Batz-Kleinman</i> controller methods for a sinusoidal variation of the pitch angle for y_2 .	74
Figure 4.35 – LQR simulation for a sinusoidal variation of the pitch angle for y_2 .	75
Figure 4.36– <i>Batz-Kleinman</i> simulation for a sinusoidal variation of the pitch angle for y_2 .	75
Figure 4.37 – Detailed pitch control and state variables comparison between the two methods for a sinusoidal variation of the pitch angle for y_2 .	75
Figure 4.38 – Single variable response comparison between LQR and <i>Batz-Kleinman</i> controller methods for a sinusoidal variation of the pitch angle for y_2 .	75
Figure 4.39 – LQR simulation for a sinusoidal variation of the pitch angle for y_1 .	76
Figure 4.40 – <i>Batz-Kleinman</i> simulation for a sinusoidal variation of the pitch angle for y_1 .	76
Figure 4.41 – Detailed pitch control and state variables comparison between the two methods for a sinusoidal variation of the pitch angle for y_1 .	76
Figure 4.42 – Single variable response comparison between LQR and <i>Batz-Kleinman</i> controller methods for a sinusoidal variation of the pitch angle for y_1 .	76
Figure 4.43 – LQR simulation for a random variation of the pitch angle for y_2 .	77
Figure 4.44 – <i>Batz-Kleinman</i> simulation for a random variation of the pitch angle for y_2 .	78
Figure 4.45 – Detailed pitch control and state variables comparison between the two methods for a random variation of the pitch angle for y_2 .	78
Figure 4.46 – Single variable response comparison between LQR and <i>Batz-Kleinman</i> controller methods for a random variation of the pitch angle for y_2 .	78
Figure 4.47 – LQR simulation for a random variation of the pitch angle for y_1 .	78

Figure 4.48 – <i>Batz-Kleinman</i> simulation for a random variation of the pitch angle for y_1 .	79
Figure 4.49 – Detailed pitch control and state variables comparison between the two methods for a random variation of the pitch angle for y_1 .	79
Figure 4.50 – Single variable response comparison between LQR and <i>Batz-Kleinman</i> controller methods for a random variation of the pitch angle for y_1 .	79
Figure A – UAV “ <i>Olharapo</i> ” 3 views drawings.	91

Blank Page

List of Tables

Chapter 3

Table 3.1 – Engine and weight specifications.	41
Table 3.2 – Inertial properties specifications.	42
Table 3.3 – Telescopic wing (VSMW) specifications.	42
Table 3.4 – Longitudinal stability derivatives specifications for the UAV <i>Olharapo</i>	43
Table 3.5 – Longitudinal control derivatives specifications for the UAV <i>Olharapo</i>	43

Chapter 4

Table 4.1 – Values for the Short-Period (SP) and Long-Period (LP) Motion Theories for all the three Categories of a Level 1, Class I Aeroplane.	50
Table 4.2 – Chosen values for eigenvalue calculation.	51
Table 4.3 – Flight modes supported by the controller.	55
Table 4.4 – Flight Safety Modes supported in the controller.....	56

Annexes

Table B – UAV's full stability and control derivatives data and aircraft's specifications.	93
Table C1 – Flight Levels.	97
Table C2 – Airplane Classes.....	97
Table C3 – Flight Categories.	98
Table C4 – Longitudinal Phugoid and Short-Period Flight Qualities Parameters.	99
Table C5 – Lateral-directional's Spiral Flight Qualities Parameters.	99
Table C6 – Lateral-directional's Roll Flight Qualities Parameters.....	99
Table C7 – Lateral-directional's Dutch Roll Flight Qualities Parameters.	100

Blank Page

List of Graphics

Chapter 3

Graphic 3.1 – Expected Pitch Moment Coefficient (C_m) distribution due to elevator deflection (δ_{V_e}).....	45
Graphic 3.2 – Wing Polars tecplot for the VSMW's maximum and minimum wingspan.	46
Graphic 3.3 – Effective drag reduction from maximum wingspan to fully retracted OMWs	46

Chapter 4

Graphic 4.1 – Graphical representation of the cosine variation of pitch	71
---	----

Blank Page

Nomenclature

α	Angle of Attack
$\dot{\alpha}$	Angle of Attack variation Rate
α_{eq}	Angle of Attack in Equilibrium Position
α_t	Angle of Attack of the tail
β	Sideslip Angle
γ	Path Angle
δ_a	Aileron Deflection
δ_b	Wingspan “Deflection” (i.e. Symmetrical extension or retraction)
δ_c	Canard Deflection
δ_e	Elevator Deflection
δ_p	Rudder Pedals Deflection
δ_r	Rudder Deflection
δ_{Sa}	Control Stick Deflection for ailerons authority
δ_{Se}	Control Stick Deflection for elevator(s) authority
δ_T	Throttle Setting
δ_y	Wing Span Variation (Dissymmetrical)
ε_T	Angle between the thrust and the aircraft’s main inertial axis
ζ	Damping Coefficient
θ	Pitch Angle
λ	Eigenvalue
ξ	Damping Ratio
π	Circle’s circumference to its diameter mathematically constant Ratio
ρ	Air Density
ρ_{eq}	Equilibrium State’s Air Density
τ	Optimization Constant
ϕ	Bank Angle
ψ	Yaw Angle
ω_n	Natural Frequency
\aleph	Fractal Numbers
C	Kinetic Moment
C_D	Drag Coefficient
C_{D_0}	Drag Coefficient for a Zero Angle of Attack
$C_{D\alpha}$	Drag Coefficient for a given Angle of Attack
$C_{D\dot{\alpha}}$	Drag Coefficient due to the Angle of Attack variation Rate
C_{Dq}	Drag Coefficient due to Pitch Rate
C_L	Lift Coefficient
C_{L_0}	Lift Coefficient for a Zero Angle of Attack
$C_{L\alpha}$	Lift Coefficient for a given Angle of Attack
$C_{L\dot{\alpha}}$	Lift Coefficient due to the Angle of Attack variation Rate
$C_{L\delta_e}$	Lift Coefficient due to Elevator Deflection
C_{Lq}	Lift Coefficient due to Pitch Rate
C_l	Roll Moment Coefficient
$C_{l\delta_a}$	Roll Moment Coefficient due to Aileron Deflection
$C_{l\delta_r}$	Roll Moment Coefficient due to Rudder Deflection

Longitudinal Flight Control with a Variable Span Morphing Wing
UBI – DCA

C_{l_p}	Roll Moment Coefficient due to Roll Rate
C_{l_r}	Roll Moment Coefficient due to Yaw Rate
C_m	Pitch Moment Coefficient
C_{m_0}	Pitch Moment Coefficient for a Zero Angle of Attack
$C_{m_{0L}}$	Pitch Moment Coefficient for a Zero Angle of Attack due to wingspan
C_{m_α}	Pitch Moment Coefficient for a given Angle of Attack
$C_{m_{\alpha t}}$	Tail's Horizontal Empennage Pitch Moment Coefficient for a given Angle of Attack
$C_{m_{\delta_e}}$	Pitch Moment Coefficient due to Elevator Deflection
$C_{m_{ac}}$	Pitch Moment Coefficient relatively to the Aerodynamic Centre
$C_{m_{c.g.}}$	Pitch Moment Coefficient relatively to the Centre of Gravity
C_{m_q}	Pitch Moment Coefficient due to Pitch Rate
C_n	Yaw Moment Coefficient
C_{n_β}	Yaw Moment Coefficient due to Sideslip Angle
$C_{n_{\delta_a}}$	Yaw Moment Coefficient due to Aileron Deflection
$C_{n_{\delta_r}}$	Yaw Moment Coefficient due to Rudder Deflection
C_{n_p}	Yaw Moment Coefficient due to Roll Rate
C_{n_r}	Yaw Moment Coefficient due to Yaw Rate
C_T	Thrust Coefficient
$C_{T_{\delta_T}}$	Thrust Coefficient due to Throttle Setting
C_y	Lateral Force Coefficient
C_{y_β}	Lateral Force Coefficient due to Sideslip Angle
$C_{y_{\delta_a}}$	Lateral Force Coefficient due to Aileron Deflection
$C_{y_{\delta_r}}$	Lateral Force Coefficient due to Rudder Deflection
C.G.	Centre of Gravity
Cp or ca	Aerodynamic Centre of Pressure
D	Drag
F_{ext}	External Force(s)
F_{int}	Internal Force(s)
I_x or I_{xx}	Inertial Moment about the Longitudinal axis
I_y or I_{yy}	Inertial Moment about the Lateral axis
I_z or I_{zz}	Inertial Moment about the Vertical axis
I_{xz}	Inertial Moment concerning the xz-plane
K_{C_D}	Drag Coefficient Factor
L	Roll Moment or Lift Force
L_{OMW_b}	Left OMW Wingspan
L_{VSMW_b}	Left VSMW Wingspan
M	Pitch Moment
M_{ext}	External Moment(s)
M_t	Tail's Horizontal Empennage Lift Moment
N	Yaw Moment
PID	Proportional-Integral-Derivative
Q	Dynamic Pressure
R_{OMW_b}	Right OMW Wingspan
R_{VSMW_b}	Right VSMW Wingspan
\mathcal{R}_0	Axis system fixed at Earth's centre
\mathcal{R}_b	Axis system fixed at the C.G. of the aircraft's body
S	Wing Area
S.P.	Short-Period Flight Mode

S_t	Tail's Horizontal Empennage Area
T	Thrust
T_p	Pughoid's Period
V	Aircraft Speed
V_{eq}	Equilibrium State's Aircraft Speed
V_T	Aerodynamic Speed Reference
W	Weight
b	Wingspan
c	Chord
\bar{c}	Mean Chord
g	Gravitational Acceleration
h	Altitude
l_t	Tail's Horizontal Empennage length
m	Mass
n	Load Factor
p	Roll Rate
q	Pitch Rate
r	Yaw Rate
s	Span
t	Time
u	Longitudinal Speed
u_{ref}	Longitudinal Speed of Reference
v	Lateral Speed
w	Vertical Speed
x	Longitudinal Position
x_{ref}	Longitudinal Position of Reference
y	Lateral Position
z	Vertical Position

Blank Page

Glossary

Aeroplane	British (UK) word for airplane.
AHM	Altitude Hold Mode
ASL	Air-to-Sea-Level Altitude (better known as MSL – Mean Sea Level)
AGL	Air-to-Ground-Level Altitude
AFCS	Automatic Flight Control System
CDDRH	Climb or Descent/Dive Rate Hold
CPU	Central Processing Unit
DCA	Department of Aerospace Science - “ <i>Departamento de Ciências Aeroespaciais</i> ”
DWM	Dissymmetrical Wing Mode
e.g.	<i>exempli gratia</i> - for example (from <i>Latin</i>)
et al.	<i>et alii</i> - and others (from <i>Latin</i>)
Fly-by-wire	An enhanced type of controller that is usually associated to an autopilot system and that enables the aircraft for superior performance under unstable flight conditions.
i.e.	<i>id est</i> - that is (from <i>Latin</i>)
IFW	Inner-Fixed Wing
In-flight	Designates an airborne vehicle flight phase , i.e. not grounded or stalling.
Level-flight	Designates an aircraft flying straight (levelled) at a constant given altitude (ASL) with no Banking, Yawing or Sliding attitudes.
LM	Landing Mode
LQR	Linear Quadratic Regulator
Mark or MK (M-series)	The M-series is a system commonly used by the military for classifying iterations of prototypes or secret technologies/ articles. Therefore, the

first iteration of a certain article is denominated by article Mark I, and the second by article Mark II and so on.

OMW	Outer-Moving Wing
PAH	Pitch Attitude Hold Mode
s.l.	<i>sine loco</i> - without location (from <i>Latin</i>)
s.n.	<i>Sine nomine</i> – without name (or publishing house) (from <i>Latin</i>)
Soaring	Flight methodology by which a glider (sailplane) pilot uses the atmospheric dynamics such as Thermals, Ridge Lift and Wave Lift to maintain the aeroplane airborne.
Stall	Refers to a situation in which the wing is not producing enough lift to maintain flight. It may occur due to insufficient airspeed or excessive angle-of- attack.
TO	Take-Off
Trimming	To trim an aircraft for the desired attitude. That is, to make a certain deflection (of a control surface) correspond to a zero deflection on the control input (e.g. control stick).
TTA	Time to Target Achievement. Refers to the required time to achieve a determined goal.
UAV	Unmanned Aerial Vehicle
UBI	University of Beira Interior
UK	United Kingdom
USA	United States of America
VSMW	Variable-Span Moving Wing
VTOL	Vertical Take-Off and Landing

Blank Page

Blank Page

Chapter 1

Introduction

Since the very beginning of the aviation history that the need for stability and control had been acknowledged by both aircraft makers and aviators (pilots). Not only it was perceived as fundamental for flight safety as, as the military operators realized the enormous potential of aircraft for combat, it became mandatory. Indeed, the fast developments in aerodynamics theory quickly led to improvements in aircraft design and its pilot-to-control-surfaces interaction, thus increasing flight stability and controllability which allowed for increased flight safety as well as the intended increase in manoeuvrability and accuracy in air-to-air combat of military aircraft. However, as military pilot's workload progressively increased with the need to operate an increasingly higher amount of complex systems and subsystems while keeping an eye on the instruments and flying the aircraft in a combat environment all at the same time, associated with the increasing need for pinpoint accuracy in weapons delivery, made such improvements insufficient. Therefore, the need to assist the pilot with automatic controls for all kind of tasks, including the flight itself, became imperative, and technological developments and research in that area were made a top priority by military authorities. In fact, even non-military aircraft required the continuous full attention of the pilot in order to fly safely, which caused severe fatigue on the pilot in longer flights. And so, when in 1914 (only eleven years after the first flight of the *Wright brothers* in 1903) the *Sperry Corporation* showed its first gyroscopic stabilizer system in a demonstration flight over Paris, it immediately caught the attention of the military [53]. That was in fact, the first mechanical autopilot in history as it allowed the aircraft to fly straight and levelled in a given compass direction, and even allowed for a controlled take-off and landing [53]. Later in the 30's, some B-17s "*Flying Fortress*" already featured the Sperry A-3 commercial autopilot. In the early 40's, the B-24 "*Liberator*" has already took the concept of controllability a step further by including a top secret *Norden Bombsight* [36][37][38][39][40]. It was so secretive, that in the brink of an airplane crash, its operator was instructed to destroy the equipment with its .45 M1911 *Colt* prior to take care about his own safety and attempts a bail-out [54]. This bombsight system utilized a gyro-stabilized sight associated to an analogical MK XV computer that, upon flight data and atmospheric parameters introduction by the operator, would take charge of the bomber stabilizing it in the right path to the locked target and automatically release the bombs on the most appropriated time [36][37][38][39][40][54]. All that was left to do to the operator was to yell "Bombs away" or "Bombs gone" so the pilot could retake the manual control of the aircraft [54]. This ingenious autopilot system allowed in its later M- versions an accuracy ratio of 40% within 500 yards (457.2 m) from an altitude of

12,000 feet (3,568 m) [36]. The Norden M- series bombsight computer is widely regarded as one of the three more crucial technological developments of the WWII era (alongside with the invention of the radar and the atomic bomb), that granted the victory to the Allies. Shortly after (after the MK XV), however, a new break-through was achieved, once again by the *Sperry* company. Its brand new S-1 Bombsight came along with the first all-electronic A-5 autopilot developed in 1940 by Mr. *Frische* from the *Sperry division* of *S. Rand Corporation*. The A-5 surpassed the previous autopilot systems in almost every aspect, and marked the beginning of the digital era of aircraft controllers [37][38][39].

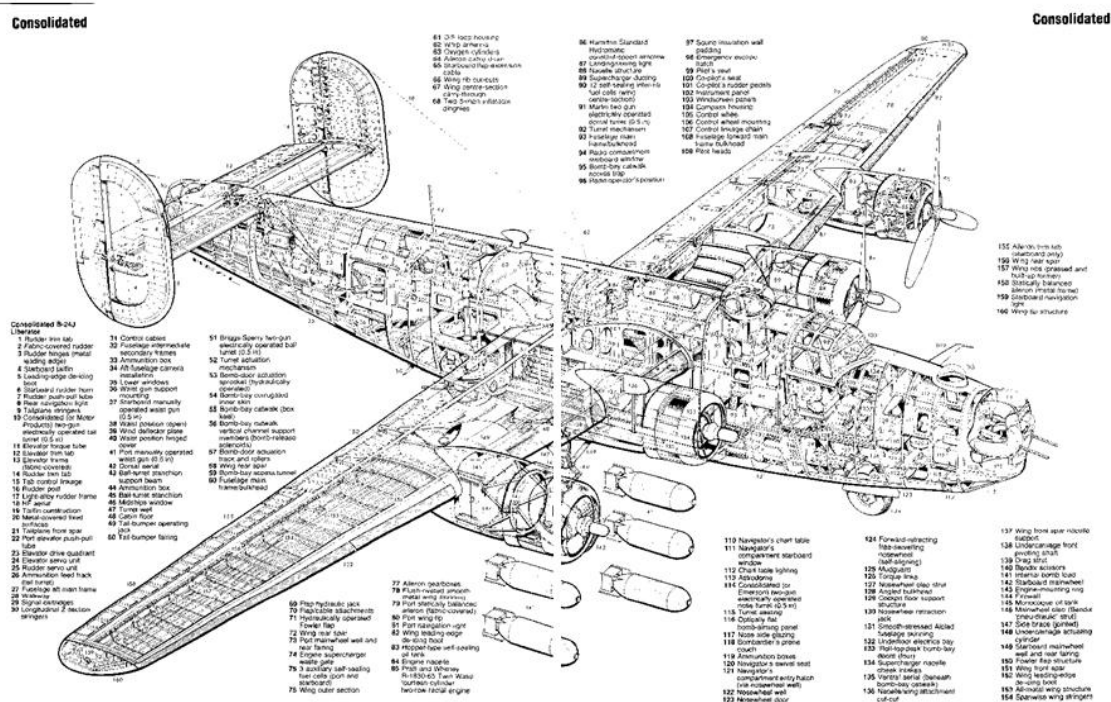


Figure 1.1 Schematic of the B-24 “Liberator” [41].

Since then, the autopilot concept and aeronautics industry itself had met great progress with many major technological advancements in context. However, modern days autopilot systems are still based in the principles of aerodynamics and flight mechanics theory applied to the standard control system of an aircraft developed in 1908 (standardized in 1909) by *Louis Blériot* and *Robert Esnault-Pelterie*. This standard model defines the linkage and control input methods for conventional aeroplanes by the usage of movable (by deflection) hinged tabs, as represented in Figure 1.2 [3][42]:

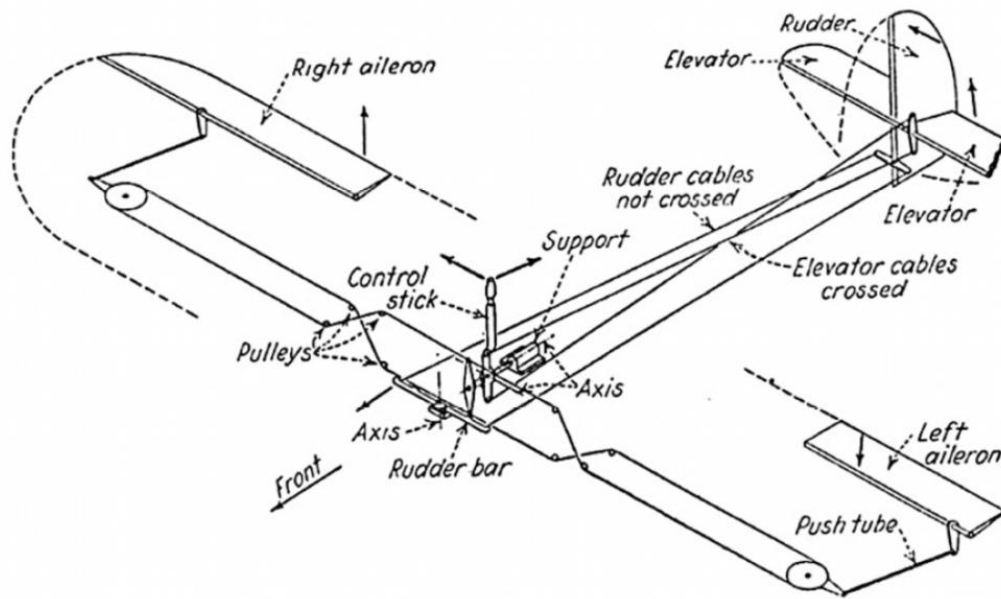


Figure 1.2 Sketch of an aeroplane's classical control system [3][18].

These control surfaces are designated ailerons for roll control, rudder(s) for yaw control and elevator(s) for pitch control. Other aircraft designs may include other tabs such as flaps (for improved lift at slow speeds) and airbrakes (to reduce airspeed by increasing drag). In some cases, it is used one single set of tabs for dual purposes. In the case of the V-Tail used in the UAV *Olharapo*, to which this work is intended, it uses ruddervators for the functions of both the elevators and the rudders.

The standard linkage of an elevators system is made trough a control stick in accordance with the following diagram in Figure 1.3:

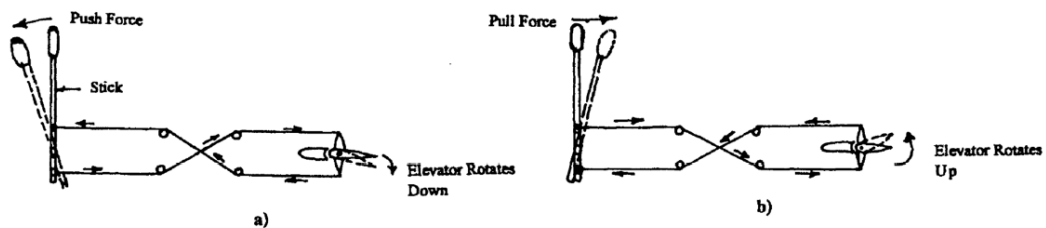


Figure 1.3 Diagram of a classical linkage between the controller stick (input) and the elevator (output). For pitch down the aeroplane, the stick is pushed forward and away from the pilot (a); To pull up (i.e. increase pitch) the stick is pulled in the direction of the pilot [3][12].

The deflection of the control surface generates a correspondent resultant force by changing the normal aerodynamic pressure distribution imposed by the airflow. So, by deflecting e.g. the elevator, it will either increase or decrease the air-pressure in the tail's horizontal stabilizer, therefore decreasing (it may even become negative) or increasing the tail's generated lift at its aerodynamic centre, that will cause a momentum around the aircraft's C.G. (Centre of Gravity), thus pitching the aircraft down or upwards.

In general, the pitch and roll attitudes are controlled with the same stick, whereas the yaw attitude is controlled via the rudder pedals (rudder bar) and the engine's thrust by a separated control designated by throttle. However, since this is an UAV, such linkage system is replaced by electrical servo-mechanisms that serve as actuators of the control surfaces by means of electrical input commands from the digital inboard controller provided by the CPU. In turn, the CPU manages the inputs sent by the operator and received through an electronic receiver or data-link and relates them with the information provided by the several onboard sensors to command the appropriate actions to the control surfaces and engine. If in autopilot mode, the CPU must rely solely on its onboard sensors and previously specified flight parameters to control the aircraft.

1.1 Morphing Technologies in Aviation

The morphing concept of a wing is not exactly new, and consists in the wing's ability to change, while in flight, its own shape or geometrical layout in order to optimize flight parameters (such as controllability, stability or efficiency) under different flight conditions. The most common reason for the development of such morphing technologies is aircraft's efficiency and performance. That is, e.g. the smaller the wingspan (b) the lower its associated drag (wing's induced drag), and thus, the greater the velocity that an aircraft can achieve without increasing its power settings, which also results on an increase in range, and thus in a better fuel or batteries consumption efficiency. It can also mean an increased flight endurance if by diminishing the aircraft's wingspan, the reduction in drag allows the aircraft to fly at the same velocity but with less thrust. Moreover, a smaller wingspan may also benefit aircraft's manoeuvrability at higher velocities. However, a smaller wingspan also implies a reduction in lift, which at lower speeds, can be fatal. Therefore, for situations that require low speed operations (such as landing) or higher lift (such as take-off), a larger wingspan is preferable and advisable.

Many of the current aircraft solve the problem by having wings designed for optimal cruise flight that can provide the extra lift necessary in landings and take-offs by the means of flaps and/or slats. In some cases, these control surfaces are part of the fly-by-wire system to aid in performance increase in manoeuvrability. The problem is that such mechanism not only do not allow a reduction of drag for airspeeds above the cruise speed, as it also represents, in some cases, an increase in drag due to flaps extension far superior to what would be expected by increasing the wingspan instead. Therefore, several concepts of morphing wings have been developed through history to allow wingspan or wing area (as it also influences both lift and drag) variation. Such concepts are represented in Figure 1.4:

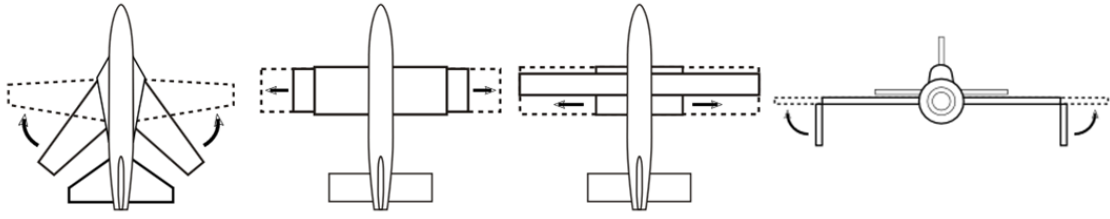


Figure 1.4 Variable geometry wing's configurations. From left to right: Variable Sweep Wing; Telescopic Wing; Extendable Wing; and Folding Wing [34].

The most commonly recognizable configuration is perhaps, the variable sweep wing present in the *F-14 "Tomcat"* or the *B-1B "Lancer"*. This configuration allows the wings to sweep back for supersonic flight (or subsonic high velocities) as it reduces the overall wingspan of the aircraft. While in slow speed operations such as take-off and landing, the wing is swept forward to its natural position to offer better control under such flight conditions. In the case of the *F-14*, it also allows the aircraft to go through the *Nimitz Class Aircraft Carrier's* elevators in pairs, and for better parking as well.

However, all these configurations were developed for symmetrical span-variation only and, although this present work deals with such type of span-variation (as it concerns mainly about longitudinal control and stability) the small scale of the UAV to which the wing was intended required a slightly different approach. Therefore it was decided to develop a new system that allowed as well for asymmetrical span-variation to induce a rolling moment without the use of the conventional ailerons. The best wing configuration for such approach is the telescopic wing configuration, and therefore, the asymmetrical system was designed for such configuration leading to the development of Dissymmetrical Telescopic Wing also known as VSMW (Variable-Span Morphing Wing).

Even though the telescopic wing concept dates back to 1931, when *Ivan Makhonine* flew the *MAK-10* in France [3], the concept has been long forgotten since the accident in 1947 with the improved *MAK-123* due to engine loss [3]. Since then, only the *Akaflieg FS-29* sailplane had made use of this concept upon its design in 1975 [3]. Even then, the lack of an engine to power the extension system required the pilot to operate the system manually, distracting him from focusing on "soaring" the glider, which contributed for the fall of the concept into oblivion once more. In the last decades, only sporadic designs, such as the *Gevers Aircraft's Genesis* in 1997, attempted such concept but there is no evidence of them ever leaving the paper drawings [3].

1.2 Dissertation's Objectives

The main objective of this work consists on the development and validation of a longitudinal flight controller method that would enable a significant increase in stability and automatization of flight for an under development UAV prototype that uses morphing technology to either symmetrically or dissymmetrically change its overall wingspan. This work

adds to the previous work about roll control [3] for this same aircraft by focusing on the longitudinal stabilization.

In order to fully understand the concept behind an automatic aircraft controller (i.e. autopilot or augmented stabilization system) it is necessary to first understand the basic concepts of flight dynamics described on the next sections of the next Chapter [Chapter 2].

Blank Page

Blank Page

Chapter 2

Theoretical Concepts of Flight Dynamics and Mechanics

In the now days modern world, where almost everything is associated with informatics and emerging technologies, it is fairly common to people to not realize how hard it can be from the programming point of view to achieve certain goals or breakthroughs, even the low impacting ones. For instance, while a pilot can reasonably fly an aircraft using only a general idea of the flight mechanics applied and his instinctive reactions on the controls to keep the aircraft under control, things get more difficult when it comes to develop electronic systems of augmented stability or full autopilot systems. Such systems lack the intuitive intelligence and instinct of a human pilot, and must therefore, rely on the a constant feed of environmental data collected through a variety of different sensors and use a CPU to analyse such data and take proper action in proper time. The problem thereby relies on how can the CPU effectively interpret the data in real time and come to a proper solution. And that's were programming skills become essential. A programmer must make full use of all the mathematical equations currently available for the intended subject and compile them in such a way that they will make sense in both informatics and electronics terms as well as in the actual physical terms, while at same time attempting to achieve the intended goals and fill in the lack of instinct and intelligence with some sort of A.I. based in logical procedures recurrent from if/else/while premises. Therefore, Chapter 2 is dedicated to an in depth overall description of the flight dynamics and mechanics inherent to a flight controller system.

2.1 Flight Dynamics Theory

In the dynamic analysis of an aeroplane, and since “a flying aircraft represents a very complicated dynamic system” (Tavares, 2011), the aircraft is considered to be a rigid-body object associated to a general axis system, and therefore elastic forces such as wing torsion are not taken into account. The axis system allows for the determination of the aircraft's C.G. position ($\mathcal{R}_b = (\vec{x}, \vec{y}, \vec{z})$) relative to the Earth ($\mathcal{R}_0 = (\vec{x}_0, \vec{y}_0, \vec{z}_0)$) as seen in Figure 1.4 a). On an in-flight aircraft act aerodynamic, traction and gravitational forces, namely Lift (L), Drag (D), Weight (W) and Thrust (T), which along with their respective angles, coefficients and variation rates represent the main variables to be considered in Aircraft's Flight Mechanics and its analysis, and are pictured on Figure 2.2.

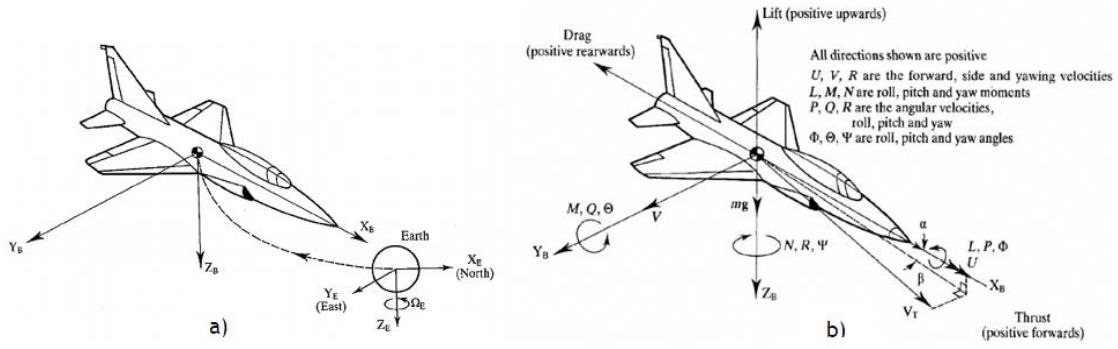


Figure 2.1 a) Axis systems of the Earth and body (aircraft); b) Forces, moments, angles and angular velocities acting on an aircraft [3][15].

All moments and forces are, by convention positive accordingly to the directions shown in Figure 2.1 b). Considering V_T as the aerodynamic speed reference for the aircraft, we obtain the angles of attack (α), sideslip (β), pitch (θ), bank (ϕ), and yaw (ψ), being the last three (θ , ϕ and ψ) the manoeuvring angles related to the corresponding axis which define the attitude of the aeroplane in flight. These are Euler angles [3][12][15][27][31], and represent the three degrees of freedom in rotation about each of their respective axes. The attitude angles are directly influenced by the control surfaces which deflection will cause them to change. For example, by deflecting the elevator (δ_e) the pitch (θ) changes accordingly, leading the aircraft into a dive or a climb according to a respectively negative or positive deflection (assuming that the aircraft is initially at a non-inverted level flight attitude and it has a conventional wings and control surfaces geometry). In the same way, a deflection of the rudder (δ_r) leads into a change of the yaw angle (ψ) and a deflection of the ailerons (δ_a) into an alteration of the bank angle (ϕ).

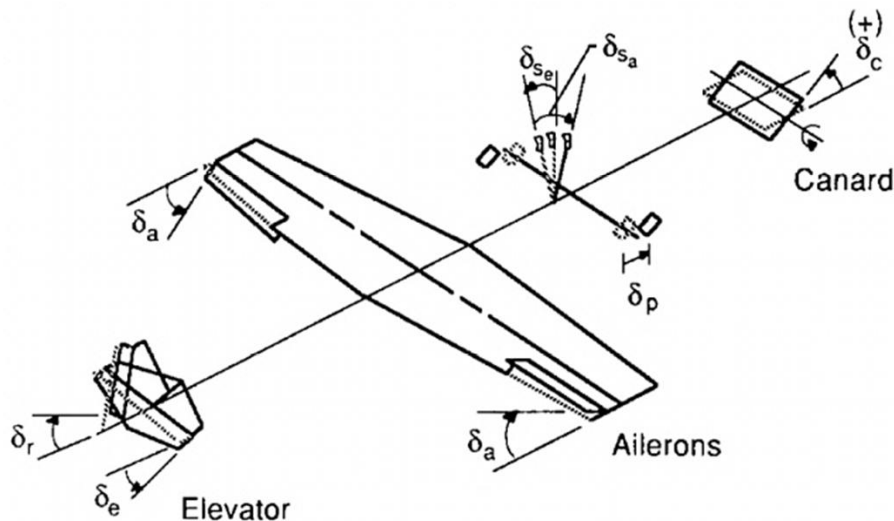


Figure 2.2 General classic control surfaces and respective positive deflections [3][15].

In order to maintain a steady flight, is advisable to reconfigure the initial zero deflection of the control surfaces associated to the neutral point of the aeroplane's centre/side-stick (or

control yoke) and rudder pedals. Doing so allows for the attitude/manoeuvring angles to remain stable reducing the pilot workload on control surfaces inputs. This is achieved by associating the neutral point with a new given deflection angle for each control surface and is called *trimming* the aircraft. However, for more complex geometries, trimming the aircraft may prove insufficient to keep an aircraft stable and therefore, the stability would rather rely on a different and much more complex computer-based control algorithm and additional control surfaces system called *fly-by-wire*.

“the time-derivatives of the Euler attitude angles may be computed from the attitude rates (p, q and r), which represent the “quantity of motion” about the respective axis. These are the basics that describe an aeroplane attitude and motion rate. To better understand the laws that manage the full dynamics of flight, it becomes necessary to formulate the equations for the force and moment coefficients.” (Tavares, 2011) [3].

To determine the motion equations that relate all the last attitude variables from flight dynamics, it is necessary to start by the Physics Fundamentals of Newton’s second law (eq. 2.1 and 2.2) [3][31] which stipulates that:

$$m\vec{V} = \sum \vec{F}_{\text{ext}} \quad (2.1)$$

$$\dot{\vec{C}} = \sum \vec{M}_{\text{ext}} \quad (2.2)$$

Where \vec{F}_{ext} and \vec{M}_{ext} represent, respectively, all the external forces and moments acting on the aircraft, and \vec{C} its kinetic moment around the C.G., that for longitudinal flight is given by equation 2.3:

$$C = I_y \dot{\theta} = I_y q \quad (2.3)$$

So, its derivative is:
$$\dot{C} = I_y \ddot{\theta} = I_y \dot{q} \quad (2.4)$$

By applying the mentioned *Newton’s second law of motion* to the moments applied to the in-flight aeroplane, we have:

$$\dot{V} = \frac{T \cos(\alpha + \varepsilon_T) - \frac{1}{2} \rho(h) V^2 S C_D}{m} - g \sin \gamma \quad (2.5)$$

$$\dot{\gamma} = \frac{T \sin(\alpha + \varepsilon_T) + \frac{1}{2} \rho(h) V^2 S C_D}{mV} - \frac{g}{V} \cos \gamma \quad (2.6)$$

$$\dot{q} = \frac{\rho(h)V^2 S \bar{c} C_m}{2I_y} \quad (2.7)$$

And from the Euler angles seen in Figure 2.1 b) and the velocity components (u, v, w) it is possible to write the general equations that describe the aircraft C.G. position along the Earth reference axis [3][12][13][27][31]:

$$\dot{x} = u \cos \psi \cos \theta + v(\cos \psi \sin \theta \sin \phi - \sin \psi \cos \phi) + w(\sin \psi \sin \phi + \cos \psi \sin \theta \cos \phi) \quad (2.8)$$

$$\dot{y} = u \sin \psi \cos \theta + v(\cos \psi \cos \phi + \sin \psi \sin \theta \sin \phi) + w(\sin \psi \sin \theta \cos \phi - \cos \psi \sin \phi) \quad (2.9)$$

$$\dot{h} = u \sin \theta - v \cos \theta \sin \phi - w \cos \theta \cos \phi \quad (2.10)$$

Where h is the altitude equivalent to the negative z (-z) axis.

By measuring the angular variation of each attitude angle, the following angular velocities are obtained:

$$p = \dot{\phi} - \dot{\psi} \sin \theta \quad (2.11)$$

$$q = \dot{\theta} \cos \phi + \dot{\psi} \cos \theta \sin \phi \quad (2.12)$$

$$r = \dot{\psi} \cos \theta \cos \phi - \dot{\theta} \sin \phi \quad (2.13)$$

The cinematic equations for the attitude angles (or attitude rates), deducted from the attitude angles and angular velocities (p, q, r) are as follows:

$$\dot{\phi} = p + (q \sin \phi + r \cos \phi) \tan \theta \quad (2.14)$$

$$\dot{\theta} = q \cos \phi - r \sin \phi \quad (2.15)$$

$$\dot{\psi} = \frac{q \sin \phi + r \cos \phi}{\cos \theta} \quad (2.16)$$

These define the G.G. position of the aircraft and its respective angle rates. But, in order to determine the complete flight equations it is necessary to define the aerodynamic coefficients which are composed by small incremental variations of the dimensionless coefficients [3][4], i.e. stability derivatives multiplied by the corresponding variables, which in turn depend on the aircraft characteristics and flight conditions.

Generally, lift (C_L), drag (C_D), and lateral force (C_Y) coefficients are defined by:

$$C_L = C_{L_0} + C_{L_\alpha} \alpha + \frac{\bar{c}}{2V} (C_{L_\alpha} \dot{\alpha} + C_{L_q} q) + C_{L_{\delta_e}} \delta_e \quad (2.17)$$

$$C_D = C_{D_0} + K_{C_D} C_L^2 \quad \vee \quad C_D = C_{D_0} + C_{D_\alpha} + \frac{\bar{c}}{2V} (C_{D_\alpha} \dot{\alpha} + C_{D_q} q) + C_{L_{\delta_e}} \delta_e \quad (2.18)$$

$$C_y = C_{y_\beta} \beta + C_{y_{\delta_a}} \delta_a + C_{y_{\delta_r}} \delta_r \quad (2.19)$$

Where C_{D_0} and K_{C_D} are constants for the used aerofoil on the aeroplane.

And roll (C_l), pitch (C_m) and yaw (C_n) coefficients are given by:

$$C_l = C_{l_\beta} \beta + \frac{b}{2V} (C_{l_p} p + C_{l_r} r) + C_{l_{\delta_a}} \delta_a + C_{m_{\delta_e}} \delta_e \quad (2.20)$$

$$C_m = C_{m_0} + C_{m_\alpha} \alpha + \frac{\bar{c}}{2V} (C_{m_\alpha} \dot{\alpha} + C_{m_q} q) + C_{m_{\delta_e}} \delta_e \quad (2.21)$$

$$C_n = C_{n_\beta} \beta + \frac{b}{2V} (C_{n_p} p + C_{n_r} r) + C_{n_{\delta_a}} \delta_a + C_{n_{\delta_r}} \delta_r \quad (2.22)$$

With:

$$\dot{\alpha} = \frac{u\dot{w} - \dot{u}w}{u^2 + w^2} \quad (2.23)$$

These allowed to obtain the following velocity equations [3][31]:

$$\dot{u} = -\frac{QS}{m} (C_D \cos \alpha \cos \beta + C_y \cos \alpha \sin \beta - C_L \sin \alpha) + \frac{T}{m} - g \sin \theta - qw + rv \quad (2.24)$$

$$\dot{v} = -\frac{QS}{m} (C_D \sin \beta - C_y \cos \beta) + g \cos \theta \sin \phi - ru + pw \quad (2.25)$$

$$\dot{w} = -\frac{QS}{m} (C_D \sin \alpha \cos \beta + C_y \sin \alpha \sin \beta + C_L \cos \alpha) + g \cos \theta \cos \phi - pv + qu \quad (2.26)$$

$$\text{With } T = \delta_T T_{\max}(V, h), \text{ for a given speed and altitude.} \quad (2.27)$$

The equations for the manoeuvring taxes are mainly determined from inertia of the aeroplane:

$$\dot{p} = \frac{1}{I_{xx}I_{yy} - I_{xz}^2} [I_{zz}(QSbC_l + (I_{yy} - I_{zz})qr) + I_{xz}(I_{xx} - I_{yy} + I_{zz})pq - I_{xz}qr] \quad (2.28)$$

$$\dot{q} = \frac{1}{I_{xx}I_{yy} - I_{xz}^2} [QScC_m + I_{xz}(r^2 - p^2) + (I_{zz} - I_{xx})rp] \quad (2.29)$$

$$\dot{r} = \frac{1}{I_{xx}I_{yy} - I_{xz}^2} [I_{xx}(QSbC_n + (I_{xx} - I_{yy})pq) + I_{xz}(QSbC_l + (I_{yy} - I_{xx} - I_{zz}))qr + I_{xz}pq] \quad (2.30)$$

Where the dynamic pressure is:

$$Q = \frac{1}{2} \rho V^2 \quad (2.31)$$

Hereupon, the dynamics of flight analysis consists henceforth in the separate analysis of both the longitudinal and lateral-directional flight dynamic characteristics. Since this work is only about the longitudinal control, it will therefore only mention the theoretical principles behind the separated analysis of the longitudinal flight dynamics.

2.1.1 Longitudinal Flight Dynamics

By considering null the effects of all non-longitudinal parameters, and thus locking the velocity vector on the longitudinal axis, it is possible to simplify the flight equations necessary to fully describe an aeroplane motion in this plane. For this matter, also the control variables are reduced to the elevator deflection (δ_e) and throttle variation (δ_T), as the aircraft is restricted to climb or descent attitudes with full disconsideration for any sideslip, yawing or bank rolling. As such, both pitch (θ) and path (γ) angles are one and the same angle while in steady, unperturbed flight, i.e. $\theta = \gamma$, as seen from the comparison between Figure 2.3 and Figure 2.4.

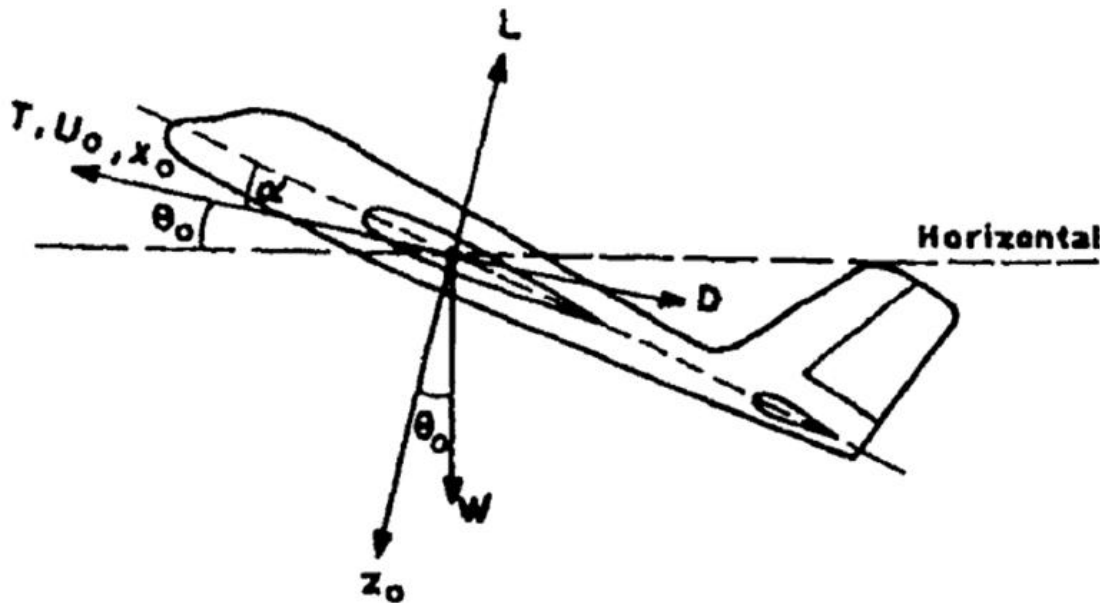


Figure 2.3 Forces and angles concerning the longitudinal flight plane analysis [3][12].

The Figure 2.3 above, shows the Lift (L), Drag (D), Thrust (T) and Weight (W) forces displacement, as well as the angle of attack (α) for an aeroplane climbing at a constant pitch angle (θ_0), where, as already mentioned, both sideslip (β), roll (ϕ), and yaw (ψ) angles are considered null:

$$\beta = 0 ; \phi = 0 ; \psi = 0 \quad (2.32)$$

The path angle formed between the velocity vector and the horizontal plane is related to the attack and pitch angles as [3][15][31]:

$$\theta = \alpha + \gamma \quad (2.33)$$

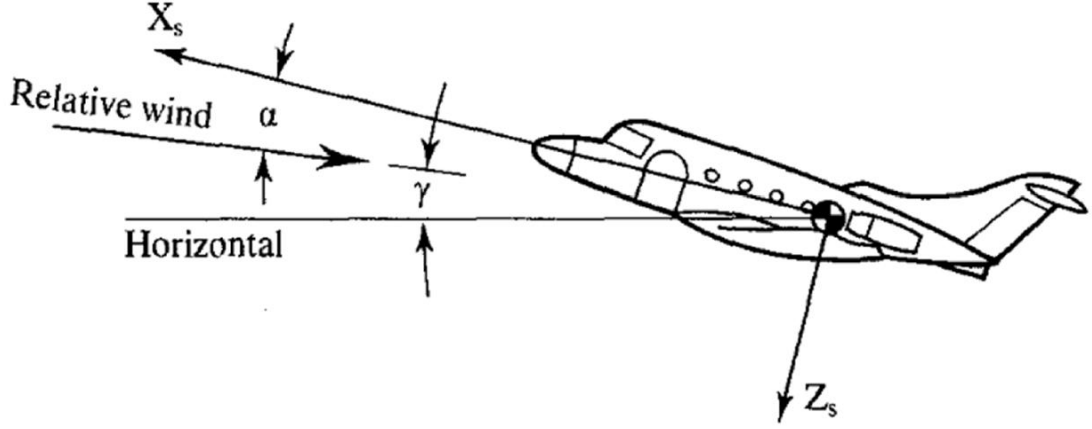


Figure 2.4 Relation between the angle of attack (α) and the path angle (γ) in perturbed flight [3][15].

While the angle of attack relates to the longitudinal and vertical velocities as [3][31]:

$$u = V \cos \alpha \quad (2.34)$$

$$w = V \sin \alpha \quad (2.35)$$

$$\alpha = \tan^{-1} \frac{w}{u} \quad (2.36)$$

Simplifying with these relations and null parameters, the only applied forces are:

$$C_D = C_{D_0} + C_{D_\alpha} \alpha + C_{D_{\delta_e}} |\delta_e| \quad (2.37)$$

$$C_L = C_{L_0} + C_{L_\alpha} \alpha + C_{L_{\delta_e}} \delta_e + C_{L_q} \frac{q\bar{c}}{2V} + C_{L_{\dot{\alpha}}} \frac{\dot{\alpha}\bar{c}}{2V} \quad (2.38)$$

$$C_m = C_{m_0} + C_{m_\alpha} \alpha + C_{m_{\delta_e}} \delta_e + C_{m_q} \frac{q\bar{c}}{2V} + C_{m_{\dot{\alpha}}} \frac{\dot{\alpha}\bar{c}}{2V} \quad (2.39)$$

Also, the necessary flight equations are reduced to:

$$\dot{u} = \frac{1}{m} \left(\frac{1}{2} \rho(h) S u^2 (1 + \tan^2 \alpha) (C_L \sin \alpha - C_D \cos \alpha) + T \cos \epsilon_T \right) - g \sin \theta - q w \quad (2.40)$$

$$\dot{w} = \frac{1}{m} \left(T \sin \epsilon_T - \frac{1}{2} \rho(h) S u^2 (1 + \tan^2 \alpha) (C_D \sin \alpha - C_L \cos \alpha) \right) + g \cos \theta + q u \quad (2.41)$$

$$\dot{q} = \frac{\rho(h) u^2 (1 + \tan^2 \alpha) S \bar{c} C_m}{2 I_{yy}} \quad (2.42)$$

$$\dot{\theta} = q \quad (2.43)$$

With

$$T = \frac{1}{2} \rho(h) S u^2 (1 + \tan^2 \alpha) C_T \quad (2.44)$$

And

$$C_T = C_{T_{\delta_T}} \delta_T \quad (2.45)$$

The interest here resides on the resulting angle of attack (α) and the sub-consequent pitch and path angles (from equation 2.33) due to a given elevator deflection (δ_e). The system works by changing the pressure distribution around the horizontal tail, which normally has a symmetric profile, and so altering the pitch moment (M) as shown in Figure 2.5 [3][12].

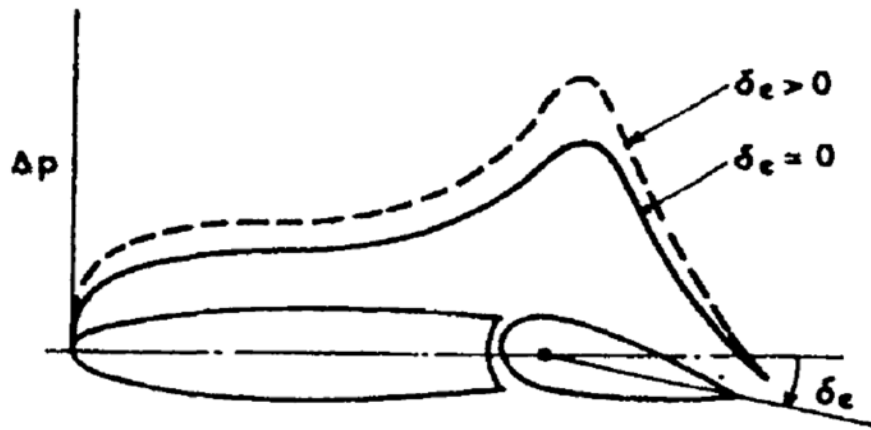


Figure 2.5 Pressure distribution along the tail's horizontal empennage and elevator and its change due to elevator deflection [3][12].

The resulting angle of attack and pitch angle and rate (α , θ and q) are obtained from the flight equations. In Figure 2.6 it is possible to see how a negative deflection of the elevator (δ_e) results in a positive angle of attack on the tail (α_t) which will also lead to a positive α on the wing and therefore to a positive pitch moment for a climbing attitude.

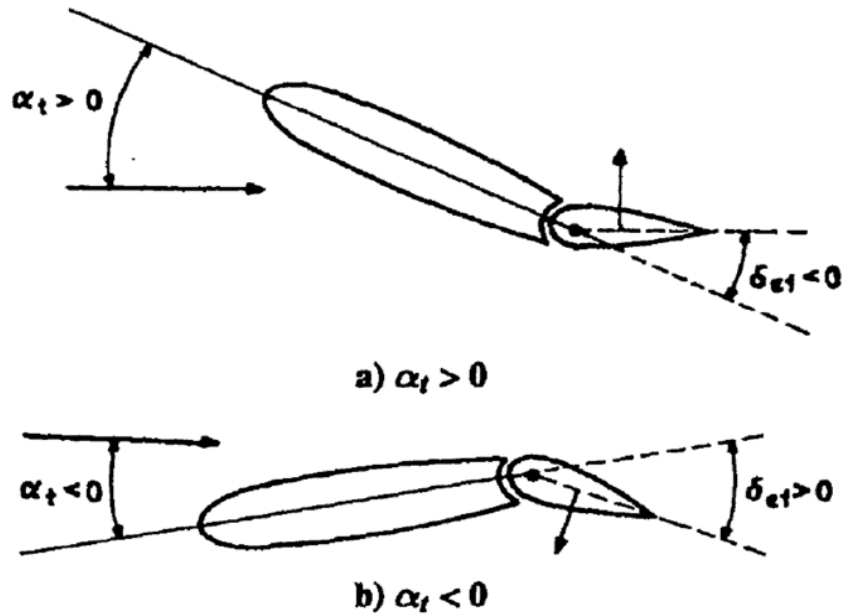


Figure 2.6 Effect of the elevator deflection on the tail's angle of attack [3][12].

This change in pitch moment is also acknowledged by the deviation in lift forces on the tail's empennage as it differs from the levelled flight lift (Figure 2.7) [3][12].

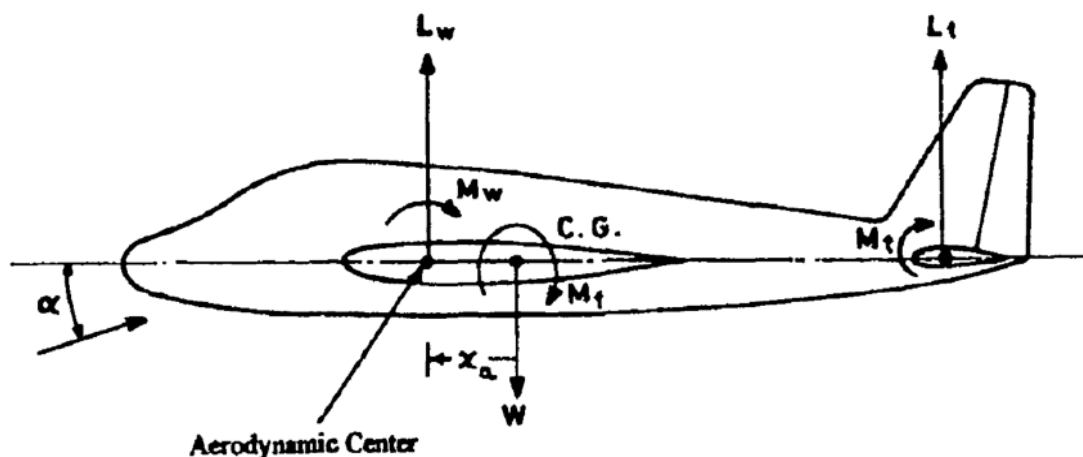


Figure 2.7 Forces and moments acting on an aircraft in levelled flight [3][12].

The thrust variation (δ_T) by the throttle also influences the attitude of the aeroplane as the increase in speed generally leads to an increase in both lift and angle of attack, which in turn adds even more lift to the wing. Therefore it may be necessary to compensate the resulting climbing attitude with a positive deflection of the elevator. A decrease in speed by throttle variation also influences the aircraft attitude as it leads to a decrease in lift and thus, a nose down attitude requiring compensation by negative elevator deflection. However, if the airspeed gets too low, it may lead the aircraft to an eminent stall, which in turn may require a different compensation approach with an increase in flaps extension/deflection.

2.2 Stability and Control Derivatives

The stability derivatives describe the change of forces and/or moments occurred due to the variations on the flight conditions and variables [3]. The control derivatives, on the other hand, describe how the same forces/moments change due to the variation on the deflection of the control surfaces and the variation in thrust. As the UAV “*Olharapo*” remains in the project phase, it is not yet possible to accurately measure the relation between the variation of the several angles and rates to their influence on the aircraft’s attitude moments and force coefficients, since it would only be possible during actual test flights or wind-tunnel tests. Therefore, both derivatives have to be previously estimated with resource to XFLR5[®] and MATLAB[®] software using known flight equations available through several books [12][13][27][33][35].

Thus, the use of XFLR5[®] software allowed for easily obtain initial values for all the needed derivatives as well as for the aircraft’s inertial moments with fairly accurate precision. Later a more elaborated analysis through the MATLAB[®] software delivered more accurate values for some of the needed derivatives which would then become the starting point to the development of the actual longitudinal controller for the UAV. However, it was necessary to proceed to a meticulous comparison between the values obtained through these two different methods and some other provided data prior to establish what final values were to be used.

2.3 Flight Stability

The equilibrium state of an aeroplane is defined by the absence of resultant forces or moments applied to its C.G.. The static stability consists on the tendency of the aircraft to return to its previous equilibrium state after a disturbance of flight. This will happen only if the aeroplane has restoring moments or forces to counter the disturbance. That is, e.g. if an aeroplane has its equilibrium state defined for level-flight with four degrees in angle of attack (α), and its wings and body geometry are such that the aircraft has a natural nose down attitude whenever α is any greater than that, then the aircraft will be able to return to level-flight if disturbed by e.g. a symmetrical interference of a thermal bubble (updraft).

The dynamic stability however, focuses on what happens to the motion of the aeroplane for the duration of the disturbance. For that matter, dynamic stability can be achieved by either oscillatory (damped or undamped) or non-oscillatory motions [3][13][15]. However, it is important to notice that although an aeroplane may be statically stable but dynamically unstable, if the aeroplane is dynamically stable, then it must be statically stable as well.

Basically, an aeroplane can be considered, as it is fairly symmetric, to describe two types of movement: Longitudinal Flight (at xOz plane) and Lateral-Directional Flight (at xOy plane). The longitudinal movements are therefore movements around the yy axis of the aeroplane like e.g. the variation in pitch angle (θ) due to the elevator deflection (δ_e), and the

longitudinal flight includes level-flight, climbing, and descending flight attitudes. The lateral-directional flight movements, on the other hand, are e.g. the yawing attitude (ψ) due to ruder deflection (δ_r). The aircraft's longitudinal and lateral-directional stability is thereby basically constituted by the forces and moments that the control surfaces have to exercise in order to recover from in-flight disturbances.

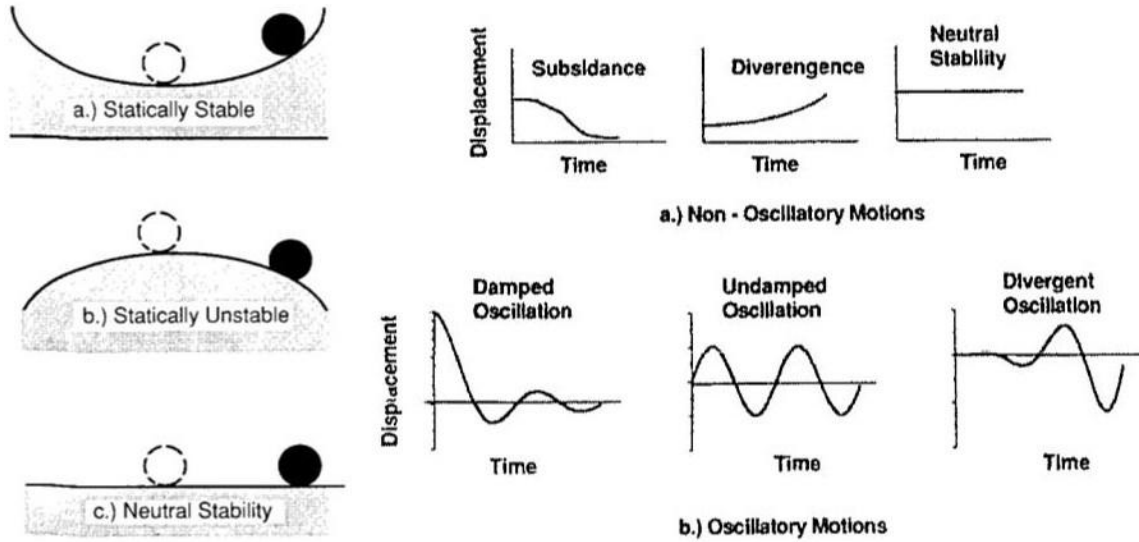


Figure 2.8 Sketches illustrating various conditions of static stability (left) and examples of stable and unstable dynamic motions (right) [13].

This theory was first developed in 1904 by *George H. Bryan*, even before knowing about Wright brother's first flight, where he showed the existence of several oscillatory and non-oscillatory longitudinal and lateral flight modes [3]. The handling qualities of an aeroplane are therefore, defined by the ability to control the aircraft in such flight modes (See Chapter 2 Section 2.4. Flight Modes (Handling Qualities)).

The oscillatory modes can be described by a second-order equation, based on the principle of a rigid body attached to a spring and a damping device [3][13]. The spring has a natural frequency of ω_n and the damping device a damping rate of ξ . The characteristic equation for this system is therefore as follows:

$$\lambda^2 + 2\xi\omega_n\lambda + \omega_n^2 = 0 \quad (2.46)$$

Where the two roots, in the complex form of $\lambda = a \pm bi$, are given by:

$$\lambda_{1,2} = -\xi\omega_n \pm \omega_n\sqrt{1 - \xi^2}i \quad (2.47)$$

2.3.1 Longitudinal Flight Static Stability

The longitudinal static stability of an aircraft is based upon the pitch moment (M) relative to the aircraft's C.G. or upon its coefficient ($C_m = M/QSb$) and the angle of attack (α). An aeroplane is statically stable in longitudinal flight in a specified equilibrium point (i.e.

equilibrium position) when it has the ability to return to its initial angle of attack in equilibrium position (α_{eq}) after a disturbance.

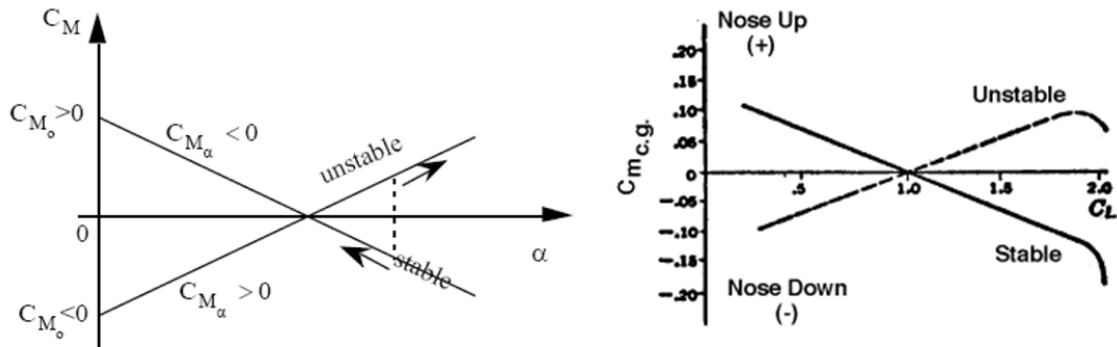


Figure 2.9 (Left) Stable and unstable static stability with regard to the relation between the pitch moment coefficient ($C_M = C_m$) and the angle of attack (α); (Right) Static stability with regard to the relation between the pitch moment coefficient relative to the centre of gravity ($C_{m.c.g.}$) and the lift coefficient (C_L) [43].

With the pitch moment coefficient for a zero angle of attack being $C_{m_0} = C_{m_{0L}}$ it is guaranteed that $C_{m_0} = C_{m_{ac}}$, where the “ac” index refers to aerodynamic centre.

For a statically stable aeroplane, the pitch moment coefficient (C_m) increases as the angle of attack (α) decreases. The pitch moment coefficient for a given angle of attack parameter (C_{m_α}), also known as pitch stiffness, is thereby the slope of the pitch moment’s polar, and is given by:

$$C_{m_\alpha} = \frac{\partial C_m}{\partial \alpha} \quad (2.48)$$

Therefore, the pre-requisite conditions for the longitudinal static stability of an aeroplane are:

$$\begin{cases} C_{m_\alpha} < 0 \\ \text{and} \\ C_{m_0} > 0 \end{cases} \quad (2.49)$$

However, comparing the C.G. and the aerodynamic centre relative positions:

$$C_m = C_{m_{c.g.}} = C_{m_{ac}} + (C_L \cos \alpha + C_D \sin \alpha)(h_{c.g.} - h_{ac}) \quad (2.50)$$

With:

$$h_{c.g.} = \frac{x_{c.g.}}{\bar{c}} \text{ and } h_{ac} = \frac{x_{ac}}{\bar{c}} \quad (2.51)$$

For small angles of attack, $\cos\alpha \cong 1$ and $\sin\alpha \cong \alpha$, thus:

$$C_m \approx C_{m_{ac}} + (C_L + C_D\alpha)(h_{c.g.} - h_{ac}) = C_{m_{ac}} + C_L \left(1 + \frac{C_D}{C_L}\alpha\right)(h_{c.g.} - h_{ac}) \quad (2.52)$$

But, for well designed wings, the drag coefficient (C_D) can be despised for below stall operation, i.e. angles of attack below the stall limit angle. Thus $C_D/C_L \cong 0$ and so, $(1 + C_D/C_L\alpha) \cong 1$. Hence:

$$C_m \approx C_{m_{ac}} + C_L(h_{c.g.} - h_{ac}) \quad (2.53)$$

Derivativating in order to α :

$$C_{m_\alpha} = \frac{\partial C_m}{\partial \alpha} = \frac{\partial C_{m_{ac}}}{\partial \alpha} + \frac{\partial C_L}{\partial \alpha}(h_{c.g.} - h_{ac}) \quad (2.54)$$

Because the aerodynamic centre is the point for which the pitch moment variation remains null as the angle of attack assumes different values, it follows that:

$$\frac{\partial C_{m_{ac}}}{\partial \alpha} = 0 \quad (2.55)$$

On the other hand, $C_{L_\alpha} = (\partial C_L / \partial \alpha)$ and $C_{m_\alpha} < 0$ is thereby equivalent to $(h_{c.g.} - h_{ac}) < 0$. Therefore, there are not one but two conditions for longitudinal stability:

Either

$$C_{m_\alpha} < 0 \text{ and } C_{m_{ac}} = C_{m_0} > 0 \quad (2.56)$$

Or

$$(h_{c.g.} - h_{ac}) < 0 \text{ and } C_{m_{ac}} = C_{m_0} > 0 \quad (2.57)$$

2.4 Flight Modes (Handling Qualities)

The handling qualities of an aircraft are the quality characteristics that determine the ease and precision with which the pilot controls that aircraft. The stability augmentation systems are means by which the appropriate handling qualities can be properly attributed to an aircraft. Such systems are based on the concepts of state feedback control that allow the improvement of the control and stability of an aircraft that does not comply with the desirable handling qualities. When a trimmed aircraft meets the required/desirable handling qualities, it performs a natural frequency motion if disturbed from its equilibrium state [3].

2.4.1 Cooper-Harper Scale

Later, in the 60's, the increase and expansion of the aeronautical industries and their applications led to the necessity of improving handling qualities. Therefore, and in order to better understand and classify the quality of an aeroplane behaviour, a new standard handling qualities evaluation system was developed [3][13][27][31]. This new system, called the *Cooper-Harper scale*, is divided in three flight phase categories (Categ. A, B and C) for each of the four aeroplane classes (Class I, II, III and IV) in any of the three possible flight levels (levels 1, 2 and 3) [13][27][31][32]. A detailed description of this classification system is presently annexed at Annex C. According to these flight levels, classes and categories, there are certain limits to the natural frequency, damping and period for each mode that define the respective flying characteristics of the aeroplane. And each mode's respective Eigen value is obtained from the characteristic equation of the state matrix A. It is important to notice that negative eigenvalues refer to converging motions, which represent dynamically stable flying modes [3].

2.4.2 Longitudinal Flight Modes

In longitudinal flight, two modes can be acknowledged: phugoid (long-period) and short-period oscillations.

The phugoid motion is created when, locking the angle of attack (α), there is a natural long-period oscillatory motion with variations of speed, altitude and attitude. In other words, the phugoid oscillation occurs as an exchange of kinetic and potential energy when there is a variation in both pitch angle (θ) and longitudinal speed (u) with almost no variation of α , that later returns to its equilibrium point [3]. This flight mode is dependant only of the equilibrium speed of a given airplane as stated by *Lanchester* in 1908 [51]. This can be acknowledged when flying a paper plane or a glider above or below the best gliding speed [3].

If the aircraft is statically stable, then any increase in longitudinal speed will increase both drag and lift leading the aircraft to assume a climbing attitude. Thus transforming kinetic energy in potential energy, which will cause the aircraft to lose speed. As its speed falls below the initial airspeed (before the disturbance) it starts to lose the acquired pitch moment

that made it climb, and eventually starts diving. This turn around, potential energy is transformed into kinetic energy increasing aircraft's speed as it loses altitude, hence increasing lift as well, leading the aircraft into a sinusoidal cycle of climbs and descents that describe the long-period mode (Figure 2.10).

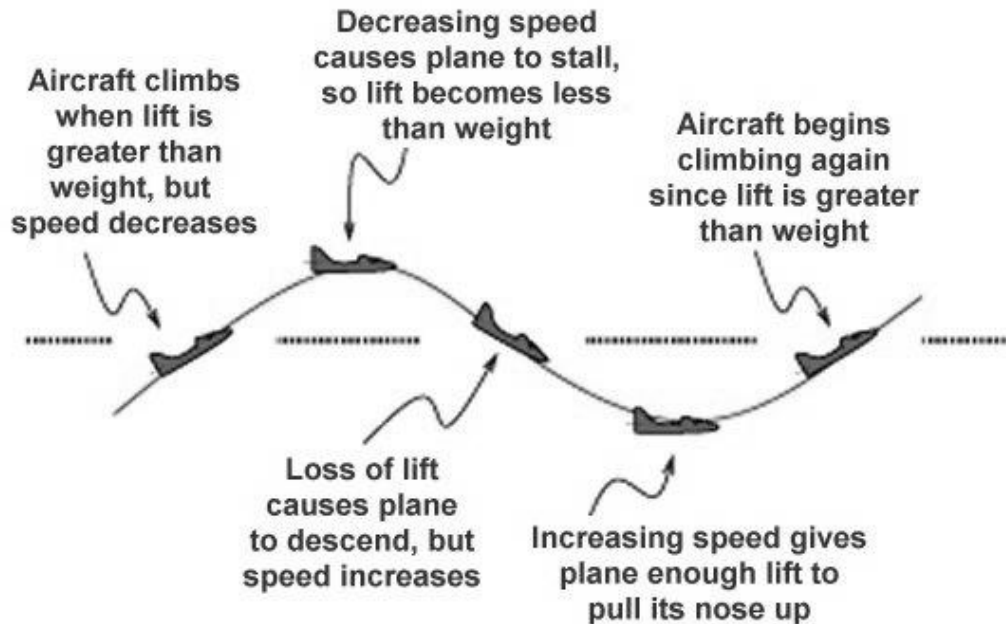


Figure 2.10 Example of an aeroplane change in altitude and attitude in a phugoid mode oscillation trough time with neutral dynamic stability. The phugoid period is generally between 20 and 100 seconds [44][51].

If the aircraft is also dynamically stable, then it may be able to return to equilibrium by actively damping the oscillation cycle. However, even if the motion remains undamped, due to the long period characteristic of this flight mode, the pilot has generally time enough to apply the necessary corrections to the control surfaces.

The short-period oscillation (Figure 2.11) consists of a rotation around the yy axis of the vehicle when affected by a vertical disturbance such as an air blast in a thermal column updraft or a downdraft on an air-pocket. During this mode the longitudinal airspeed remains constant as the vertical draft disturbance causes a variation of the angle of attack (α) which in turn leads to a variation in lift causing a pitch moment that disrupts attitude equilibrium. In the short-period mode the aircraft may not have the ability to return to its initial attitude equilibrium depending on the severity of the disturbance and on the fact of the aeroplane being either dynamically stable or unstable. By other words, the short-period mode is a usually heavily damped oscillation with a period of only a few seconds where the fast pitching of the aircraft about its C.G. generates a variation of the angle-of-attack (α). As the name suggests, the short-period has a shorter oscillation period than the phugoid, which prevents a promptly response of the pilot to correct aircraft's attitude, and thereby requiring a proper damping by the aircraft itself in order to sustain longitudinal dynamic stability. In fact, the

period is so short that the speed does not have time to change. However, this allows the identification of each conjugated eigenvalue, obtained from the state-matrix A of the linear mode, where the period is determined by [3][51]:

$$T_p = \frac{2\pi}{\omega_n \sqrt{1 - \xi^2}} \quad (2.58)$$

The real and imaginary parts for each eigenvalue are determined by equation 2.47. Then, to identify which oscillations are phugoid and which are short period, the period (T_p) must be calculated for each pair of conjugated eigenvalues as follows:

$$\begin{aligned} \left. \begin{matrix} \lambda_1 \\ \lambda_2 \end{matrix} \right\} &\Rightarrow \left\{ \begin{matrix} \omega_{n1} \\ \xi_1 \end{matrix} \right\} \Rightarrow T_{p1} = \frac{2\pi}{\omega_{n1} \sqrt{1 - \xi_1^2}} \\ \left. \begin{matrix} \lambda_3 \\ \lambda_4 \end{matrix} \right\} &\Rightarrow \left\{ \begin{matrix} \omega_{n2} \\ \xi_2 \end{matrix} \right\} \Rightarrow T_{p2} = \frac{2\pi}{\omega_{n2} \sqrt{1 - \xi_2^2}} \end{aligned} \quad (2.59)$$

With

$$\omega_n = |\lambda| \quad (2.60)$$

and

$$\xi = -\frac{a}{\omega_n} \quad (2.61)$$

Therefore, since the phugoid has a longer period than the short-period mode is easy to conclude that if T_{p1} is higher than T_{p2} , then such oscillation is part of the phugoid mode. Else, if T_{p1} is lower than T_{p2} , such oscillation belongs to the short-period mode.

The pitch moment about the C.G. of an aircraft due to a slight variation of the pitch angle ($\Delta\theta$) from its equilibrium state is given by:

$$M = \frac{1}{2} \rho_{eq} V_{eq}^2 S \bar{c} C_{m\alpha} \Delta\theta \quad (2.62)$$

The lift moment of the tail's horizontal empennage about its C.G. is:

$$(\Delta M)_t = \frac{1}{2} \rho_{eq} V_{eq} S_t C_{mat} l_t^2 \frac{d(\Delta\theta)}{dt} \quad (2.63)$$

And therefore, the motion equation is given by:

$$I_y \frac{d^2(\Delta\theta)}{dt^2} = \frac{1}{2} \rho_{eq} V_{eq} S_t C_{mat} l_t^2 \frac{d(\Delta\theta)}{dt} - \frac{1}{2} \rho_{eq} V_{eq}^2 S \bar{c} C_{m\alpha} \Delta\theta \quad (2.64)$$

It is yet important to observe how the following factors intervene on the undamped natural frequency's magnitude of the short-period flight mode:

1. The $C_{m\alpha}$ affects the position of the center of gravity (C.G.) in relation to the aerodynamic center (Cp) of the aeroplane. The S.P.'s frequency is usually higher for a more over the front C.G. than for a more over the rear one.
2. Due to the Dynamic Pressure, the frequency, at any altitude, is higher the higher is the speed.
3. Due to Inertial Moment while pitching, the frequency is higher the lower is the aircraft's inertial moment.

It is also important to notice that, when in hands free flight mode (e.g. when flying a trimmed aircraft), it may occur an neutral damping with an extremely short period of only one to two seconds, which leads to dangerously high load factors ($n = L/W$) possibly incurring on structural damage to the wings and the aircraft's main frame.

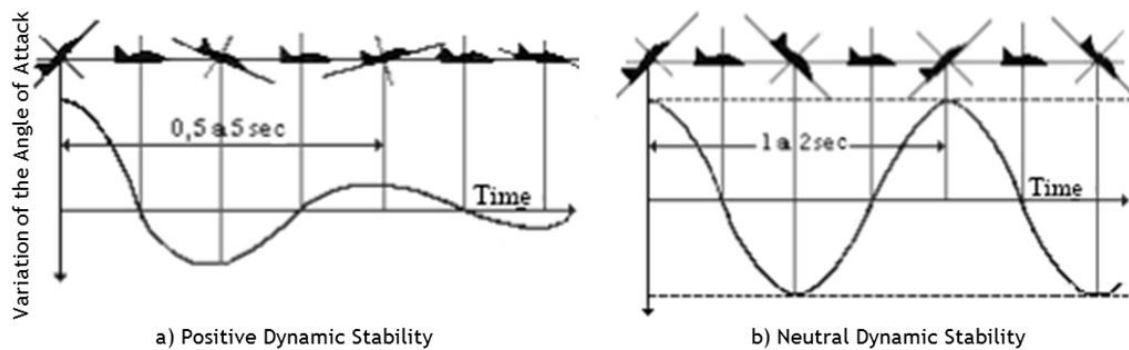


Figure 2.11 Short Period movement characterization [51]

Therefore, by defining the longitudinal flight modes of the aeroplane in accordance with the Cooper-Harper Scale system (presented in Annex C), it's now possible to define the parameters of the controller's algorithm.

2.5 System Linearization

According to the *Lyapunov's* Theorem of the Local Linearity, a non-linear dynamic system has a linear behaviour in the vicinity of its equilibrium points. Therefore, a linearized system is closely similar to its non-linear model in the vicinity of such points. As it is simpler to use a linear system instead of a non-linear one to study an aircraft's behaviour around its equilibrium state, and since it is required in order to use the more up-to-date controller methods, it is thereby necessary to linearize the previous flight equations system relatively to an equilibrium state, generally defined as levelled (trimmed) flight [3][51]. This linearization method is based on the *Taylor's* expansion described by the following theorem.

2.5.1 Generalized *Taylor's Theorem*

Suppose that $D \in \mathbb{R}^n$, ($n \in \mathbb{N}^*$), and that $f: D \rightarrow \mathbb{R}$ has partial derivatives up to $(p + 1)$ order in D . Then, for any $l = (l_1, \dots, l_n) \in D$ such that $(x_0 + l) \in D$, there is a real number θ with $0 < \theta < 1$ such that [51]:

$$f(x_0 + l) = \sum_{r=0}^p \frac{1}{r!} (l \cdot \nabla)^r f(x_0) + \frac{1}{(p+1)!} (l \cdot \nabla)^{p+1} f(x_0 + \theta l) \quad (2.65)$$

Where the partial differential operator is defined by:

$$(l \cdot \nabla)^k = \sum_{\substack{0 \leq i_1, \dots, i_n \leq k \\ i_1 + \dots + i_n = k}} \frac{k!}{i_1! \dots i_n!} l_1^{i_1} \dots l_n^{i_n} \frac{\partial^k}{\partial x_1^{i_1} \dots \partial x_n^{i_n}} \quad (1.66)$$

The linearization of the function f around x_0 (that represents a given equilibrium point for the aeroplane) consists in replacing f 's expression in the vicinity of x_0 by the first order *Taylor's* expansion of f on that point with null remainder. That is:

$$f(x_0 + \Delta x) \cong f(x_0) + \sum_{k=1}^n \Delta x_k \frac{\partial f}{\partial x_k}(x_0) = f(x_0) + (\nabla f(x_0))^T \Delta x \quad (2.67)$$

Where $\Delta x = (\Delta x_1, \dots, \Delta x_n) = l$ is the considered (x) point's deviation from x_0 .

The linearization of a mono-variable f function is given by:

$$f(x_0 + \Delta x) \cong f(x_0) + \Delta x \cdot f'(x_0) \quad (2.68)$$

Given an equilibrium or reference state, this linearization method can be used for longitudinal stabilization in small flight disturbances.

Δu and Δw designate, respectively the incremental variations of longitudinal (u) and vertical (w) velocities around their respective equilibrium or reference conditions designated by u_0 and w_0 . In fact: $u = u_0 + \Delta u$ and $w = w_0 + \Delta w$. Δq , $\Delta \alpha$, $\Delta \gamma$ and $\Delta \theta$ can be defined in the same way, and the non-linear model can be described by either the u , w , q and θ variables or the u , α , q and θ ones given the relation:

$$\tan \alpha = \frac{w}{u} \quad (2.69)$$

Therefore, the flight model linearization can be achieved by the following procedure:

Be it $X_0 = [V_0 \ \gamma_0 \ q_0 \ \theta_0]^T$ the equilibrium state vector, and $U_0 = [\delta_{e_0} \ \delta_{T_0}]^T$ its equilibrium control vector, then $F(X_0, U_0) = 0$.

So, for example, for the following equation of the non-linear model, given earlier by (2.5):

$$\dot{V} = \frac{T \cos(\alpha + \varepsilon_T) - \frac{1}{2} \rho(h) V^2 S C_D}{m} - g \sin \gamma \quad (2.70)$$

Once $\dot{V}_0 = f_V(X_0, U_0) = 0$ for the equilibrium point, the *Taylor's* expansion of the 1st order f_V about (X_0, U_0) results in (equation 2.71):

$$\overbrace{\dot{V}_0 + \Delta \dot{V}}^{\dot{V}} = \Delta \dot{V} = f_V(X_0 + \Delta X, U_0 + \Delta U) = f_V(X_0, U_0) + (\nabla f_V(X_0, U_0))^T \begin{bmatrix} \Delta X \\ \Delta U \end{bmatrix} = (\nabla f_V(X_0, U_0))^T \begin{bmatrix} \Delta X \\ \Delta U \end{bmatrix}$$

With (equation 2.72):

$$(\nabla f_V(X_0, U_0))^T = \left[\frac{\partial f_V}{\partial V}(X_0, U_0) \quad \frac{\partial f_V}{\partial \gamma}(X_0, U_0) \quad \frac{\partial f_V}{\partial q}(X_0, U_0) \quad \frac{\partial f_V}{\partial \theta}(X_0, U_0) \quad \frac{\partial f_V}{\partial \delta_e}(X_0, U_0) \quad \frac{\partial f_V}{\partial \delta_T}(X_0, U_0) \right]$$

Designating by $\nabla_X f_V(X_0, U_0)$ the gradient of $f_V(X_0, U_0)$ related to the state vector X and by $\nabla_U f_V(X_0, U_0)$ its gradient in relation to the control vector U results:

$$\Delta \dot{V} = (\nabla_X f_V(X_0, U_0))^T \Delta X + (\nabla_U f_V(X_0, U_0))^T \Delta U \quad (2.73)$$

With:

$$(\nabla_X f_V(X_0, U_0))^T = \left[\frac{\partial f_V}{\partial V}(X_0, U_0) \quad \frac{\partial f_V}{\partial \gamma}(X_0, U_0) \quad \frac{\partial f_V}{\partial q}(X_0, U_0) \quad \frac{\partial f_V}{\partial \theta}(X_0, U_0) \right] \quad (2.74)$$

and

$$(\nabla_U f_V(X_0, U_0))^T = \left[\frac{\partial f_V}{\partial \delta_e}(X_0, U_0) \quad \frac{\partial f_V}{\partial \delta_T}(X_0, U_0) \right] \quad (2.75)$$

Then, replacing $(\nabla_X f_V(X_0, U_0))^T$ by its state vector related *Jacobian* matrix A and $(\nabla_U f_V(X_0, U_0))^T$ by its control vector related *Jacobian* matrix B , the linearized model assumes its final form as the following linear differential system:

$$\Delta \dot{X} = A \Delta X + B \Delta U \quad (2.76)$$

2.5.2 Butcher's Algorithm

To obtain the best possible approximation of the state vector x , an iterative calculation method based in the *Runge-Kutta* methods is used. The method is called the Butcher's algorithm and consists of the following:

For the model of a controlled system described by:

$$\dot{x} = f(x, u), \quad x \in \mathbb{R}^n; \quad u \in \mathbb{R}^m \quad (2.77)$$

Being u the control vector and assuming a given x_0 , then the system states $t_1, t_2, \dots, t_k, \dots, t_n$ are determined by:

$$x_{k+1} = x_k + \frac{1}{90}(7k_1 + 32k_3 + 12k_4 + 32k_5 + 7k_6) \quad (2.78)$$

With:

$$k_1 = dt \cdot f(x_k, u_k) \quad (2.79)$$

$$k_2 = dt \cdot f\left(x_k + \frac{1}{4}k_1, u_k\right) \quad (2.80)$$

$$k_3 = dt \cdot f\left(x_k + \frac{1}{8}k_1 + \frac{1}{8}k_2, u_k\right) \quad (2.81)$$

$$k_4 = dt \cdot f\left(x_k - \frac{1}{2}k_2 + k_3, u_k\right) \quad (2.82)$$

$$k_5 = dt \cdot f\left(x_k + \frac{3}{16}k_1 + \frac{9}{16}k_4, u_k\right) \quad (2.83)$$

$$k_6 = dt \cdot f\left(x_k - \frac{3}{7}k_1 + \frac{2}{7}k_2 + \frac{12}{7}k_3 - \frac{12}{7}k_4 + \frac{8}{7}k_5, u_k\right) \quad (2.84)$$

With all the information presented so far, it is now possible to implement the controller itself.

2.6 LQR Controller

As part of an integrated automatic control system (autopilot) or AFCS, its longitudinal controller component must comply with the requirements and general design of such system. Since the *Sperry Brothers* proved in 1914 that it was indeed possible to maintain the attitude of an airborne aeroplane even through an array of several random disturbances, provided that the aeroplane is dynamically stable, control and stabilization methods have improved

greatly [39][53]. The advent of guided missiles and modern air combat had played a major role in the development of modern control systems that allow even dynamically unstable aircrafts such as the *F-117A "Nighthawk"*, the *F-16 "Fighting Falcon"* or the *B-2A "Spirit"* to be safely handled with ease by the pilots. These systems, known as "*fly-by-wire*", even allow certain aircrafts, such as the *F-22A "Raptor"* or the Su-27 "*Flanker*" to execute highly complex air combat manoeuvres such as the "*Pugachev's Cobra Manoeuvre*" and "*Thrust Vectoring*" as well as crucially accurate VTOL operations performed with great precision by aircrafts such as the *F-35B "Lightning II"*.

Despite the several control and stabilization methods available today, the most commonly used is the PID controller (proportional-integral-derivative controller) [3][50]. The PID calculates an error value as the difference between a measured process variable and a desired objective point, and then attempts to minimize this error by adjusting the process control inputs. However, a LQR controller is a better and more suitable alternative for this project.

LQR stands for *Linear Quadratic Regulator* and the implementation of such controller implies operating a dynamic system at minimum cost with supplied weight factors (R and Q matrices). This dynamic system must be described by a set of linear differential equations, which, had to be linearized, as explained earlier, from the non-linear flight equations from section 2.5.



Figure 2.12 An F-35B performing a vertical take-off and landing test (left) [45]; and a Mig-29 performing the *Pugachev's Cobra Manoeuvre* (right) [46]

In a LQR controller, the time-continuous linear system is described by [3][12][15][18][27][31]:

$$\begin{cases} \dot{x} = Ax + Bu \\ y = Cx + Du \end{cases}, \quad x \in \mathbb{R}^n \text{ and } u \in \mathbb{R}^m \quad (2.85)$$

The cost function is defined as:

$$J = \int_0^{+\infty} F(x, u) dt \quad (2.86)$$

With:

$$F(x, u) = x^T Q x + u^T R u \quad (2.87)$$

Where Q and R are the weighting matrices for, respectively, the state and control variables, and must be positive-definite in the following way:

- Matrix $Q \geq 0$, i.e. Q is a positive-semidefinite matrix: $\forall x: x^T Q x \geq 0$;
- Matrix $R > 0$, i.e. R is a positive-definite matrix: $\forall u: u^T R u > 0$.

As for longitudinal flight, A is the *Jacobian* matrix of F concerning the aircraft's state vector x and B the *Jacobian* matrix concerning the aircraft's control vector u obtained from linearization.

$$A = \begin{bmatrix} (\nabla_x f_V(x_0, u_0))^T \\ (\nabla_x f_\gamma(x_0, u_0))^T \\ (\nabla_x f_q(x_0, u_0))^T \\ (\nabla_x f_\theta(x_0, u_0))^T \end{bmatrix}; \quad B = \begin{bmatrix} (\nabla_u f_V(x_0, u_0))^T \\ (\nabla_u f_\gamma(x_0, u_0))^T \\ (\nabla_u f_q(x_0, u_0))^T \\ (\nabla_u f_\theta(x_0, u_0))^T \end{bmatrix} \quad (2.88)$$

$$x = [V \ \gamma \ q \ \theta]^T; \quad u = [\delta_e \ \delta_T]^T \quad (2.89)$$

Where u must be such that:

$$u: \longrightarrow u(x) \text{ minimizes } J(u) = \int_0^{+\infty} (x^T Q x + u^T R u) dt \quad (2.90)$$

The feedback control law that minimizes the cost equation in 2.86 is described by:

$$u = -Kx \quad (2.91)$$

Where $K \in \mathbb{R}^{m \times n}$ is the system's gain matrix determined by:

$$K = R^{-1} B^T P \quad (2.92)$$

This cost function (equation 2.86) is often defined as a sum of the deviations of key measurements from their desired values. In fact, this algorithm strives to find the proper controller settings that minimize the undesired deviations, like e.g. deviations from the desired attitude. However, the main problem while properly scaling a LQR controller, i.e. fine-tuning the controller for optimal performance, resides in finding the adequate weighting factor's Q and R matrices. In general LQR design, Q and R are simply determined by *Bryson's method* [3][31], where each state (Q matrix) and control (R matrix) parameter is calculated in relation to its maximum amplitude as diagonal elements of a diagonal matrix:

$$Q_{ii} = \frac{1}{x_{i,\max}^2} \quad R_{ii} = \frac{1}{u_{i,\max}^2} \quad (2.93)$$

Although this method being a good starting point for trial-and-error iterations on the search for the intended controller results, it is somehow limited by its maximum state values as, even though the control values are limited only by their control surface's maximum physical properties, they lack a more proper optimization algorithm.

However, is available since 1995 a better alternative method for the Q and R matrices estimation proposed by *Jia Luo* and *C. Edward Lan* [16]. The R matrix is still determined using Bryson's method [3][31] (equation 2.93), as the problem lies, as noted before, in the determination of the optimal state values of the Q matrix. In this method, the cost function J (equation 2.86) is minimized by a Hamiltonian matrix H, which is used to determine P.

Considering the Theorem whereby a symmetrical matrix has only real eigenvalues, it can be deduced that when $Q = Q^T, Q \geq 0$, all its eigenvalues are $\lambda_i(Q) \geq 0$ and, when $R = R^T, R > 0$, then all its eigenvalues are $\lambda_i(R) > 0$.

The R matrix is therefore a Penalization (or Ponderation) matrix of the control vector, which allows a certain flexibility upon its generation, and is therefore calculated by *Bryson's method* (equation 2.93). However the Q matrix must be such that its eigenvalues match the eigenvalues from a group I Hamiltonian matrix H. Accordingly to the principle of the *Pontriagin's Maximum*, the Hamiltonian matrix is associated to the LQR's "P Problem" in the following way:

$$P \left\{ \begin{array}{l} \dot{x} = Ax + Bu \\ J(u) = \int_0^{+\infty} (x^T Q x + u^T R u) dt \end{array} \right. \Rightarrow H = \begin{bmatrix} A & -BR^{-1}B^T \\ -Q & -A^T \end{bmatrix}, \quad H \in \mathbb{R}^{2n \times 2n}; A \in \mathbb{R}^{n \times n} \quad (2.94)$$

The Hamiltonian eigenvalues are:

- For Group I: $\lambda_1, \dots, \lambda_n$ with $\text{Re}(\lambda_i) < 0, i = 1, \dots, n$;
- For Group II: $\lambda_{n+1}, \dots, \lambda_{2n}$ with $\text{Re}(\lambda_k) > 0, k = n + 1, \dots, 2n$.

The eigenvalues of H are thereby symmetrically distributed in relation to the imaginary axis, thus having positive and negative symmetrical real parts only. And as the "P Problem" is part of the \hat{A} matrix of the LQR's feedback system described as follows:

$$\hat{A} = A - BR^{-1}B^TP \quad (2.95)$$

P is found by solving the continuous time algebraic *Riccati's* equation [3][16][31] in equation 2.96:

$$A^TP + PA - PBR^{-1}B^TP + Q = 0 \quad (2.96)$$

As the eigenvalues of \hat{A} are the same of those of the Group I of the Hamiltonian matrix H , they can be specified as:

$$\begin{cases} \lambda_1 = \mu_1 + i\omega_1; & \text{Re}(\lambda_1) = \mu_1 < 0 \\ & \vdots \\ \lambda_n = \mu_n + i\omega_n; & \text{Re}(\lambda_n) = \mu_n < 0 \end{cases}$$

Therefore, the state matrix Q must be determined such that:

$$\forall i: \det(\lambda_i I - H) = 0 \quad (2.97)$$

Where I is an Identity matrix.

Although this last equation (2.97) may be used to directly determine the Hamiltonian eigenvalues, choosing rather to directly calculate the Q matrix by assigning iteratively assumed values to the Hamiltonian eigenvalues that comply with such requirement (equation 2.97), which can improve optimization capabilities by allowing the fine-tuning of such eigenvalues. For simplified calculations it is enough to use the state matrix A 's eigenvalues, but in order to minimize the cost function J (2.86) under certain imposed flight qualities, and therefore, these eigenvalues must be subjected to such impositions. The Q matrix is thereby defined as a diagonal matrix composed by a single vector $q_i = [q_1 \ q_2 \ \dots \ q_n]^T$. Using the Group I Hamiltonian eigenvalues to satisfy the prior condition (equation 2.97), q_i must be such that:

$$\forall i: f_i(q_i) = \det(\lambda_i I - H(q_i)) = 0 \xrightarrow{\text{in order to minimize}} J(q) = \sum_{i=1}^n (f_i(q))^2, \text{Re}(\lambda_i) < 0 \quad (2.98)$$

As Q is positive-semidefinite, the “diagonal vector” is rather defined as $q_i = [q_1^2 \ q_2^2 \ \dots \ q_n^2]^T$ to prevent the case of any of the determined q_i values being negative, and therefore:

$$Q = \begin{bmatrix} q_1^2 & & & \\ & q_2^2 & & \\ & & \ddots & \\ & & & q_n^2 \end{bmatrix} \quad (2.99)$$

As the control law given by (2.86) forces the controller feedback system to stabilize around zero, i.e. it only stabilizes the aircraft around its default neutral levelled flight's stability (equilibrium point), a reformulation of the equation is needed. Therefore, to force a convergence (i.e. stabilization) to any given equilibrium state, the control points $(x_{\text{ref}}, u_{\text{ref}})$ that define such state must be included in the control law as [3]:

$$u = u_{\text{ref}} - K(x - x_{\text{ref}}) \quad (2.100)$$

This allows the LQR controller to fully stabilize an aircraft state and control variables for optimized R and Q weighting matrices.

2.7 Batz-Kleinman Controller

This method is in all identical to the LQR method, except by the gain matrix, now defined by the following L matrix [3][52]:

$$L = B^T(P(\tau))^{-1} \quad (2.101)$$

Where P is now defined by the *Gramian* as [3][52]:

$$P(\tau) = \int_0^\tau e^{-At} B B^T e^{-A^T t} dt \quad (2.102)$$

Where an always positive assumed variable τ appears to limit the integration interval for optimization purposes. The smaller the variable τ , the larger the control amplitude, and the faster the convergence for optimal values [52].

The control law is, therefore the same as that of the LQR but with the gain matrix L instead of the previous K one:

$$u = u_{ref} - L(x - x_{ref}) \quad (2.103)$$

It must be mentioned that although several other control methods are available. These ones are the most efficient ones, and therefore the most appropriated to use in this work.

2.8 Block Diagram of a Control System

The amount of energy required to operate an aeroplane (specially an unstable intended one (generally for improved manoeuvrability purposes)) is indeed one of main reasons that justifies the need for an optimal control system as it minimizes the energy loss in the stabilization process. Therefore it is crucial to understand the concept of a full system block diagram when designing a full state regulator that is later intended for actual physical implementation. The scheme is composed by the controller itself and all the systems and subsystems that influence the aircraft's attitude. That mainly includes pilot's direct inputs, control surfaces status, guidance systems (such as the GPS, INS or ILS) and atmospheric data. Such information is retrieved through several different types of sensors and avionics and transmitted to the flight controller that analyses it and takes proper action through several actuators and other control mechanisms. More complex systems may even integrate data related to the aircraft situational awareness provided by TCAS or radar, and in the case of military aircraft, also a variety of other data directly or indirectly related to e.g. weapon's employment, damage assessment, ACM and engagement tactics, TFTA or other complex inboard systems or technologies such as thrust vectoring. However, most aircraft's control systems are still based on the more elementary scheme of a general AFCS (Automatic Flight Control System) as depicted on Figure 2.13:

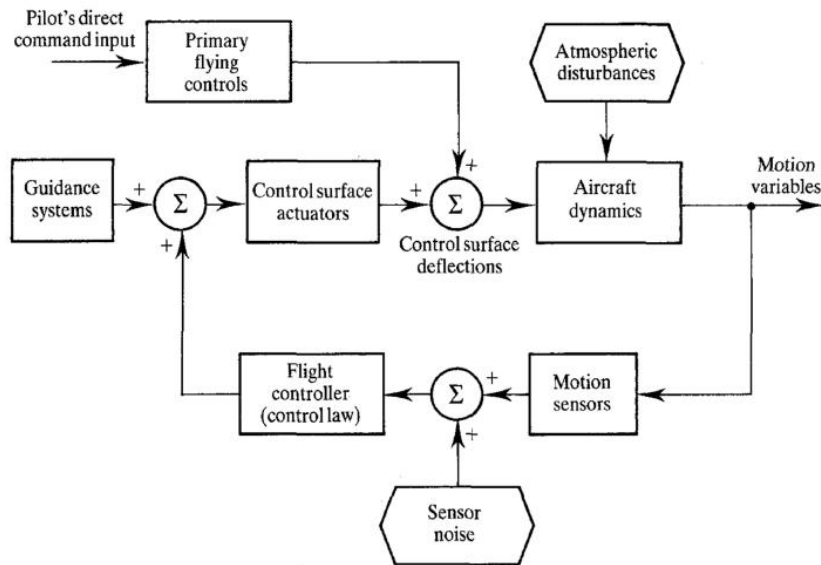


Figure 2.13 General block diagram of an AFCS [3][15].

Therefore, a Longitudinal Flight Controller may be perceived as a component of an AFCS, that generally is part of a larger system known as FMS (Flight Management System) and it is responsible for the monitoring and control of the aircraft's longitudinal speed and attitude (climb, dive, or levelled-flight attitudes) via elevators, throttle, flaps and airbrakes actuators and can be represented by the block diagram of Figure 2.14:

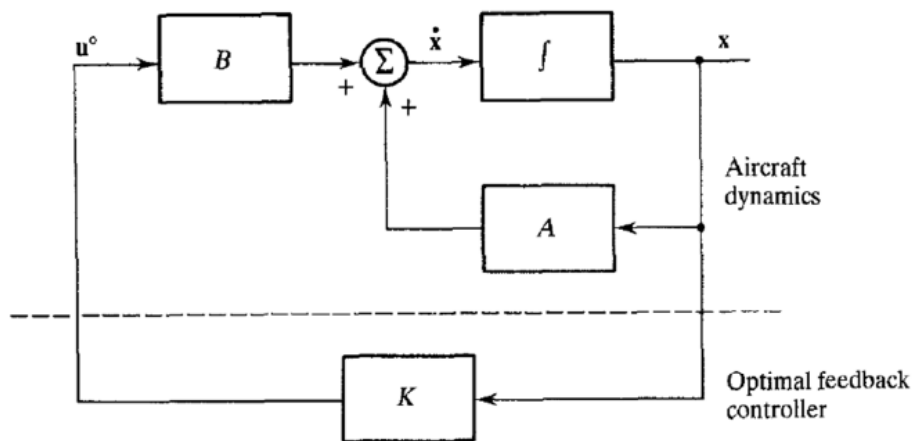


Figure 2.14 Closed loop state regulator with optimal feedback [3][15].

Figure 2.14 exemplifies how the control variables (u) obtained from the system linearization for a given equilibrium state are iterated to allow the stabilization of the state variables (x) by means of the control surface's actuators in a LQR controller. Blocks A , B and K represent respectively the state, control and gain matrices explained earlier in this Chapter. Whereas the integral block (f) represents the solution of the differential equation $\dot{x} = Ax + Bu$ achieved by using K in the LQR's control law. Analogously, Figure 2.14 would also represent a

Batz-Kleinman controller if the K block was replaced by an L block indicating the use of an L matrix instead of the K matrix in the control law.

A general schematic of the control surface's actuation by the controller is provided by Figure 2.15:

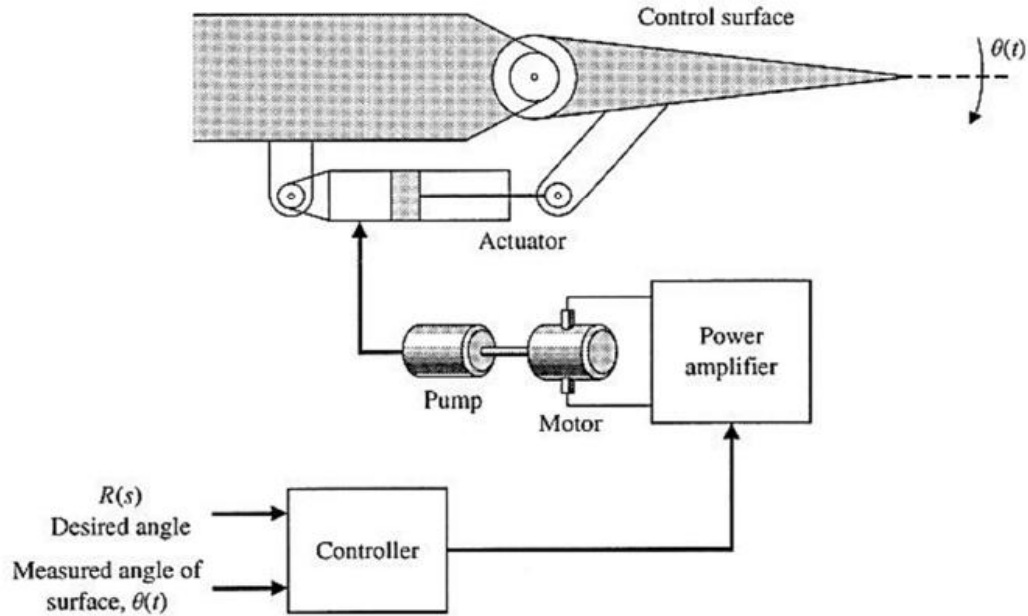


Figure 2.15 Actuator's control system scheme [3][49].

Next, Chapter 3 provides an overview over the global aspects of the UAV and the VSMW to which the controller design of this work is intended.

Blank Page

Chapter 3

VSMW (Variable-Span Morphing Wing)

This Chapter describes the fundamentals behind the aircraft and its VSMW system for which the controller is primarily designed. The aircraft is a UAV prototype designated as *Olharapo* and is described in the following sections.

3.1 UAV *Olharapo*

The *Olharapo*'s Project dates back to 2001 [23][24] when Professor *Pedro Gamboa* from UBI-DCA suggested to his students at the course of Aircraft's Design and Project I to develop a new UAV. Since then the project has received several core modifications and upgrades, resulting on several prototypes of the aircraft. Intended as an observation aircraft, the current prototype now mainly serves as a practical modular multi-systems integration and testing platform for several of the recently developed work from Master's Degree students in aeronautical engineering at the university in their respective theses. The actual handwork of each prototype is usually done entirely by students of the course of Aircraft's Design and Project II under the supervision of the same professor.



Figure 3.1 *Olharapo* light UAV prototype featuring its standard wing configuration [48].

3.2 *Olharapo's* Dissymmetrical Telescopic Wing

The VSMW (Variable-Span Morphing Wing) is the direct result of the stated capacity of the UAV *Olharapo* to serve as a multi-systems integration and testing platform. Initially developed by Master's student *J. Mestrinho* and then perfected by *J. Felício* at their respective Master's Theses, VSMW consists of a totally new modular telescopic wing for that UAV that uses dissymmetrical wingspan variation for the role of conventional aircraft's control surfaces such as the ailerons and flaps, and taking the concept of flapprons to an all new level. Although not totally new in concept, the OLHARPO's VSMW is actually one of the very firsts that takes it into reality at such reduced scale. The wing itself is easily interchangeable with the primary *Olharapo's* native wing and consists of two inner-fixed wings (IFWs) connected by two carbon fiber spars and the servo-actuators compartment at (see Figure 3.2) the centre and two outer-moving wings (OMWs). The two OMWs slide inside each of the respective IFW by means of two independent servo-actuators that operate the two, also independent, aluminium racks connected to each of the OMWs as shown in Figure 3.3.

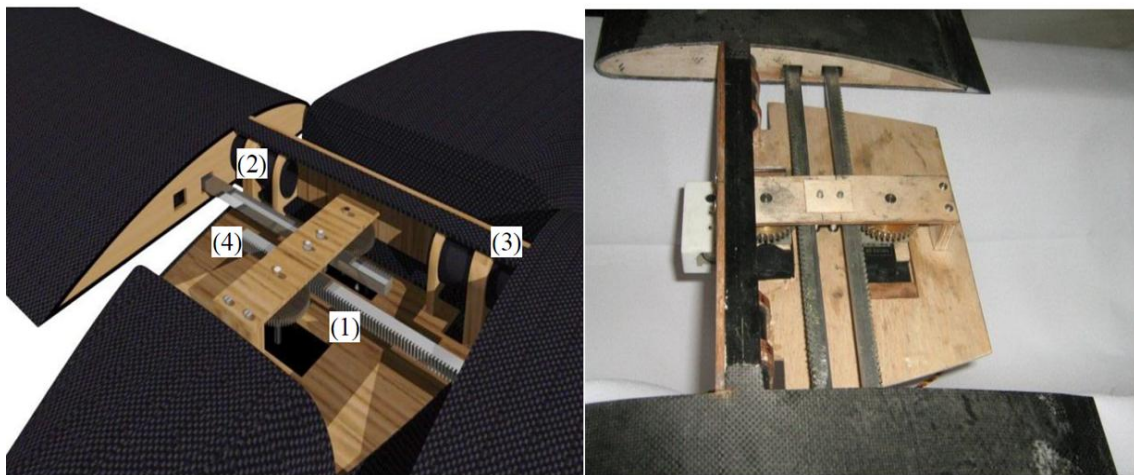


Figure 3.2 CAD Drawing (left) and the actual actuation system (right) with: 1- Support Board; 2- Board Linkage; 3- Wing to Fuselage Connection; and 4- Upper Board [26].

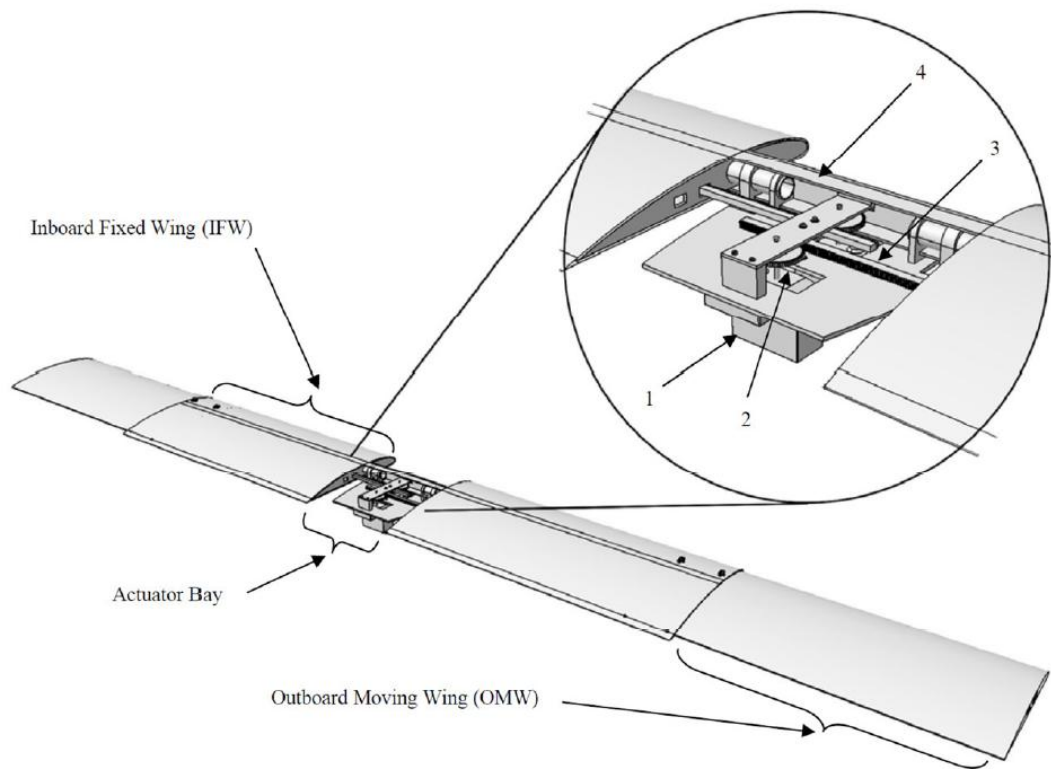


Figure 3.3 VSMW mechanical system (1- servo-motor; 2- transmission pinion; 3- transmission rack; 4- carbon spar) [3][48].

The actual UAV prototype was built in 2010 by students of the Aeronautics Engineering course at the Portuguese University of Beira Interior. The team assigned to the VSMW was composed by *J. Felicio*, *P. Santos* and *T. Sanches* under the supervision of the Professor *P. Gamboa*. The overall aspect of the UAV equipped with the telescopic wing can be observed in Figure 3.4.



Figure 3.4 *Olharapo* UAV prototype equipped with the VSMW: (a) fully retracted wing; and (b) fully extended wing [48].

3.3 UAV Specifications

In 2011, a study by *Gamboa et al* [25] demonstrated the relationship between the VSMW's wingspan and the UAV's airspeed and its resulting drag reduction relatively to the standard wing. The results of that study are presented in Figure 3.5.

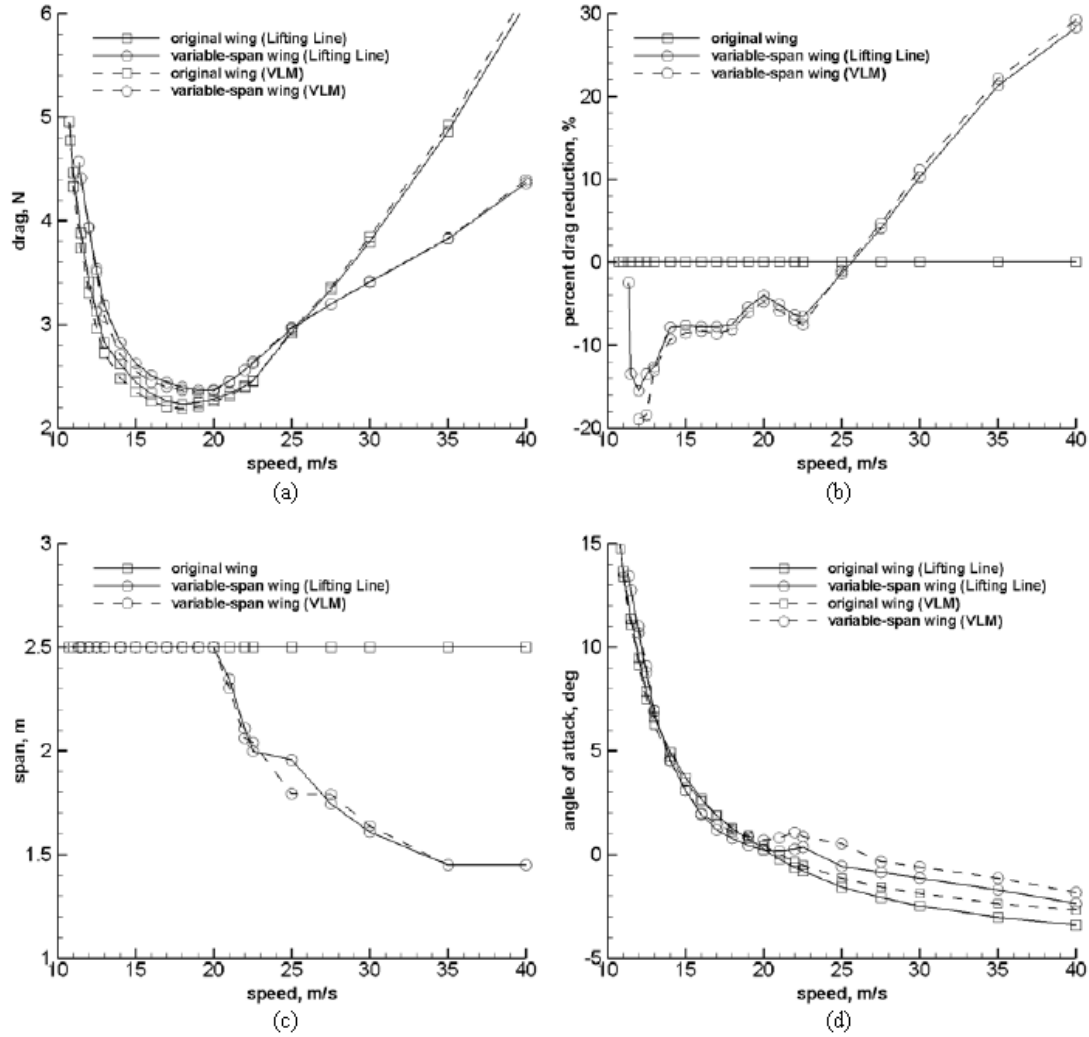


Figure 3.5 (a) Drag variation with flight speed; (b) Drag reduction with the VSMW relative to the original standard wing; (c) Wingspan variation with flight speed; (d) Angle of Attack variation with flight speed [25].

The most important information to extract from this study is, that for the purpose of extracting the maximum efficiency of the VSMW, the wingspan (b) must be maximal to speeds (V) lower than 20 m/s and minimal to speeds above 35 m/s, varying almost linearly between this two critical flight speed values. Whereas for the angle of attack (α), it must vary, for speeds above 10 m/s, in a non-linear way that can be approximated by the equation 3.1:

$$(3.1)$$

$$\alpha(V) = \frac{2}{(V - V_{\min})/\alpha_{\max}} + \alpha_{\min}$$

Which, in order to match the values of the graphic (d) of Figure 2.6 becomes:

$$\alpha(V) = \frac{2}{(V - 11)/15} - 3,5 \quad (3.2)$$

The angle of attack (α) assumes therefore, a maximum amplitude (α_{\max}) of 15 degrees at minimum flight speed (V_{\min}) and then decreases according to equation 3.2 until it stabilizes at approximately 3.5 negative degrees (α_{\min}) for flight speeds above 40 m/s.

The equation that gives an approximate output for the variation of the wingspan (b) in between the two critical flight speeds is given by equation 3.3.

$$b(V) = -\frac{(V - V_m)}{\zeta} + b_{\max} \quad (3.3)$$

Where V_m is the critical flight speed value below which, the wingspan must be maximal so that the aircraft doesn't go into a stall. b_{\max} represents the maximum wingspan, and the Greek letter koppa (ζ) represents the value that approximates the function to the desired values. The function then becomes as in equation 3.4.

$$b(V) = -\frac{(V - 20)}{14.2858} + 2.5 \quad (3.4)$$

Both equations 3.2 and 3.4 were achieved by trial and error, but both give good approximations of the intended values.

In order to proceed with the program script, several data about the *Olharapo's* specifications and its control and stability derivatives were compiled for use in the program and are specified in Tables 3.1 to 3.5 (Also present in Annex B).

Module	Parameter	Value	Units
Weight	Empty Weight	3.7000*	[kg]
	Max. Take-Off Weight	6.7000	[kg]
Engine	Maximum Thrust	25.000*	[N]

Table 3.1 Engine and weight specifications [3]. *Assumed value.

Module	Parameter	Value	Units
Inertial Properties	lxx	0.6175	[kg.m ²]
	lyy	0.3410	[kg.m ²]
	lzz	0.9345	[kg.m ²]
	lxy	0.0000	[kg.m ²]
	lxz	0.0391	[kg.m ²]

Table 3.2 Inertial properties specifications.

Module	Parameter	Value	Units
VSMW Geometry	Fuselage Span (at wings intersection section)	0.2000	[m]
	IFW span	0.6250	[m]
	OMW span	0.6250	[m]
	IFW-OMW overlap span	0.1000	[m]
	Max. VSMW wingspan	2.5000	[m]
	Min. VSMW wingspan	1.4500	[m]
	IFW chord	0.2830	[m]
	OMW chord	0.2500	[m]
	VSMW mean chord	0.2665	[m]
	Max. VSMW Area	0.6663	[m ²]
	Min. VSMW Area	0.3864	[m ²]

Table 3.3 Telescopic wing (VSMW) specifications [14][26].

As mentioned in Chapter 2, the control and stability derivatives were obtained by third parties using the software XFLR5[®] at first, and afterwards utilizing extensive calculations with the use of MATLAB[®] software. With incomplete data originated from different sources it was necessary to filter all data and chose the best values by direct comparison, filling in the blanks of the most reliable source with data from other sources. The filtration method was applied to all data, including the lateral-directional derivatives, but for the purpose of this work, only the longitudinal data is presented in Tables 3.4 and 3.5.

Longitudinal Stability Derivatives			
Sub-Module	Parameter	Value	Units
Zero Angle of Attack	C_{L_0}	0.110	rad^{-1}
	C_{D_0}	0.089	rad^{-1}
	C_{m_0}	0.060	rad^{-1}
Aerodynamic Coefficients	C_L	0.610	N
	C_D	0.259	N
Given an Angle of Attack	C_{L_α}	4.580	rad^{-1}
	C_{D_α}	0.173	rad^{-1}
	C_{m_α}	-2.540	rad^{-1}
Given a Pitch Rate	C_{L_q}	4.888	rad^{-1}
	C_{D_q}	0.000	rad^{-1}
	C_{m_q}	-7.995	rad^{-1}
Given an Angle of Attack due to Pitch Rate	$C_{L_{\dot{\alpha}}}$	0.000	rad^{-1}
	$C_{D_{\dot{\alpha}}}$	0.000	rad^{-1}
	$C_{m_{\dot{\alpha}}}$	0.000	rad^{-1}

Table 3.4 Longitudinal stability derivatives specifications for the UAV *Olharapo*.

Because the aeroplane is intended for subsonic flight, some of the stability derivatives ($C_{L_{\dot{\alpha}}}$, $C_{D_{\dot{\alpha}}}$, $C_{m_{\dot{\alpha}}}$ and C_{D_q}) can be considered null [3][8][13]. Besides, in the particular case of $C_{m_{\dot{\alpha}}}$, it can be almost always considered null, particularly for levelled flight, since the wing's contribution for the pitch moment coefficient in such flight condition is negligible.

Longitudinal Control Derivatives			
Module	Parameter	Value	Units
V-Tail Elevator	$C_{L_{\delta V_e}}$	0.127	rad^{-1}
	$C_{D_{\delta V_e}}$	0.036	rad^{-1}
	$C_{m_{\delta V_e}}$	-1.884	rad^{-1}

Table 3.5 Longitudinal control derivatives specifications for the UAV *Olharapo*.

Because the UAV *Olharapo* is equipped with a V-Tail rather than a standard T-Tail, its control surfaces have the dual purpose of serving as both elevators and rudders. This makes it necessary to account for the disposition angle of the tail's stabilizers relatively to the horizontal plane in order to calculate the (δ_{V_e}) V-Tail Elevator's Derivatives. However, as mentioned in Chapter 1, the XFLR5[®] software can easily deliver fairly accurate initial data for an aircraft's control and stability derivatives, even for less common geometries. These control surfaces have an actuation's amplitude of sixty degrees, i.e. they can deflect to a maximum value of thirty degrees in each positive or negative direction.

From Table 3.3 it's possible to see that each wing can extend outwards by a maximum of 0.525 meters, which means the total variation of wingspan, when wings are deflected symmetrically, can be up to 1.05 meters, almost doubling the aircraft's wingspan from 1.45 to 2.50 meters.

Although this work focuses in the longitudinal flight dynamics evaluation for control and stabilization purposes, it is also important to take into account some particularities regarding the lateral-directional proprieties of such complex span-variation system. While for symmetrical extension/retraction of the OMWs the variable representing such deflection can be simply given by b (overall wingspan), where a positive deflection of b (δ_b) corresponds to an increase in its value (i.e. it corresponds to an increase in wingspan), and a negative δ_b corresponds to a decrease in the overall wingspan. For dissymmetrical variations of the wingspan, a new variable was created to reflect such parameter, designated Dissymmetric Wing Variation or just Wing Deflection (δ_y). This new parameter represents the dissymmetrical deflection of the OMWs acting as ailerons up to a maximum of 0.525 meters, meaning that for a $\delta_y = -0.525$ m, the left OMW is fully extended while the right OMW is fully retracted for maximum left roll rate attitude. The concept of this new parameter can be better understood by observing Figure 3.6.

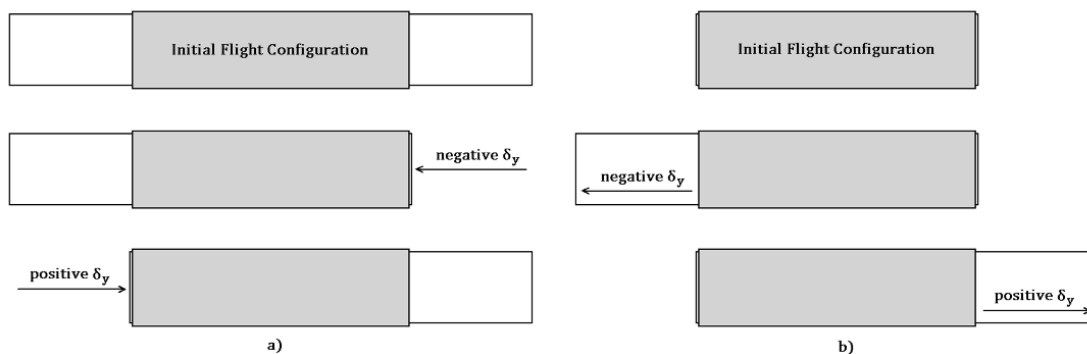
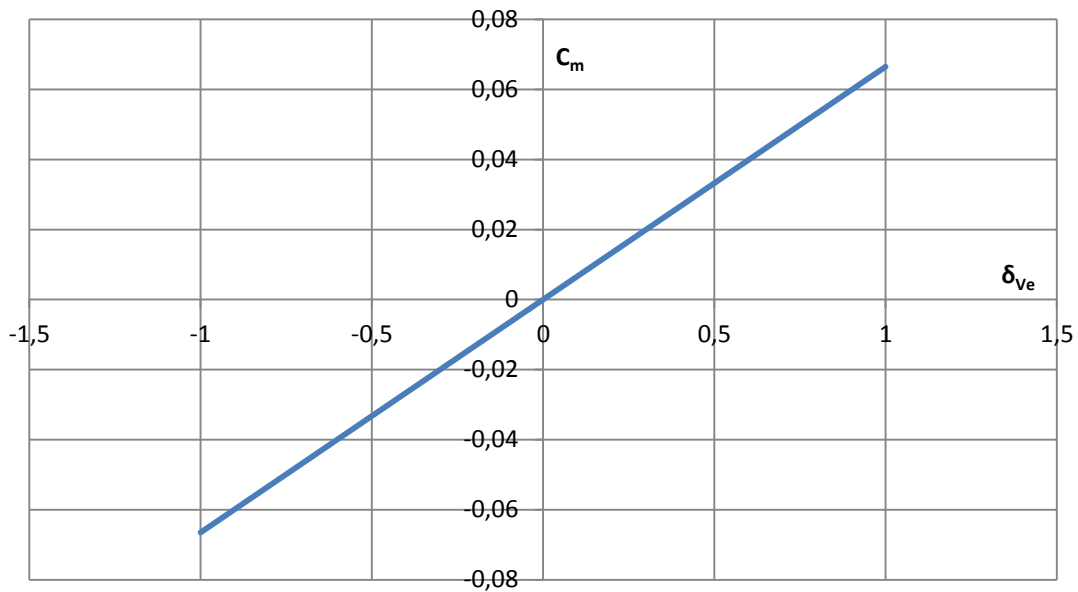


Figure 3.6 Dissymmetrical Wing Variation (δ_y). A positive deflection of the wing corresponds to a relocation of the aerodynamic centre of pressure to the right by δ_y meters leading to a left roll attitude [3].

The specificities of such system and the equations that correlate them can be found in detail through several works, books and publications, and they must be taken into account in order to observe the longitudinal behaviour of the aircraft during a dissymmetrical deflection of the wing or while suffering lateral-directional disturbances or performing a roll or turn manoeuvre [3][14][22][25][26][48].

From the data provided by XFLR[®], it was possible to foresee some of the aircraft flight characteristics prior to simulation itself.

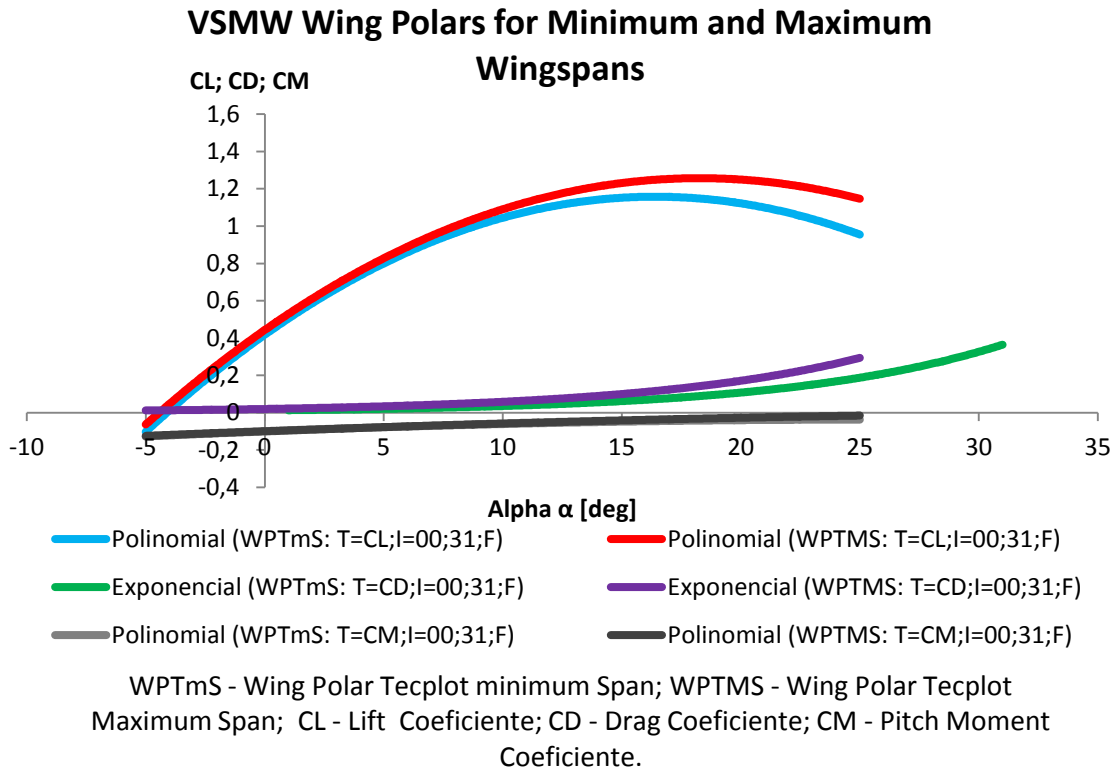


Graphic 3.1 Expected Pitch Moment Coefficient (C_m [rad⁻¹]) distribution due to elevator deflection (δ_{ve} [%]) percentage.

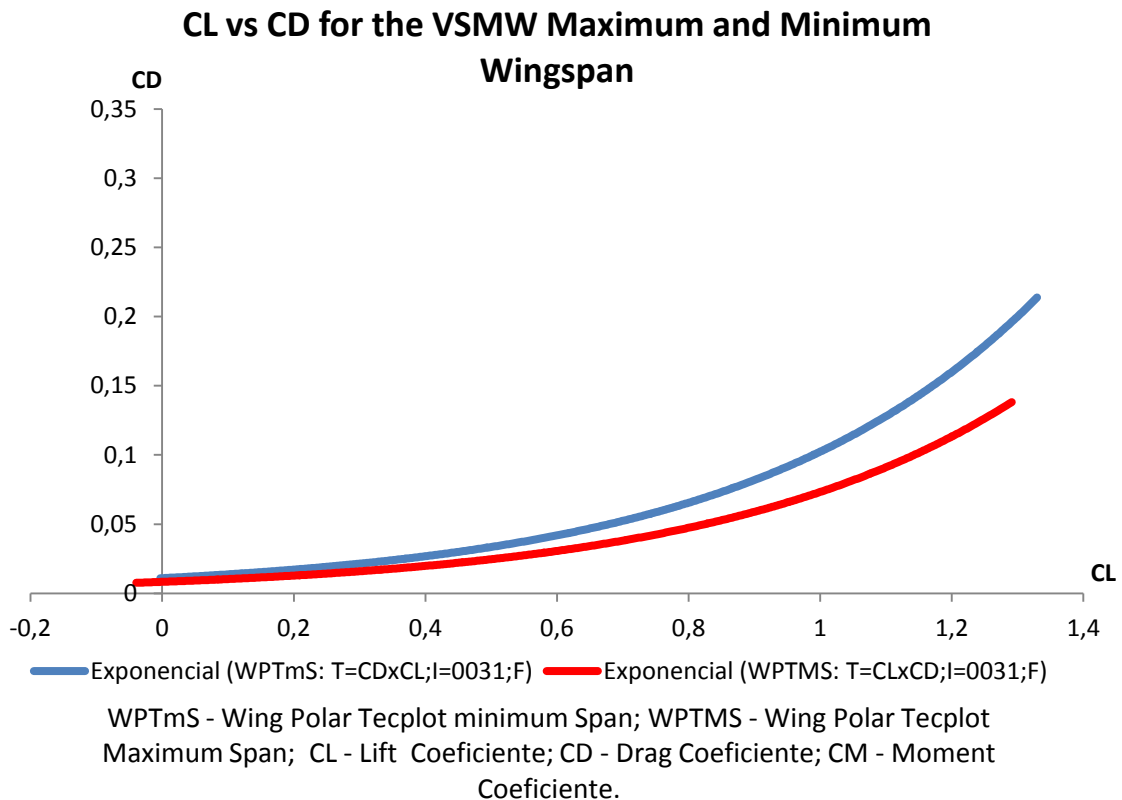
Graphic 3.1 shows how the Pitch Moment Coefficient is expected to behave while the UAV's V-Tail Elevator is deflected. Therefore, it's expected that the aircraft reaches a maximum C_m of 0.068 when a maximum deflection of the elevator (15 degrees) is achieved.

Graphic 3.2 represents the expected wing polars at both maximum and minimum wingspan and associated effects on drag reduction and increased lift for the lift, drag and pitch moment coefficients (C_L , C_D and C_m respectively), for an airspeed of 20 m/s at sea level. One interesting conclusion is that the aircraft can increase its lift in order to climb by extending its wings without the necessity of an increase in pitch or power. Such capability is even more evident at angles of attack (α) higher than 10 degrees.

Graphic 3.3 offers a different perspective on the drag reduction ratio due to wingspan decrease with the VSMW.



Graphic 3.2 Wing Polars tecplot for maximum and minimum wingspan of the telescopic wing.



Graphic 3.3 Effective drag reduction from maximum wingspan to fully retracted OMWs.

Blank Page

Blank Page

Chapter 4

Simulation and Tests

The actual M-File, or MATLAB® file, that allows for the longitudinal stabilization and control of the *Olharapo* UAV uses robust algorithms in interaction with each other following the basic principles of flight dynamics and stabilization presented in Chapter 2. The program is scripted in a very structured and modular way so it can be easier to understand, operate and edit, without prejudice of the performance of the controller. As an additional, self-imposed goal, such modular structure allows the program to be utilized with any different configuration of the UAV or even for a totally different aircraft by means of minor editing of the existent modules and/or by the addition of new ones. Therefore, it also allows for an easier integration of new modules in order to become a full autopilot system. The program does not only serve as an actual controller for the aircraft, as it has indeed the ability to simulate the aircraft response to given disturbances defined by the user. In fact, for the purpose of this work, such simulation capability was essential to validate the controller system since the UAV's prototype is not yet in test-flights phase and it would be advisable, if not even required, to have some degree of knowledge about the predicted flight behaviour of the aircraft using such stabilization method prior to actual flight.

Therefore, the program uses for the simulation purpose, an integrated mathematical atmosphere model and a simulated disturbances module in conjunction with flight dynamics, linearization and control modules necessary to control the aircraft in accordance with the handling qualities required for the different flight phases.

4.1 Imposed Flight Qualities

The theory behind flying qualities has already been described in Chapter 2, Section 2.4. These values are applied in the controller method using the theory developed by *Jia Luo* and *C. Edward Lan*, also resumed in Chapter 2. The values are thereby inputted in the λ vector used for the Q matrix estimation. When using the eigenvalues given by the characteristic equation of the state matrix A, the controller stabilizes the aircraft attitude after a short time as long as it remains dynamically stable and controllable. Therefore the controller is unable to correctly provide augmented stability in certain unstable flight modes (such as e.g. a flat spin) and may even worsen the situation in its attempts to re-establish a stable flight for an inherent unstable flight mode to which it was not designed. It does however have some degree of authority over some less critical unstable flight modes, and could e.g. allow a stall

recovery under certain conditions. Although no controller optimization had been performed for such flight modes, and its utilization in such situations is thus not recommended. However, it was possible to optimize the controller for more common flight modes, such as levelled cruise flight and landing, by inverting the determination of the flying qualities into predetermined data, which easily allowed the finding of the corresponding optimal values to be applied in λ vector. i.e. by imposing the flight qualities of Level 1, Class I, Cat. B for cruise flight and Level 1, Class I, Cat. C for Take-off and Landing (see Annex C – Handling Qualities Data for detailed information) it was possible to optimize the values of the λ vector and thus the controller itself for these flight modes. This predetermined data can be found through various books [13][15][31] and is presently annexed to this work. The optimization is then accomplished by solving the frequency and damping equations in order to both the real and imaginary parts of each value.

The values for each of the three categories of a Level 1, Class I aeroplane are summarized in table 4.1:

Longitudinal Motion Theory values for a Level 1, Class I Aeroplane				
Motion Theory		ω_n	ξ	T_2
Cat. A	SP	0.4 to 0.6	0.5 to 0.9	—
	LP	—	> 0.04	< 55 s
Cat. B	SP	0.4 to 0.6	0.5 to 0.9	—
	LP	—	> 0.04	< 55 s
Cat. C	SP	0.4 to 0.6	0.5 to 0.9	—
	LP	—	> 0.04	< 55 s

Table 4.1 Values for the Short-Period (SP) and Long-Period (LP) Motion Theories for all the three Categories of a Level 1, Class I Aeroplane [15][32].

The Short-Period oscillation parameter limits were obtained from Figure 4.1. As it can be observed, the best controllability and responsiveness is obtained inside the *Satisfactory* area of the graphic. By imposing oscillation values within this area it is possible to obtain handling parameters that can be equally applied to any of the categories of flight of a Level 1, Class I UAV (Table 4.1) such as the *Olharapo*.

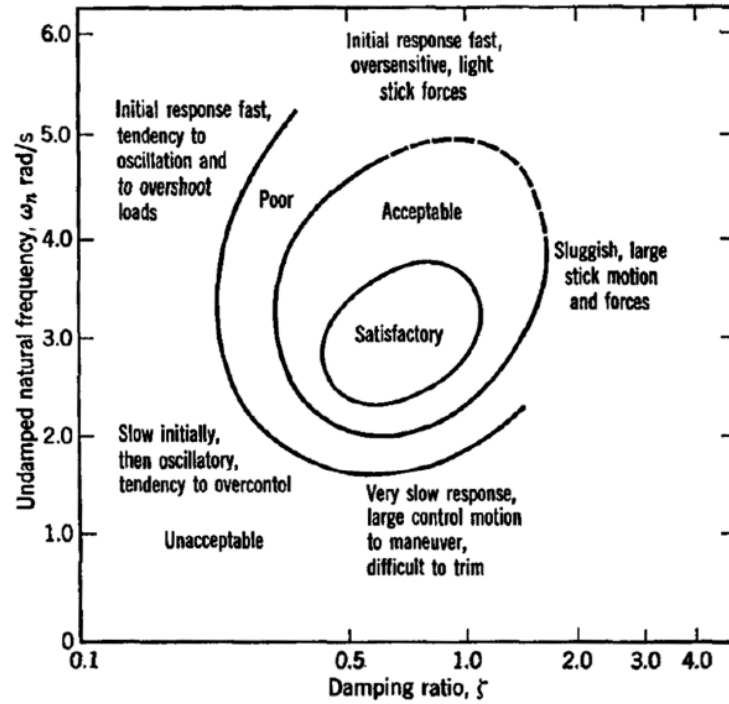


Figure 4.1 Short-Period parameters definition based on pilot opinions.

The values for the Long-Period mode were obtained from the equations 2.51 to 2.52 mentioned in Chapter 2, Section 2.4, solved in order to the real and imaginary parts using the data from Table 4.1. Therefore, the Long-Period respective eigenvalue takes the complex form of the equation 4.1:

$$\lambda_{LP} = a \pm bi = -\xi\omega_n \pm \omega_n\sqrt{1 - \xi^2} \quad (4.1)$$

Replacing the variables with values from Table 4.1, it is possible to obtain the optimal values for a Level 1, Class I UAV in any flight category. The imposition of these eigenvalues to the controller allows the optimization of the Q matrix, resulting in an optimal longitudinal controller for any flight phase. The values used in the controller are presented in table 4.2:

Longitudinal Motion Theory values for a Level 1, Class I Aeroplane			
Motion Theory	ω_n	ξ	T_2
Short-Period	3	0.75	—
Long-Period	—	0.40	10 s

Table 4.2 Chosen values for eigenvalue calculation.

The eigenvalues vector (or eigenvector) composed by these calculated values is then given by:

$$\lambda = [\lambda_{SP} \ \lambda_{LP}] = [-2.25 \pm 19843i \quad -0.0693 \pm 0.1588i] \quad (4.2)$$

Three simulation types were then performed to completely prove the working concept and reliability of this Longitudinal Controller System.

4.2 Classical Control Method (Disturbances Response)

When designing a controller or stabilization system for a specified vehicle, there are, as for a general damping system (i.e. damper, spring and mass), two main approaches possible: frequency domain and time domain [3]. The first consists of integrated open and closed-loop systems, where the open-loop design allows independent control variables (i.e. input variables do not depend on previous output results), whereas in the closed-loop design, the input variables receive feedback from output, increasing the accuracy of the controller response [3][13]. The design of such frequency domain controller is based in transfer functions (*Laplace* transforms) for each control component, and the root locus technique for finding the best roots of the characteristic equation (eigenvalues), which tends to be a trial-and-error method involving great amount of calculations in the process, making this design really tricky and complex for large control systems implementation [3].

The time domain method, on the other hand, offers a much easier concept where the control variables are described by first-order differential equations easily solved with computational software like the MATLAB® and applied to the controller using the most efficient and up-to-date controller methods available on modern control theory of LQR and *Batz-Kleinman* as described in Chapter 2 [3].

The most classic method of analyzing a controller design is by simulating the state variable response of the trimmed aircraft to an atmospheric disturbance [3]. Therefore, the code script for the digital longitudinal controller follows the diagram scheme of Figure 4.2.

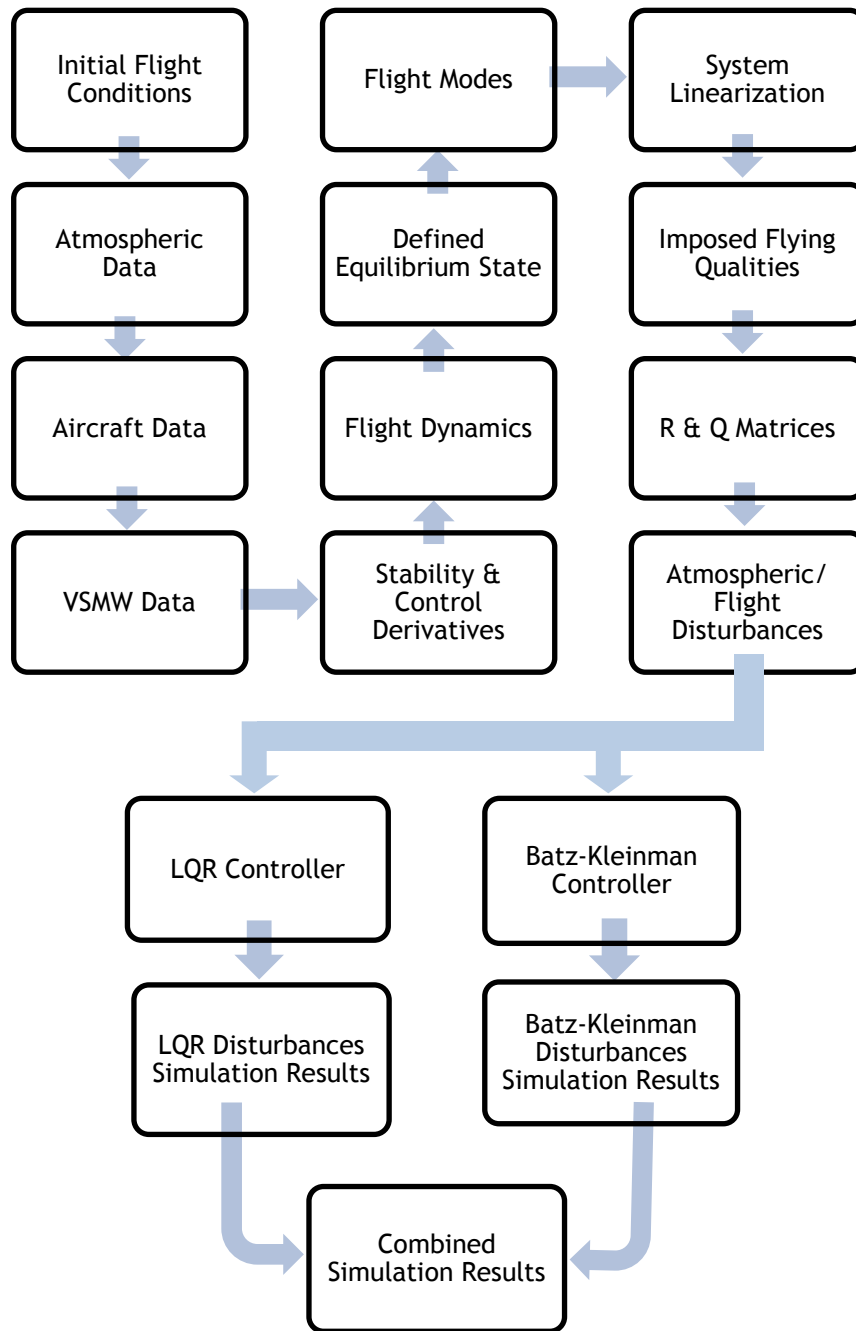


Figure 4.2 Diagram of the general path scheme of the simulation code. Each block represents a program module that can be edited or (in some cases) deactivated for different requirements or aircraft compatibility.

The disturbance suffered by the aeroplane can be defined as a uniform fractional divergence from the pre-established variables for equilibrium state vector $x = [u \ w \ q \ \theta]^T$, obtained by linearization of the flight equation systems (refer to Chapter 1) using the *Taylor's* equation [3][31]. In the simulation however, the atmospheric disturbances are inputted values defined

by the user and imposed to the controller by means of a new vector designated x_1 or disturbances vector.

In fact, two symmetrical disturbances vectors (x_1 and x_2) were created to provide enough prove of work to each controller module.

$$x_1 = \begin{bmatrix} +2 \\ -2 \\ -0.03 \\ -0.03 \end{bmatrix} \text{ and } x_2 = \begin{bmatrix} -2 \\ +2 \\ +0.03 \\ +0.03 \end{bmatrix} \quad (4.3)$$

Therefore, when applying Disturbances Case 1 (x_1 disturbances vector), the UAV is deviated from its equilibrium state, by suffering an increase in forward longitudinal airspeed of 2 m/s, as well as an increase of 2 m/s in vertical speed (the vertical axis w points in direction to Earth as opposed to what happens with the more easily perceived concept of an altitude axis pointing in the opposite direction. Refer to Chapter 2), a decrease of 0.03 rad/s on pitch rate (meaning the nose is pitching up by the same reason of w being positive when pointing down to Earth) and the same reduction in pitch angle. That results in a new after-disturbances state vector (x_i) that the controller will have to return to the original equilibrium state values of vector x by applying the appropriate controls in control surfaces and throttle. In this case, a given vector x , e.g. $x = [30 \ 1 \ -0.2 \ 0.2]^T$ would become, after suffering the disturbances of case 1, $x_i = x + x_1 = [32 \ -1 \ -0.23 \ 0.17]^T$. The equilibrium state and control vectors are calculated to each flight mode specific simulation prior to any disturbances by solving $f(x_{eq}, u_{eq}) = f(x_0, u_0) = 0$.

Note that the x vector replaces the theoretical variables of V , γ and α by the longitudinal and vertical components of the velocity vector (V) and the pitch rate (q). That happens because, as seen in the previous Chapters, the angle of attack (α) depends directly of longitudinal velocity of the aircraft, while the path angle (γ) is, by definition dependent of both α and θ angles. For that reason this two variables are the direct result of longitudinal velocity (u), pitch angle (θ) and pitch rate (q) and are therefore calculated separately (i.e. the LQR or *Batz-Kleinman* controller do not act directly over that two variables, rather controlling them indirectly through the declared x vector variables). Besides there was the necessity to split the velocity in its three components in order to have direct control over the two main longitudinal parameters: longitudinal and vertical velocities. In fact, for better analyze the longitudinal behaviour of the aircraft in the case of wings dissymmetry it was necessary to implement all the lateral-directional theory described in the previous work for the roll motion control [3] and the actual equilibrium state and control vectors used for this longitudinal controller simulation are the same as those used in that work ($X = [u \ w \ q \ \theta \ v \ p \ r \ \phi]^T$ and $U = [\delta_{V_e} \ \delta_T \ \delta_y \ \delta_{V_r}]^T$). However, for all the other longitudinal flight modes those lateral-directional variables are null and therefore, they not need to be represented in those modes.

The 3D velocity vector can be decomposed in its unidimensional components by using this simple formula:

$$V = \sqrt{u^2 + v^2 + w^2} \quad (4.4)$$

The program features 7 main flight modes in which the controller is able to stabilize the aircraft in the intended equilibrium state given any of disturbances cases described by either vector x_1 or x_2 . These flight modes are described in Table 4.3.

Flight Mode	Description
Altitude Hold Mode	This is the main flight mode of the aircraft and allows the aircraft to maintain levelled flight at the desired barometric (or GPS) altitude and at any desired airspeed.
Pitch Hold Mode	This mode is mainly intended for use in final approach in integration with the Landing mode allowing the aircraft to descend in a nose up attitude to allow touch down on the main landing gear. Or to quickly change to a climb by applying full throttle in the case of miss approach or go-around on short runways.
Climb or Descent/Dive Mode	This mode allows a stable climb or dive by defining either the desired climb/descent rate or the pitch angle (using the pitch hold mode). The descent differs from diving by using the pitch hold mode to keep the aircraft in a nose up attitude.
Landing Mode	Landing mode establishes a standard descent rate for the UAV to follow during the approach and then automatically flares the aircraft to allow a smooth touchdown in the main landing gear. Alternatively, it can use the pitch hold mode to keep the aircraft in a nose up attitude during the entire final approach to a short runway.
Take-Off Mode	This mode simply imposes full throttle until the aircraft reaches take-off speed and then establishes a standard climb attitude.
TFTA	This mode enables the aircraft to use a radar altimeter to set an AGL altitude at which the UAV must follow the terrain changes keeping the desired radar altitude.

Dissymmetrical Wings Mode	This mode attempts to stabilize the aircraft at a given altitude and path while suffering a dissymmetric wing displacement. It is essentially an experimental simulation mode not intended for use in the actual aircraft.
---------------------------	--

Table 4.3 Flight modes supported by the controller.

The program also features two safety modes that are imposed over the mentioned flying modes and are described in Table 4.4.

Flight Safety Modes	Description
Minimum Altitude Safety	When not in Landing or Take-Off Mode, this safety procedure is activated whenever the altitude drops below a preset value and takes proper action to return the aircraft to a safe altitude.
Automatic Stall Recovery	This safety procedure automatically detects a stall and takes proper action to recover from it by adding full power to the UAV on nose down attitude of 45°, after recovery, the system will engage climb mode until reaching an altitude preset and then switch to Hold Altitude Mode. However this procedure will not work if the UAV enters a spin and it may be impossible to the system to automatically recover from stall if the altitude drops below the minimum safety value.

Table 4.4 Flight Safety Modes supported in the controller.

The simulation results are presented in the next section of this Chapter (Chapter 4, Section 4.3).

4.3 Simulations Results

An example of the full raw data output from MATLAB® is available for consult in Annex B. However, due to the long extension of data provided in each simulation, the results presented in this Section (Chapter 4, Section 4.3) are reduced to only the most essential data and graphs required to demonstrate and prove the controller capabilities and efficiency. By the same reason, only one example for each of the modules is presented. Therefore, although several simulations have been undertaken for each individual module including both cases of disturbances presented before, the actual results presented for each module consists of one single simulation related to only one of the disturbance's cases.

4.3.1 Altitude Hold Mode

For altitude stabilization at 60m ASL levelled flight of the UAV *Olharapo* when fully loaded and at an airspeed of 25m/s, the controller response to a simulated disturbance is as follows:

Normal Simulation

Disturbances Case 2

Altitude Hold Mode Selected

Automatic Symmetrical Wingspan Variation with Flight Speed Mode Activated

b = 2.1500 (VSMW overall wingspan)

Longitudinal Stability Achieved

$$X = \begin{bmatrix} 25.000 \\ 0.0000 \\ 0.0000 \\ 0.0416 \end{bmatrix} \text{ and } U = \begin{bmatrix} -0.0242 \\ 0.8676 \end{bmatrix}$$

The System is Longitudinally Controllable

The System is Longitudinally Observable

Handling Qualities: Cruise Mode Selected (Level 1, Class I, Category B)

$$\lambda = \begin{bmatrix} -2.2500 \pm 1.9843i \\ -0.0693 \pm 0.1588i \end{bmatrix}$$

$$X_i = \begin{bmatrix} 23.0000 \\ 2.0000 \\ 0.0300 \\ 0.0716 \end{bmatrix}$$

$$\text{ATTITUDE} = \begin{bmatrix} \text{Velocity [m/s]} \\ \text{Altitude [m]} \\ \text{Pitch Angle [deg]} \\ \text{Wingspan [m]} \\ \text{Bank Angle [deg]} \\ \text{Vertical Speed [m/s]} \\ \text{Latral Speed [m/s]} \\ \text{Angle of Attack [deg]} \\ \text{Trajectory Angle [deg]} \\ \text{Pitch Rate [rad/s]} \end{bmatrix} = \begin{bmatrix} V \\ h \\ \theta \\ b \\ \phi \\ w \\ v \\ \alpha \\ \gamma \\ q \end{bmatrix} = \begin{bmatrix} 25.0000 \\ 60.0000 \\ 2.3809 \\ 2.1500 \\ 0.0000 \\ 0.0000 \\ 0.0000 \\ 5.6429 \\ -3.2620 \\ 0.0000 \end{bmatrix}$$

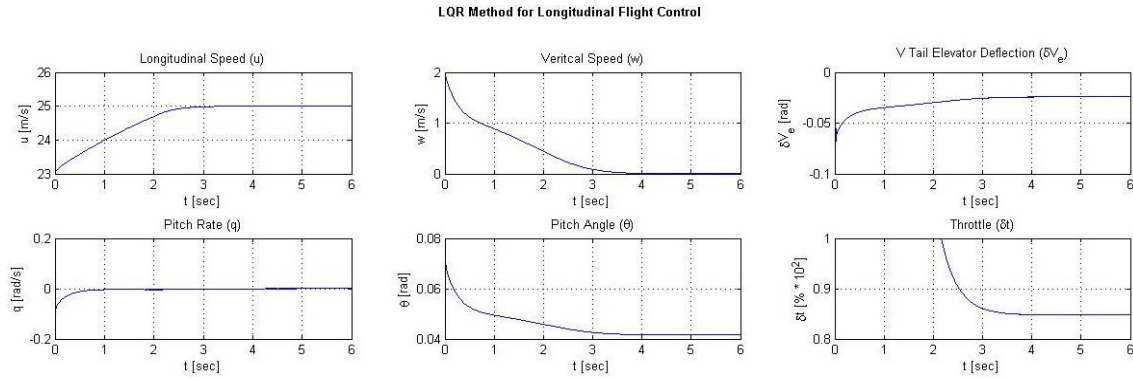


Figure 4.3 Classic disturbance simulation response with LQR for disturbances case 2 (x_2).

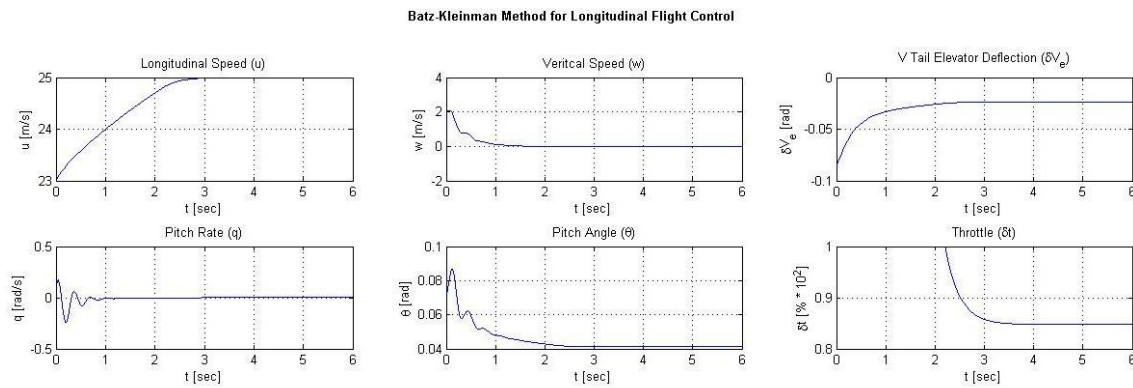


Figure 4.4 Classic disturbance simulation response with the *Batz-Kleinman* controller for disturbances case 2 (x_2).

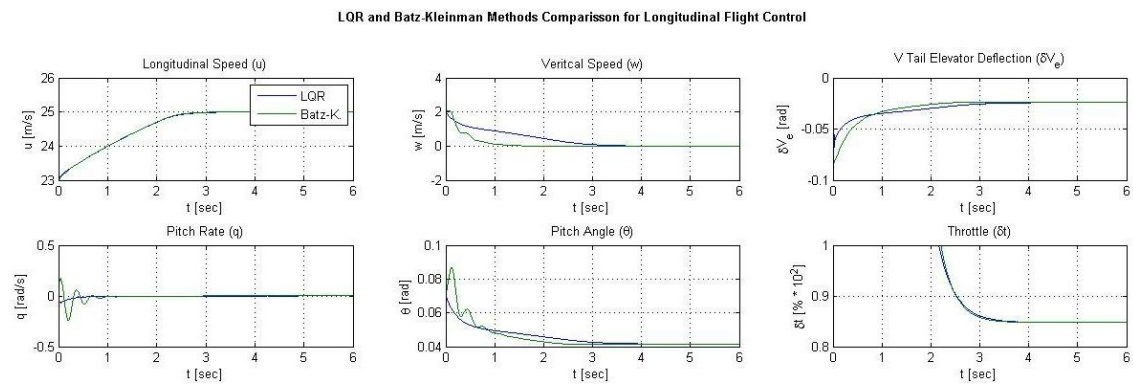


Figure 4.5 Comparison between the simulation responses of both methods with x_2 .

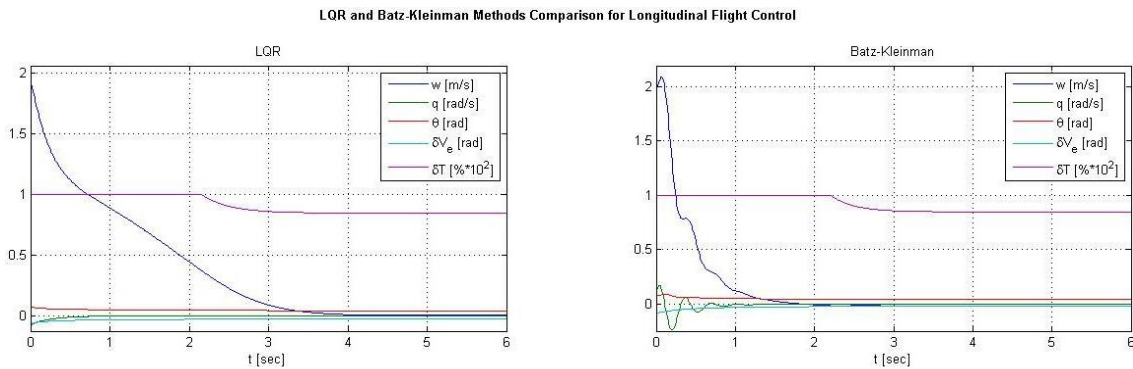


Figure 4.6 Detailed comparison between the longitudinal responses for both methods with x_2 .

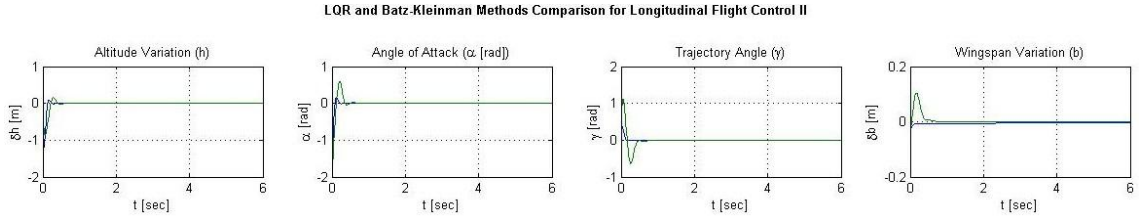


Figure 4.7 Complementary longitudinal parameters response results with \mathbf{x}_2 .

Note that cruise flight at 25 m/s levelled at 60m of altitude (ASL) requires, in accordance with the ISA (International Standard Atmosphere) model for STP (Standard Temperature and Pressure) conditions, about 87% of power (i.e. Throttle settled for 87% of full power meaning $\delta_T = 0.87$) and an elevator trim of $\delta_{v_e} = -0.02 \text{ rad}^{-1}$, meaning a slight upwards deflection of the elevator (i.e. as in a nose up attitude).

The objective of the simulated controller is to stabilize the aircraft after small atmospheric disturbances within six seconds. As seen from Figures 4.3 to 4.7, all values converge to their equilibrium values within the established time limit on this simulation.

The Attitude vector gives the final aircraft attitude after the actuation of the controller to stabilize it on levelled flight. However, that vector gives angles as a relationship between them, and must thereby be manually converted to the body axis system. Therefore after the simulation the aircraft is returned to stable flight levelled ($\gamma = \arctan(w/u) = 0$) at 60m of altitude, 25 m/s of indicated airspeed, nose slightly down ($\theta = 0.74$ degrees), and an angle of attack of 3.26 degrees.

4.3.2 Pitch Attitude Hold Mode

For a specified pitch angle of 3.7 degrees simulating a nose up attitude for the UAV while losing altitude during a landing approach at an airspeed of 20m/s and at 60m MSL, the results are as follows:

Normal Simulation

Disturbances Case 2

Pitch Attitude Hold Mode Selected

Automatic Symmetrical Wingspan Variation with Flight Speed Mode Activated

Longitudinal Stability Achieved

$$\mathbf{X} = \begin{bmatrix} 19.7998 \\ 2.8224 \\ 0.0000 \\ 0.0645 \end{bmatrix} \text{ and } \mathbf{U} = \begin{bmatrix} -0.0551 \\ 0.6646 \end{bmatrix}$$

The System is Longitudinally Controllable

The System is Longitudinally Observable

Handling Qualities: Cruise Mode Selected (Level 1, Class I, Category B)

$$\lambda = \begin{bmatrix} -2.2500 \pm 1.9843i \\ -0.0693 \pm 0.1588i \end{bmatrix}$$

$$X_i = \begin{bmatrix} 21.7998 \\ 4.8224 \\ 0.0300 \\ 0.0945 \end{bmatrix}$$

$$\text{ATTITUDE} = \begin{bmatrix} \text{Velocity [m/s]} \\ \text{Altitude [m]} \\ \text{Pitch Angle [deg]} \\ \text{Wingspan [m]} \\ \text{Bank Angle [deg]} \\ \text{Vertical Speed [m/s]} \\ \text{Lateral Speed [m/s]} \\ \text{Angle of Attack [deg]} \\ \text{Trajectory Angle [deg]} \\ \text{Pitch Rate [rad/s]} \end{bmatrix} = \begin{bmatrix} V \\ h \\ \theta \\ b \\ \phi \\ w \\ v \\ \alpha \\ \gamma \\ q \end{bmatrix} = \begin{bmatrix} 20.0000 \\ 60.0000 \\ 3.6935 \\ 2.5000 \\ 0.0000 \\ 2.8224 \\ 0.0000 \\ 0.1193 \\ -3.1398 \\ 0.0000 \end{bmatrix}$$

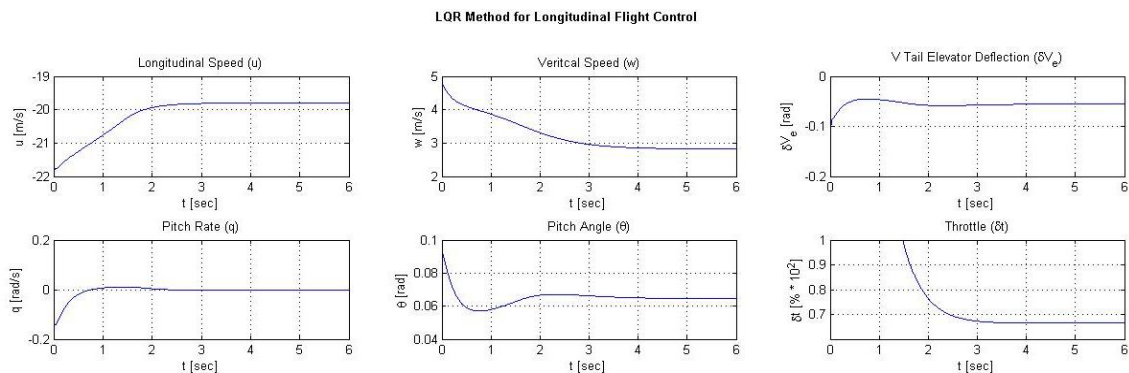


Figure 4.8 Classic disturbance simulation response with LQR for disturbances case 2 (x_2).

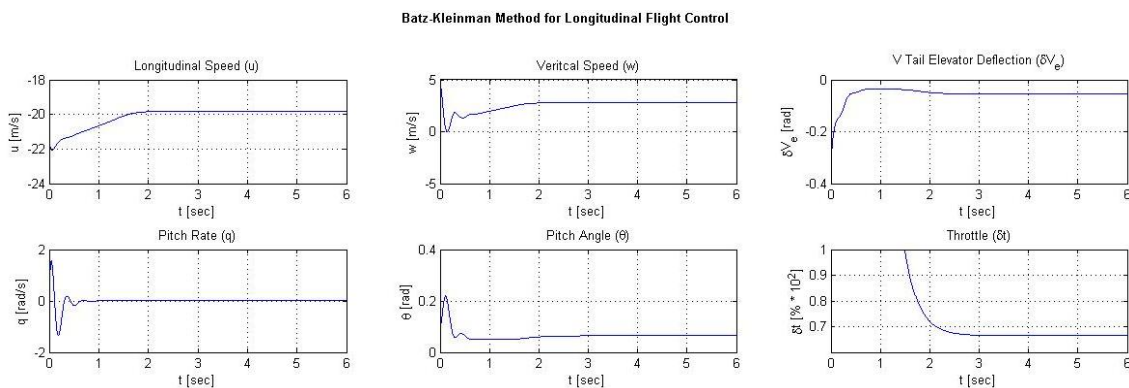


Figure 4.9 Classic disturbance simulation response with the *Batz-Kleinman* controller for disturbances case 2 (x_2).

LQR and Batz-Kleinman Methods Comparison for Longitudinal Flight Control

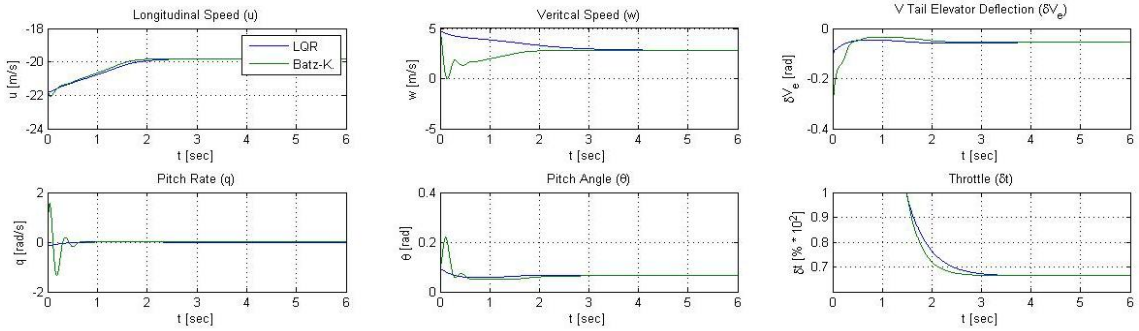


Figure 4.10 Comparison between the simulation responses of both methods with x_2 .

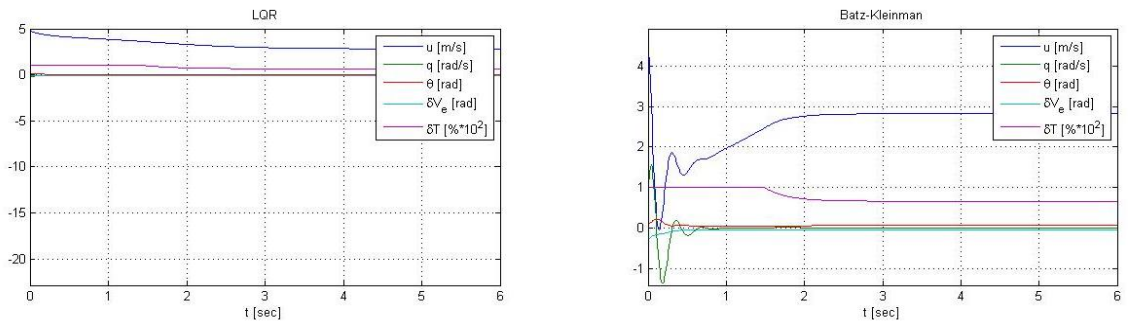


Figure 4.11 Detailed comparison between the longitudinal responses for both methods with x_2 .

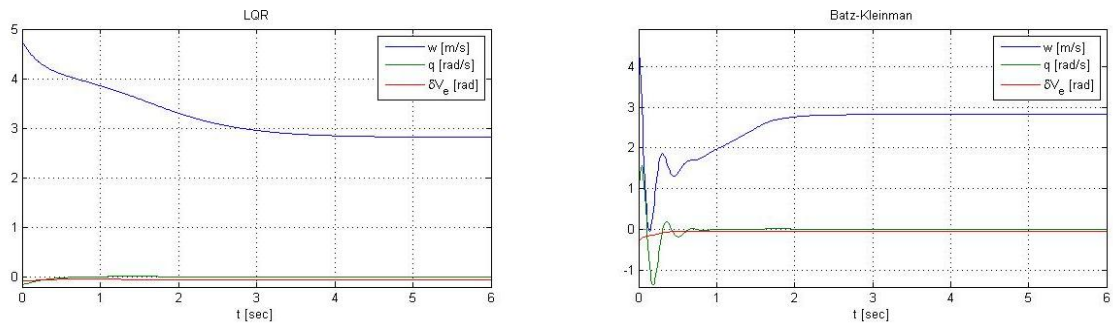


Figure 4.12 Detailed comparison between the vertical velocity, pitch rate and elevator responses for both methods with x_2 .

From this simulation results, it is possible to observe how a slight nose up attitude of only 3.7 degrees ($\theta = 3.7$ deg.) allows for a smooth descent of the aircraft at an adequate rate of nearly 3 m/s on a path angle of $\gamma = -8.0$ degrees. This slow descent ratio associated to the nose up attitude should provide a smooth touch down on the main landing gear after flaring the aircraft, or otherwise, by maintaining this attitude trough all of the final approach and touchdown stages.

For this particular case, it is clear that the LQR method is the most recommended during landing procedures, as it offers far smoother responses when in comparison with the *Batz-Kleinman* method, while retaining the same time target achievement (from now on

abbreviated to TTA) capabilities, i.e. it stabilizes the aircraft in the same time limit than the *Batz-Kleinman* method. In this case, both methods have a TTA of less than 3 seconds.

It is also important to notice that, for an unknown reason, an error occurs in the graphical representation of the longitudinal velocity (u) as it is shown in negative values instead of the expected positive ones. However, the error lies only on the graphical representation of such variable, thus not affecting any of the results.

4.3.3 Climb or Descent/Dive Rate Hold Mode

For a specified climb rate of 5 m/s ($w = -5$ m/s) from a base altitude of 60 m at an initial airspeed of 20 m/s, the disturbances simulation results as follows:

Normal Simulation

Disturbances Case 2

Climb/Descent Rate Hold Mode Selected

Automatic Symmetrical Wingspan Variation with Flight Speed Mode Activated

$b = 2.5000$ (VSMW overall wingspan)

Longitudinal Stability Achieved

$$X = \begin{bmatrix} 19.3649 \\ -5.0000 \\ 0.0000 \\ 0.0645 \end{bmatrix} \text{ and } U = \begin{bmatrix} -0.0551 \\ 0.6646 \end{bmatrix}$$

The System is Longitudinally Controllable

The System is Longitudinally Observable

Handling Qualities: Cruise Mode Selected (Level 1, Class I, Category B)

$$\lambda = \begin{bmatrix} -2.2500 \pm 1.9843i \\ -0.0693 \pm 0.1588i \end{bmatrix}$$

$$X_i = \begin{bmatrix} 17.3649 \\ -3.0000 \\ 0.0300 \\ 0.0945 \end{bmatrix}$$

$$\text{ATTITUDE} = \begin{bmatrix} \text{Velocity [m/s]} \\ \text{Altitude [m]} \\ \text{Pitch Angle [deg]} \\ \text{Wingspan [m]} \\ \text{Bank Angle [deg]} \\ \text{Vertical Speed [m/s]} \\ \text{Lateral Speed [m/s]} \\ \text{Angle of Attack [deg]} \\ \text{Trajectory Angle [deg]} \\ \text{Pitch Rate [rad/s]} \end{bmatrix} = \begin{bmatrix} V \\ h \\ \theta \\ b \\ \phi \\ w \\ v \\ \alpha \\ \gamma \\ q \end{bmatrix} = \begin{bmatrix} 20.0000 \\ 60.0000 \\ 3.6935 \\ 2.5000 \\ 0.0000 \\ -5.0000 \\ 0.0000 \\ 0.1193 \\ -3.1398 \\ 0.0000 \end{bmatrix}$$

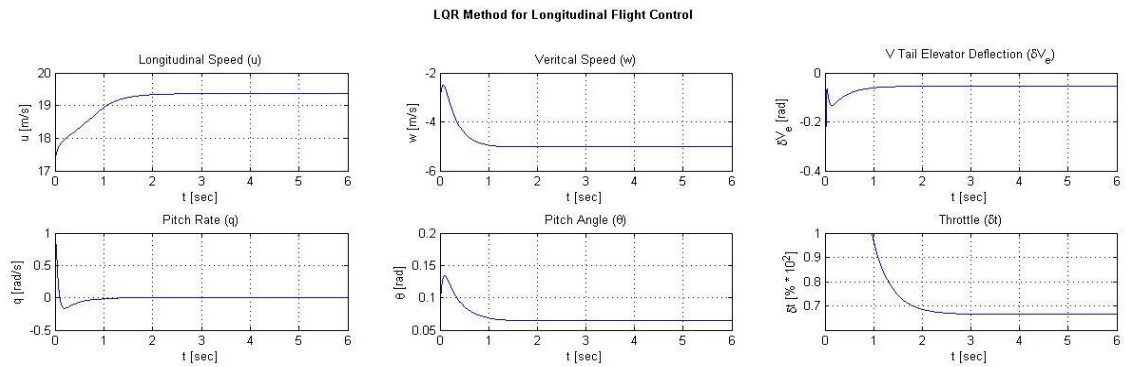


Figure 4.13 Classic disturbance simulation response with LQR for disturbances case 2 (x_2).

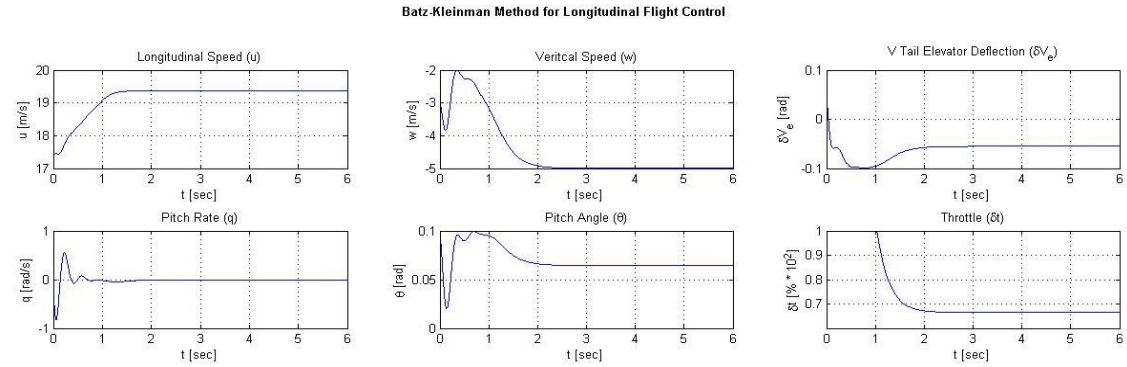


Figure 4.14 Classic disturbance simulation response with the *Batz-Kleinman* controller for disturbances case 2 (x_2).

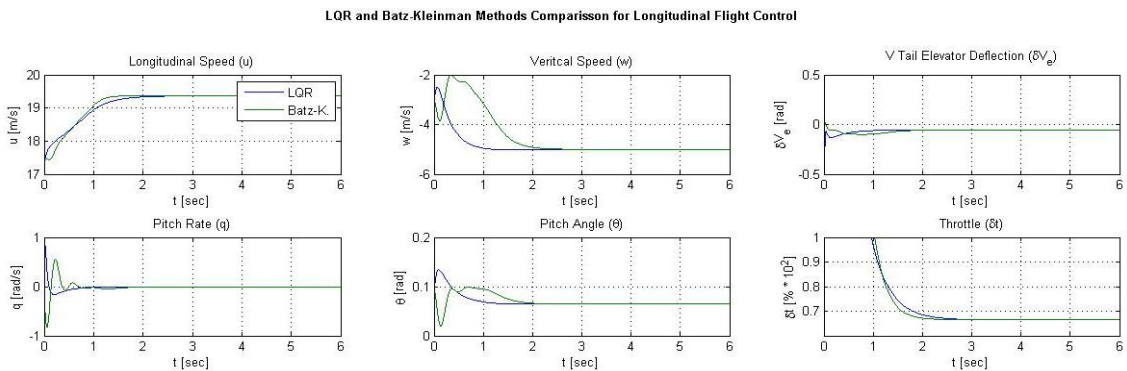


Figure 4.15 Comparison between the simulation responses of both methods with x_2 .

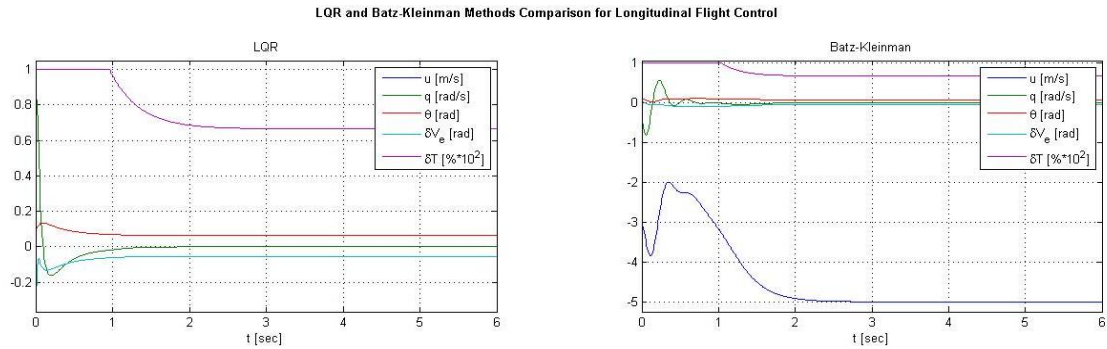


Figure 4.16 Detailed comparison between the longitudinal parameters responses for both methods with x_2 .

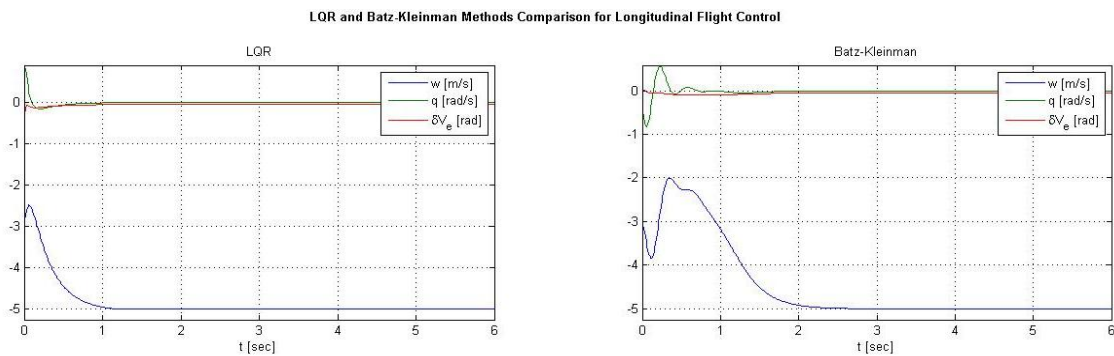


Figure 4.17 Detailed comparison between the vertical velocity, pitch rate and elevator responses for both methods with x_2 .

After applying the necessary angle corrections, it is verifiable that the aircraft is actually climbing at 5 m/s at a path angle of 14 degrees and with a pitch angle of nearly 4 degrees.

4.3.4 Landing Mode

In the landing mode the aircraft is set to follow a standard approach to the runway at a constant given airspeed and vertical speed (or descent rate). Independently of the selected approaching parameters, the controller will automatically flare the UAV to allow a smooth touch-down on the main landing gear. The controller assumes that procedure when the UAV is at 3 m above the ground, and then trims the aircraft for about 3 degrees of pitch angle and a climb rate of -2 m/s. For this simulation purpose, the aircraft is set for a final approach to the runway, beginning at 60 m AGL at the same speed and climb rate indicated for touch-down, which means that the aircraft will, theoretically, not have the necessity to flare before touch-down. The simulation assumes the aircraft is already aligned with the runway, and that no lateral-directional disturbances exist.

Note that although the controller does not directly takes into account external factors such as the ground effect, such effects would translate into deviations of the longitudinal flight parameters from their equilibrium state, and therefore interpreted as atmospheric disturbances by the controller.

The controller may use the signal of a radar altimeter and/or GPS receiver to increase the accuracy of the flare manoeuvre at the right trigger altitude.

The simulation results are shown below:

Normal Simulation

Disturbances Case 2

Landing Mode Selected

Automatic Symmetrical Wingspan Variation with Flight Speed Mode Activated

b = 2.5000 (VSMW overall wingspan)

Radar Altimeter On

Longitudinal Stability Achieved

$$X = \begin{bmatrix} 20.0000 \\ 2.0000 \\ 0.0000 \\ 0.0636 \end{bmatrix} \text{ and } U = \begin{bmatrix} -0.0539 \\ 0.6699 \end{bmatrix}$$

The System is Longitudinally Controllable

The System is Longitudinally Observable

Handling Qualities: Take-Off/Landing Mode Selected (Level 1, Class I, Category C)

$$\lambda = \begin{bmatrix} -2.2500 \pm 1.9843i \\ -0.0693 \pm 0.1588i \end{bmatrix}$$

$$X_i = \begin{bmatrix} 18.0000 \\ 4.0000 \\ 0.0300 \\ 0.0936 \end{bmatrix}$$

$$\text{ATTITUDE} = \begin{bmatrix} \text{Velocity [m/s]} \\ \text{Altitude [m]} \\ \text{Pitch Angle [deg]} \\ \text{Wingspan [m]} \\ \text{Bank Angle [deg]} \\ \text{Vertical Speed [m/s]} \\ \text{Latral Speed [m/s]} \\ \text{Angle of Attack [deg]} \\ \text{Trajectory Angle [deg]} \\ \text{Pitch Rate [rad/s]} \end{bmatrix} = \begin{bmatrix} V \\ h \\ \theta \\ b \\ \phi \\ w \\ v \\ \alpha \\ \gamma \\ q \end{bmatrix} = \begin{bmatrix} 20.0998 \\ 60.0000 \\ 3.6428 \\ 2.5000 \\ 0.0000 \\ 2.0000 \\ 0.0000 \\ 0.1193 \\ -3.1905 \\ 0.0000 \end{bmatrix}$$

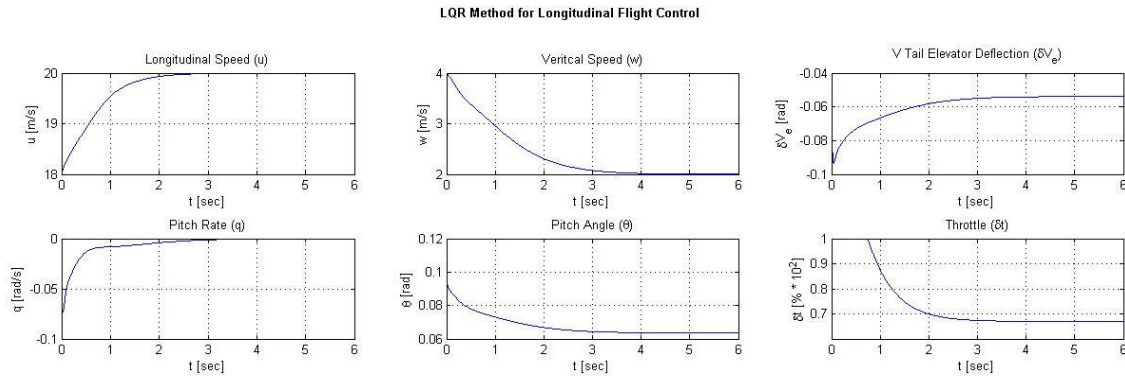


Figure 4.18 Classic disturbance simulation response with LQR for disturbances case 2 (x_2).

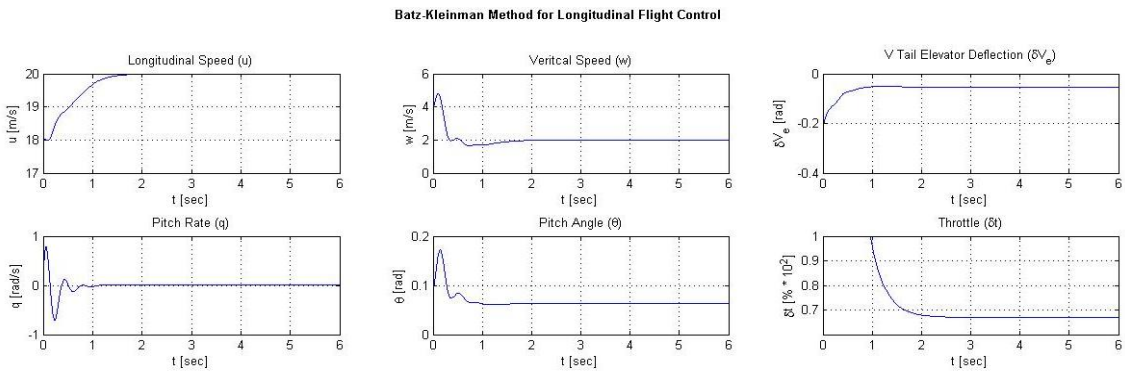


Figure 4.19 Classic disturbance simulation response with the *Batz-Kleinman* controller for disturbances case 2 (x_2).

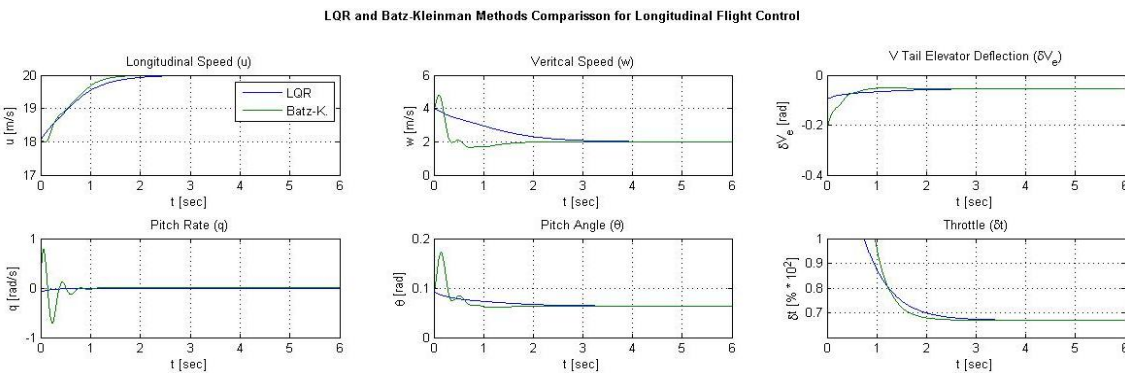


Figure 4.20 Comparison between the simulation responses of both methods with x_2 .

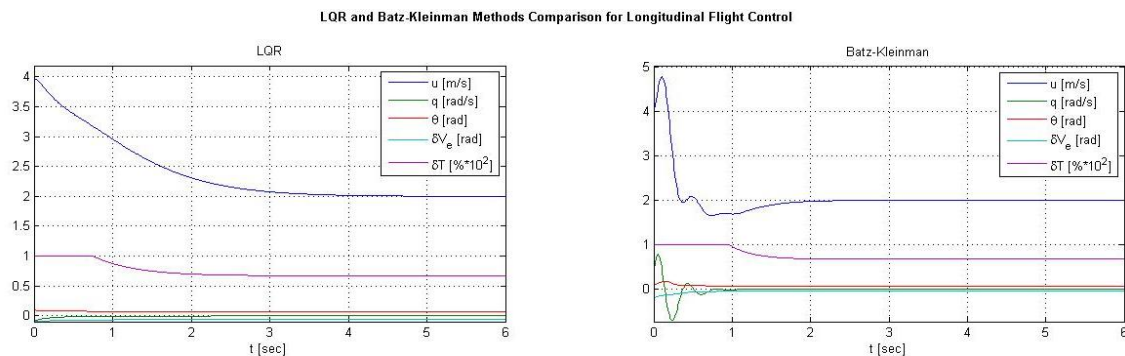


Figure 4.21 Detailed comparison between the longitudinal parameters responses for both methods with x_2 .

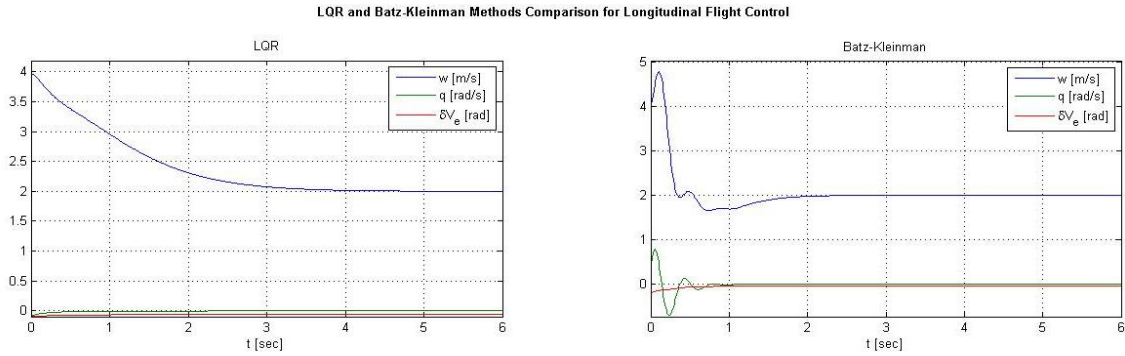


Figure 4.22 Detailed comparison between the vertical velocity, pitch rate and elevator responses for both methods with x_2 .

After the necessary corrections have been applied, it is found that the aircraft is descending in an optimal touch-down attitude in preparation for landing. The VSI (Vertical Speed Indicator) and the IAS (Indicated Airspeed) Indicator would indicate a smooth descent of 2 m/s ($w = 2$ m/s) at an airspeed (u) of 20 m/s with a nose up attitude of 3.6428 degrees in pitch (θ , indicated by the Attitude Indicator) with an AoA (Angle of Attack or α) of nearly 2 degrees on a path angle (γ) of -5.68 degrees.

4.3.5 Take-Off Mode

The take-off mode simply adds full power to the UAV's engine until minimum take-off airspeed is achieved, then the controller switches to Climb Mode until a pre-defined altitude is reached. At that altitude, the controller switches again for Altitude Hold Mode.

4.3.6 TFTA Mode

This mode works exactly the same as the Altitude Hold Mode. The only difference is that this mode allows the use of a radar altimeter and/or a GPS receiver to calculate its altitude relatively to the ground, and engages a standard climb or dive mode whenever the altimeter reads an altitude deviation of 10 m (assumed value) of the assigned flight altitude.

4.3.7 Dissymmetrical Wing Mode

This module of the program is intended to provide an insight in the longitudinal behaviour of the UAV while suffering a lateral-directional disturbance. For this case, a momentaneous failure of the wing mechanism is simulated inducing the aircraft into a roll. The initial span deflection (δ_y) is of 0.2m (i.e. a wing span dissymmetry of 0.2m) at 20 m/s and 60 m MSL. The results are shown below:

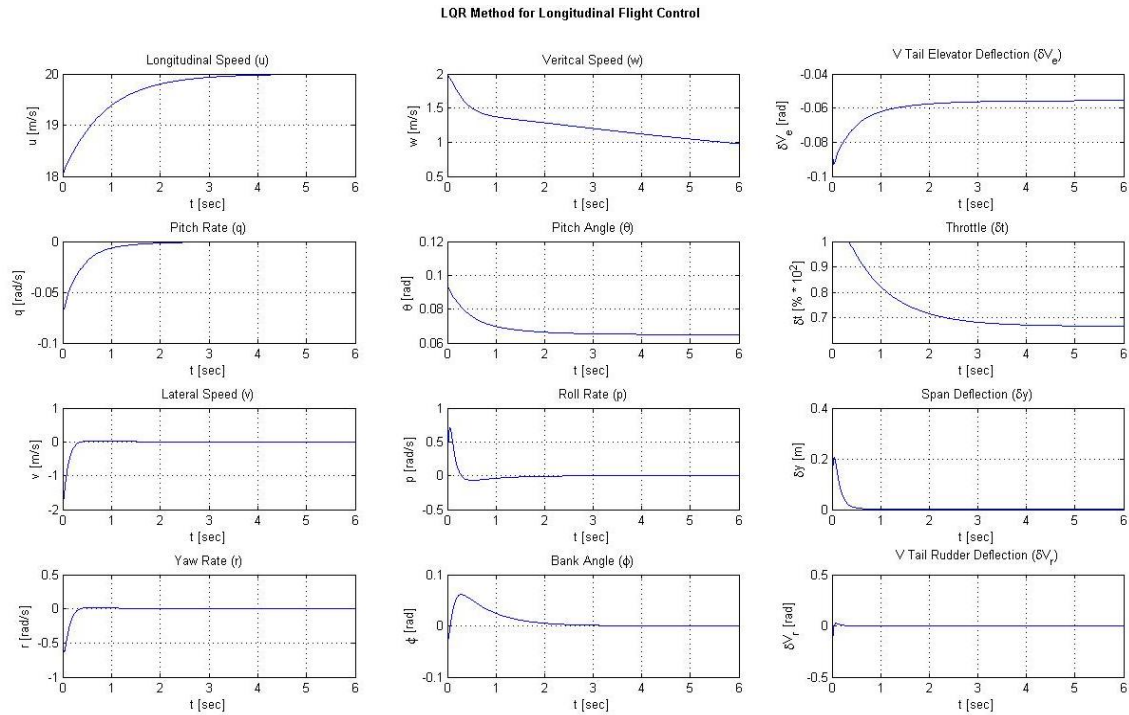


Figure 4.23 Classic disturbance simulation response with LQR for disturbances case 2 (x_2).

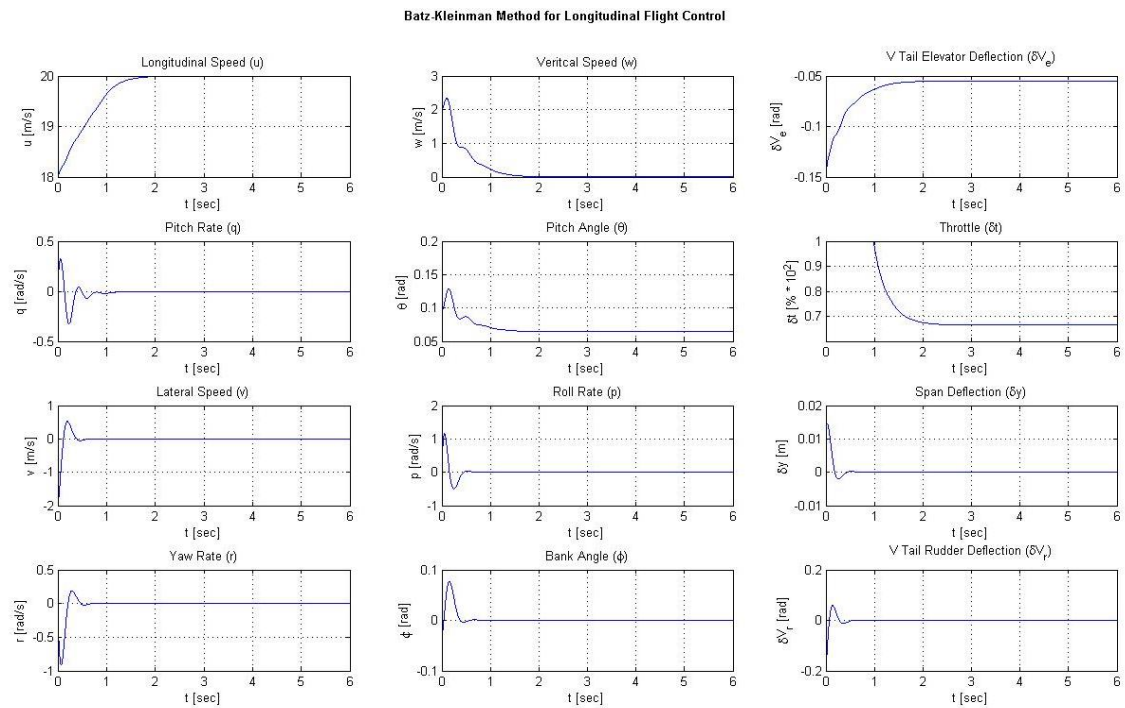


Figure 4.24 Classic disturbance simulation response with the *Batz-Kleinman* controller for disturbances case 2 (x_2).

LQR and Batz-Kleinman Methods Comparison for Longitudinal Flight Control

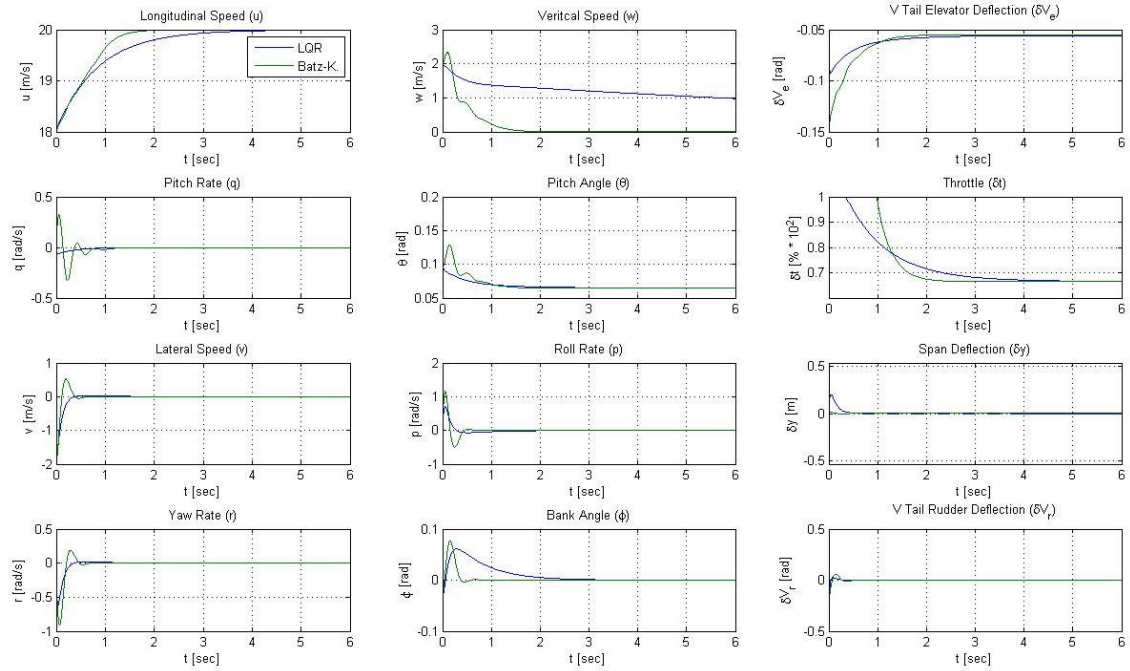


Figure 4.25 Comparison between the simulation responses of both methods with x_2 .

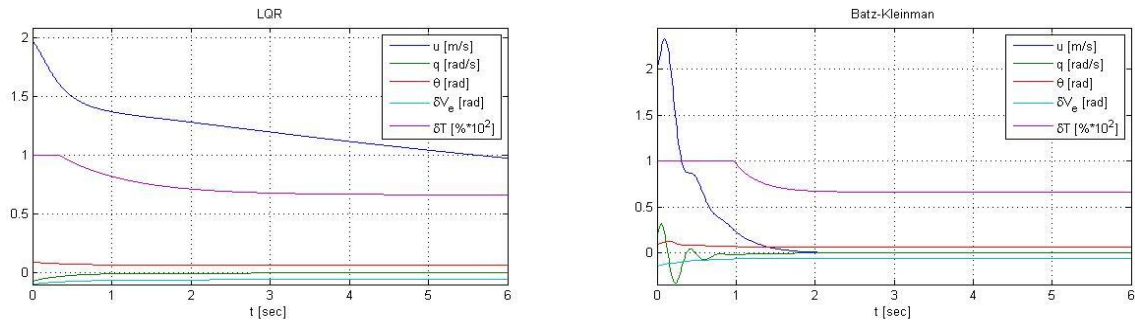


Figure 4.26 Detailed comparison between the longitudinal parameters responses for both methods with x_2 .

As seen from this simulation, the controller has the ability to maintain longitudinal stability during small and temporary lateral-directional disturbances (of atmospheric or mechanical origins). Up to what extent it is possible to compensate a permanent jam of the wing mechanism with the rudders and elevators however, remains to be ascertained in future studies.

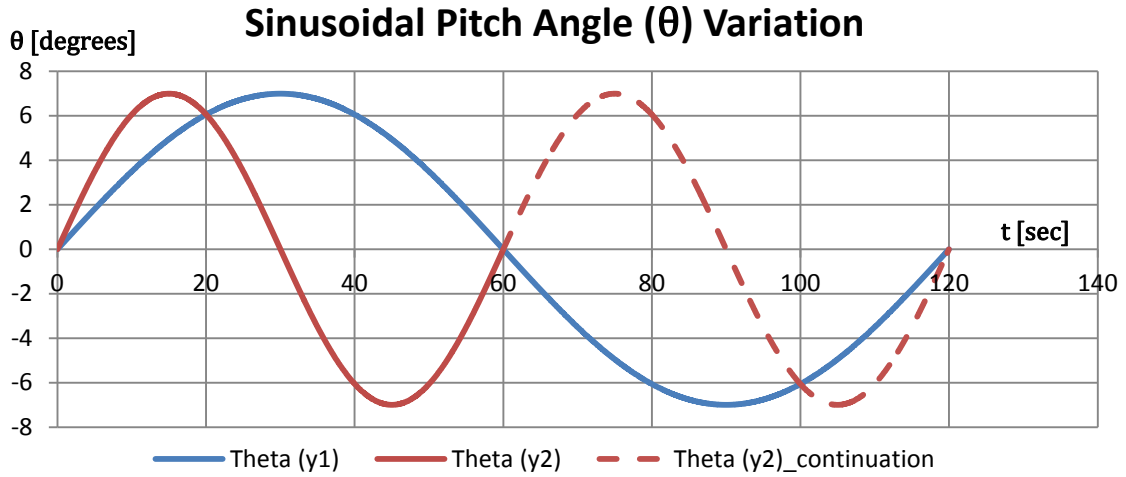
4.4 Pitch Angle Sinusoidal Variation Test Response

Although the classical simulation results allow a clear observation of the aircraft's state response to an atmospheric disturbance, it somehow lacks such observation clarity when it comes to the direct relationship between the induced control inputs and the consequent reaction in state variables. Therefore, there was the need to perform a more complex analysis regarding such relationship. In this simulation, a larger number of equilibrium states had to be calculated, in order to simulate the aircraft's response to a sinusoidal variation of the pitch angle (θ) up to a maximum of 7 degrees. The simulation's code script is mostly the same as the one used in previous simulations regarding the classical disturbances method. It is set to simulate the aircraft's control surfaces (elevators) and engine's power while attempting to maintain a levelled flight at 20 m/s at sea level and with the wings extended to its maximum wingspan. As explained before all aircraft data, including the imposed handling qualities, remain the same. The simulation works by systematically forcing the UAV to change its pitch angle every fixed amount of time (a few seconds), and then calculating the associated equilibrium state and control vectors. The objective of such simulation is to analyze the reactions of the state and control variables to a dynamic variation of the pitch attitude as it is prone to happen during actual flight, proving that both the concept mechanism behind the controller and the controller itself work properly and are thus, theoretically viable to be implemented in the actual aircraft prototype for test flight purposes. In order to enhance the reliability of the test results, the simulation was performed for two different sets of regular (i.e. periodic) time intervals (y_1 and y_2) between equilibrium points. y_1 represents a 6 seconds time span between equilibrium points, whereas y_2 represents a 1.5 seconds time span. To induce a smooth fully symmetrical amplitude variation in pitch, a sinusoidal (more precisely, a cosine) variation of the pitch angle (θ) using the following equation (4.5):

$$\theta = \frac{|\theta_{\max} - \theta_{\min}|}{2} \cos \left[\left(\frac{2\pi}{(t_{\max} - t_{\min})} \right) \left(t + \frac{3}{4}(t_{\max} - t_{\min}) \right) \right] \quad (4.5)$$

With $-\theta_{\min} = \theta_{\max} = 7$ degrees.

Which is graphically represented in graph (4.1):



Graphic 4.1 Graphical representation of the cosine variation of the pitch angle (θ) for the two different time spans (maximum pitch angle of 7 degrees).

The controller creates a total of 20 equilibrium points for each simulation independently of the time span chosen, which means that, for the time span of 6 seconds of y_1 , the total simulation time is of $t_{\max} = 20 \times 6 = 120$ sec, while for y_2 is of only 30 sec. However, in order to enable the graphic visualization of the variables returning to their initial values, the simulation was extended by a time factor of $t_{\max}/20$, which means that the actual simulation duration is of $t_{\max} + t_{\max}/20$, meaning a total time of 126 sec to y_1 and 31.5 sec to y_2 .

Both the LQR and the *Batz-Kleinman* controller methods were analyzed for each set of time span (y_1 and y_2) as seen in Figures 4.27 to 4.30.

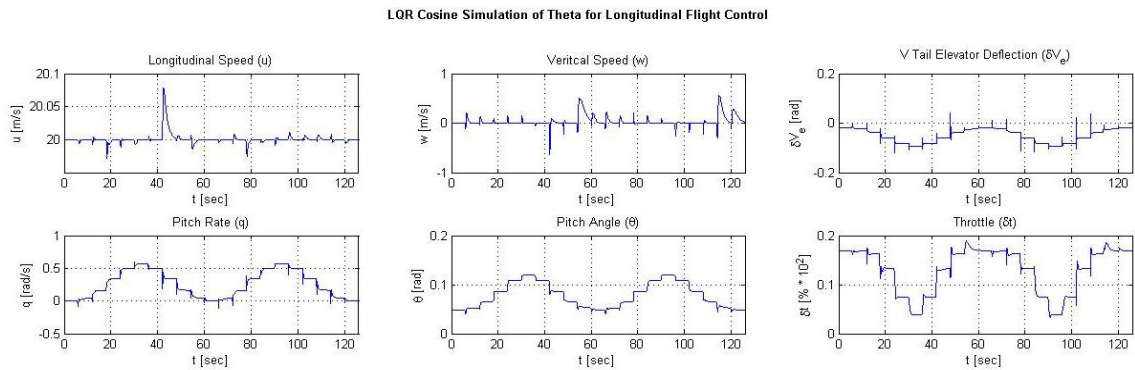


Figure 4.27 LQR simulation for a sinusoidal variation of the pitch angle for y_1 .

The figure above (Figure 4.27) shows how control variables respond to the variation in the pitch angle (θ) influencing the pitch rate (q) and the velocities in order to maintain the aircraft on a level flight at the intended airspeed (u). From the vertical speed graph, it is visible the high peaks occurring immediately after the UAV starts pitching down, depicting the sudden increase in the Climb Ratio (i.e. an increase in the absolute value as the UAV is actually descending instead of climbing [remember: $w = 1\text{m/s}$ indicates that the aircraft as a

positive vertical speed along the z axis which points towards the centre of the Earth, or in other words that the aircraft is descending with a negative climb rate]) towards the ground influenced by the gravity pull aid.

Another important observation to be noticed is the substantial decrease in required thrust when compared with the values obtained in the classical method simulations. While it may simply be due to the altitude difference, since the previous simulations were performed for an altitude of 60m whereas this one was set for sea level (0m), the reduction in the required power is indeed significant and therefore, the possibility of an error in the program code script regarding the thrust equations or the control and stability derivatives can't be completely discarded. In fact, such was the case as described later on.

The remaining graphical results of this simulation are presented in Figures 4.28 through 4.30.

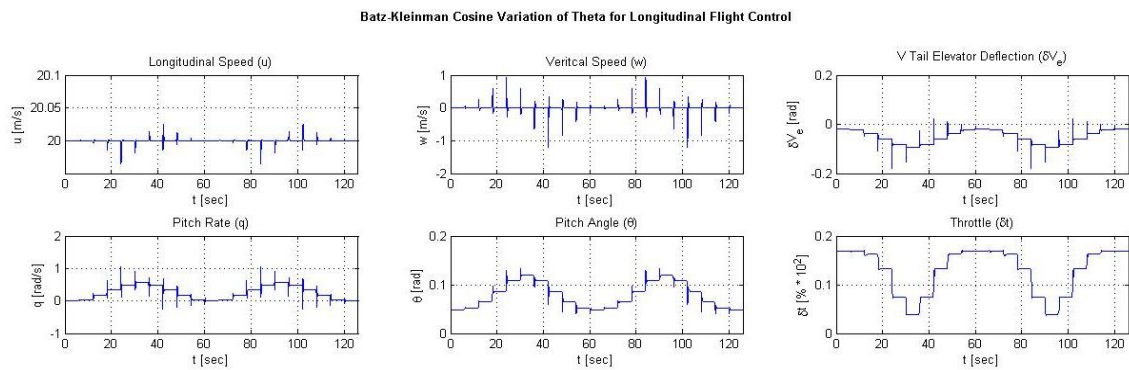


Figure 4.28 *Batz-Kleinman* simulation for a sinusoidal variation of the pitch angle for y_1 .

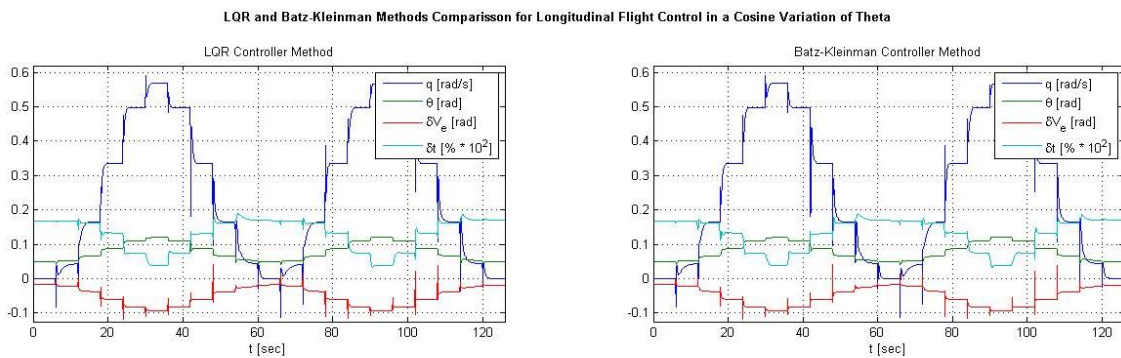


Figure 4.29 Detailed pitch control and state variables comparison between the two methods for a sinusoidal variation of the pitch angle for y_1 .

LQR & Batz-Kleinman Cosine Variation of Theta Simulation Comparison for Longitudinal Flight Control

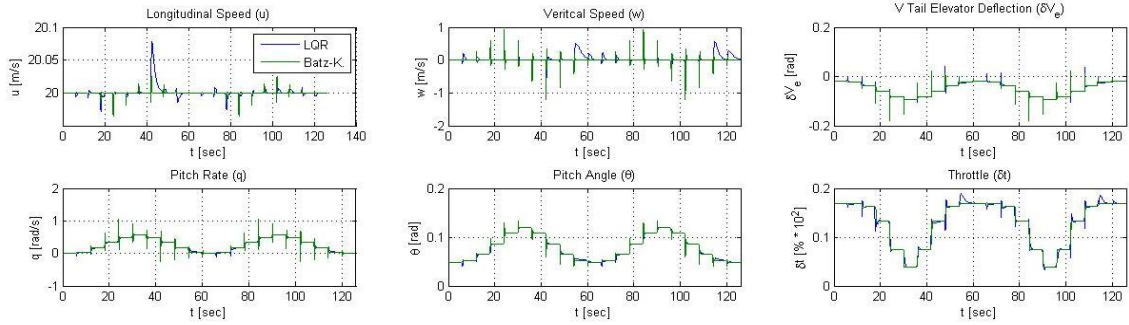


Figure 4.30 Single variable response comparison between LQR and *Batz-Kleinman* controller methods for a sinusoidal variation of the pitch angle for y_1 .

From the observation of figure 4.30 it is possible to see that, although very similar, the LQR controller seems to offer an overall better controllability of the aircraft, particularly in regard to the longitudinal (u) and vertical (w) velocities stabilization.

Figures 4.31 To 4.34 now illustrate the same test responses, but for the y_2 case.

LQR Cosine Simulation of Theta for Longitudinal Flight Control

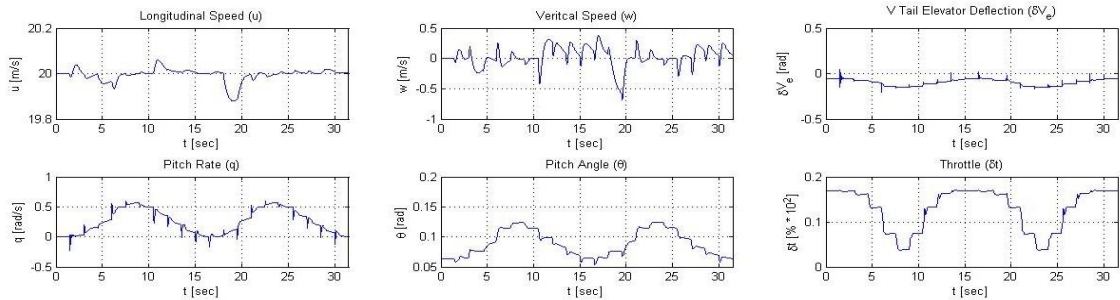


Figure 4.31 LQR simulation for a sinusoidal variation of the pitch angle for y_2 .

Batz-Kleinman Cosine Variation of Theta for Longitudinal Flight Control

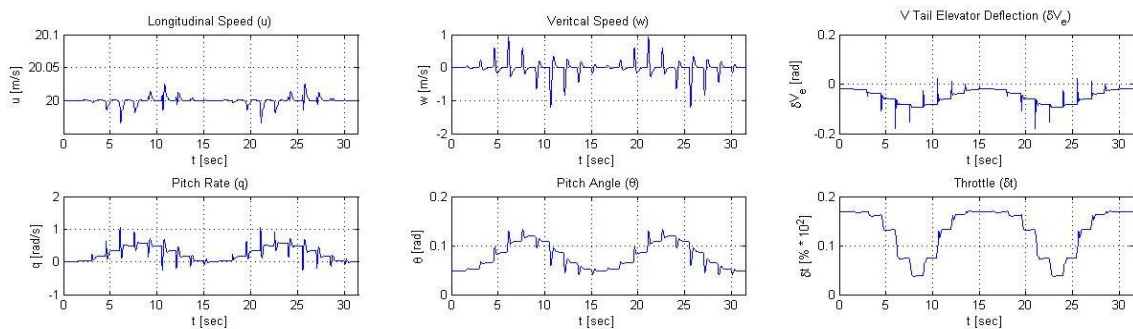


Figure 4.32 *Batz-Kleinman* simulation for a sinusoidal variation of the pitch angle for y_2 .

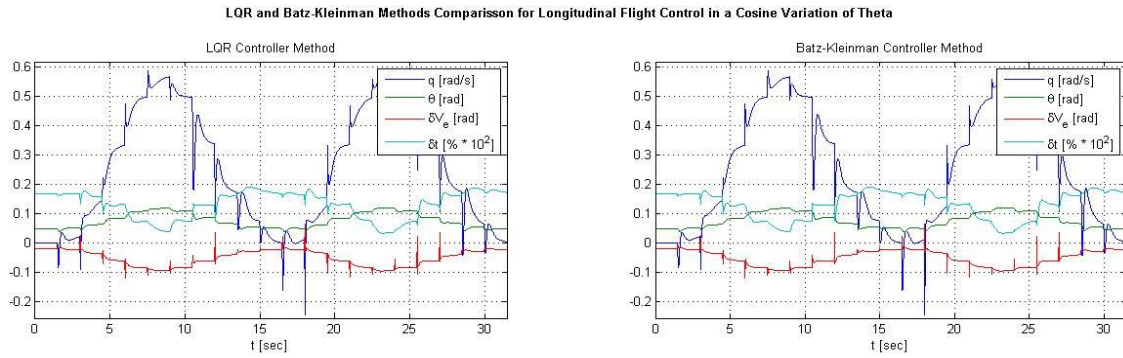


Figure 4.33 Detailed pitch control and state variables comparison between the two methods for a sinusoidal variation of the pitch angle for y_2 .

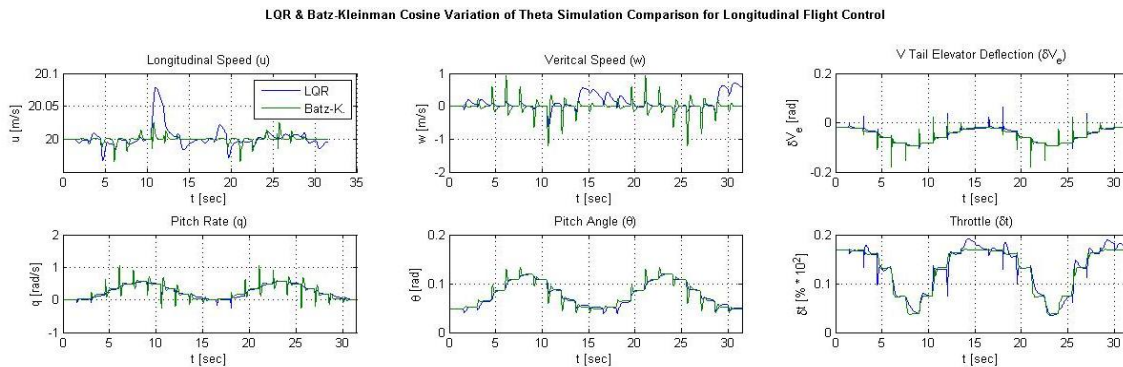
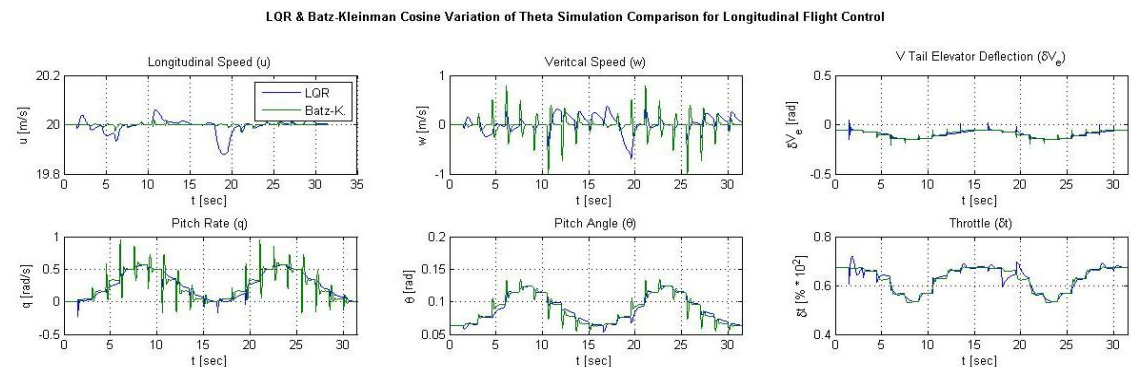
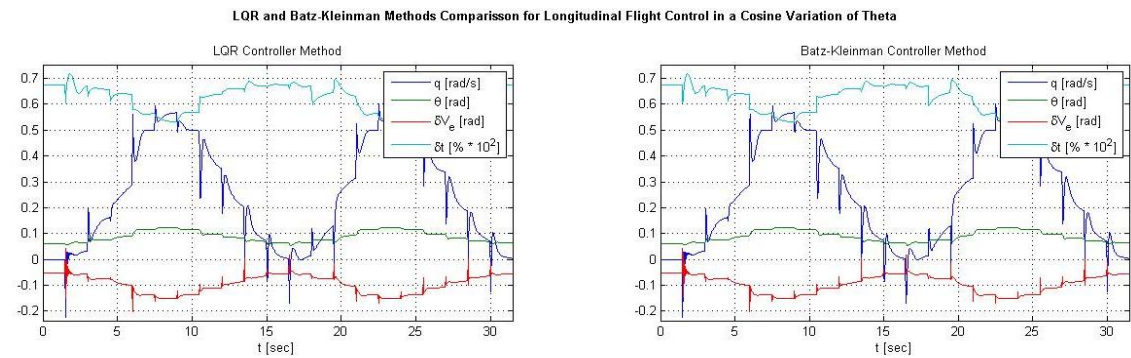
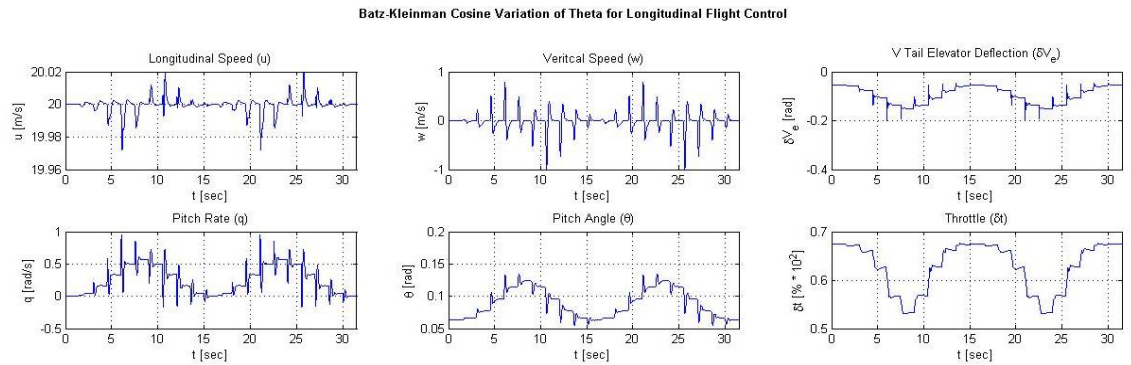
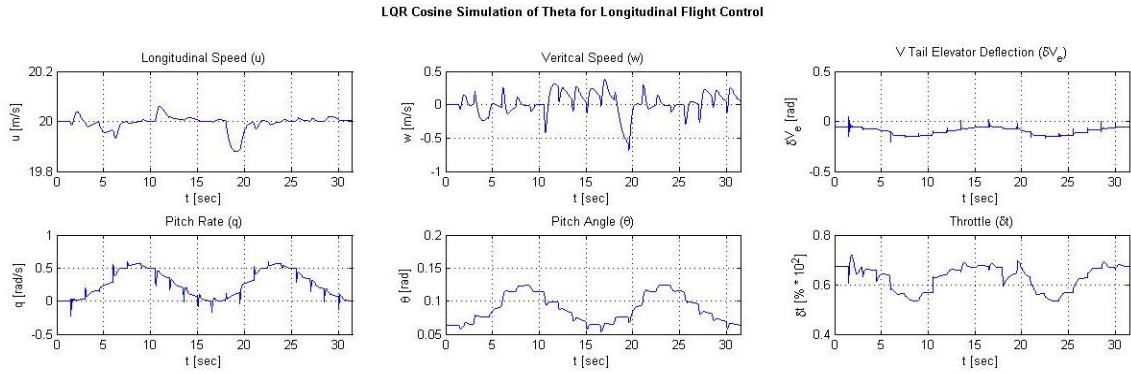


Figure 4.34 Single variable response comparison between LQR and *Batz-Kleinman* controller methods for a sinusoidal variation of the pitch angle for y_2 .

With this test response simulation, the main longitudinal variables responses can now be fully observed in detail, revealing the actual aircraft motion parameters and their relationship. It is now clear that, as expected, a sinusoidal variation on pitch angle leads to a similar sinusoidal response of both the elevators and engine power controls that in turn results in an also sinusoidal pitch rate variation in order to maintain the aircraft stable at levelled flight and at the intended velocity.

After a careful review of the program script, we indeed, detected errors in the assigned values to the stability and control derivatives that caused the unusually low value of throttle “deflection” reported earlier. After proceeding to the necessary corrections, the simulation now delivers the expected results as shown in Figures 4.35 to 4.42. However, the previous results were maintained in this report as an alert and reminder of the extreme complexity and attention to detail that are required when dealing with such controllers scripts. Just a small mistake when assigning one single value can easily lead results completely off the expected ones.



LQR Cosine Simulation of Theta for Longitudinal Flight Control

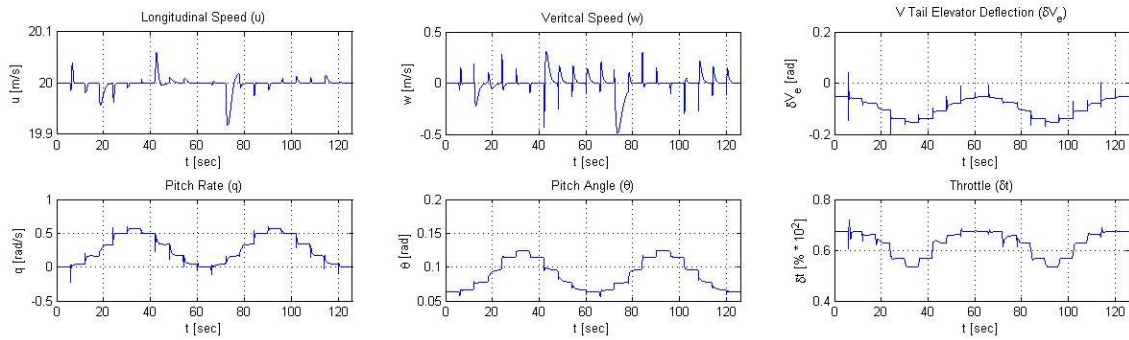


Figure 4.39 LQR simulation for a sinusoidal variation of the pitch angle for y_1 .

Batz-Kleinman Cosine Variation of Theta for Longitudinal Flight Control

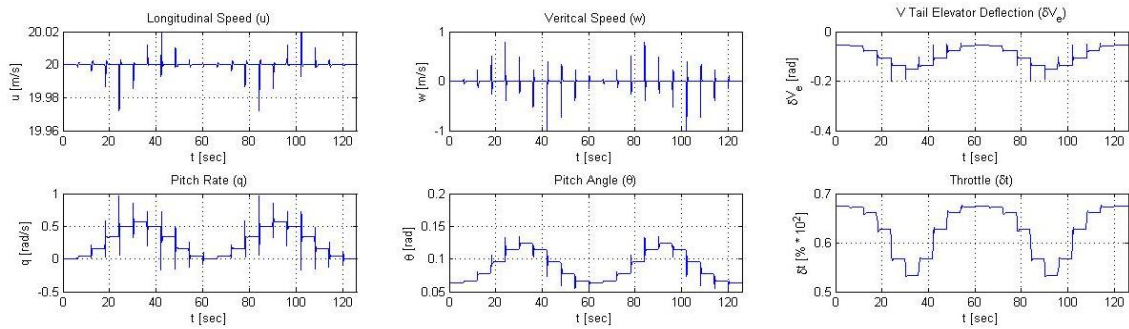


Figure 4.40 Batz-Kleinman simulation for a sinusoidal variation of the pitch angle for y_1 .

LQR and Batz-Kleinman Methods Comparison for Longitudinal Flight Control in a Cosine Variation of Theta

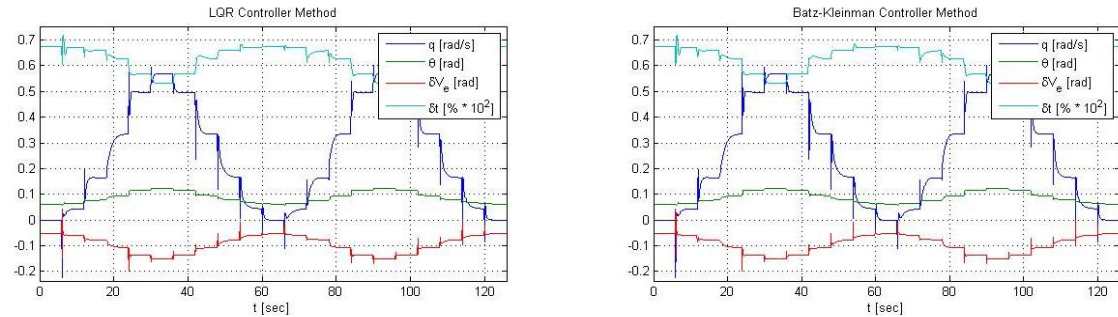


Figure 4.41 Detailed pitch control and state variables comparison between the two methods for a sinusoidal variation of the pitch angle for y_1 .

LQR & Batz-Kleinman Cosine Variation of Theta Simulation Comparison for Longitudinal Flight Control

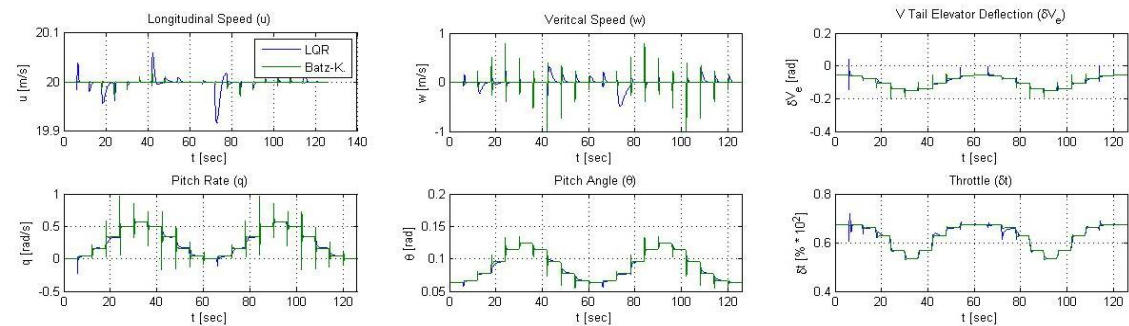


Figure 4.42 Single variable response comparison between LQR and Batz-Kleinman controller methods for a sinusoidal variation of the pitch angle for y_1 .

4.5 Random Pitch Angle Variation

The previous Classical Disturbances and Sinusoidal Pitch Variation simulations already describe and validate the working concept of this flight controller. However, to validate the controller for actual use, a more complex simulation had to be performed. For that effect, a random simulation of the pitch angle was created in order to evaluate the controller's ability to stabilize the aircraft under such harsh and unpredictable conditions.

This random simulation uses the same base code script and equilibrium states as the ones used in the previous sinusoidal simulation. However, in this simulation, the program chooses a random point every t seconds no more than n steps above or below the previous equilibrium point. That means that, since the same equilibrium points of the sinusoidal simulation are being used, the program will always choose the equilibrium point immediately after, the equilibrium point immediately before, the second equilibrium point immediately after, or the second equilibrium point immediately before the current equilibrium point. Because the equilibrium points are the same as those of the sinusoidal simulation, it will always mean an increase or decrease in pitch angle accordingly to the current equilibrium point. By that same reason, the variation in pitch will be smaller if the random chosen point is closer to the current equilibrium point and vice-versa.

Once again, two simulations were carried out. In the first one (y_1), $t = 6$ seconds, meaning that a new random point is selected every 6 seconds, while in the second one (y_2), $t = 3$ seconds. The random variable that determines the next equilibrium point was created using only MATLAB®'S commands [33].

The results of these two simulations are presented in the following Figures:

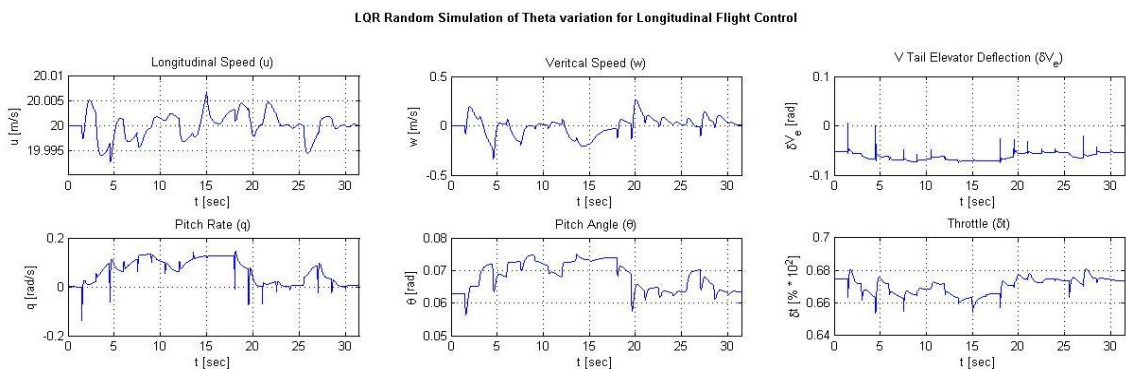


Figure 4.43 LQR simulation for a random variation of the pitch angle for y_2 .

Batz-Kleinman Random Variation of Theta for Longitudinal Flight Control

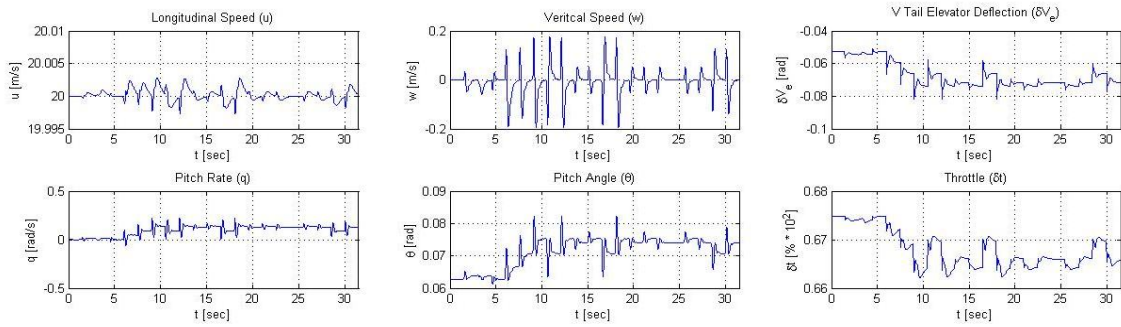


Figure 4.44 *Batz-Kleinman* simulation for a random variation of the pitch angle for y_2 .

LQR and Batz-Kleinman Methods Comparison for Longitudinal Flight Control in a Random Variation of Theta

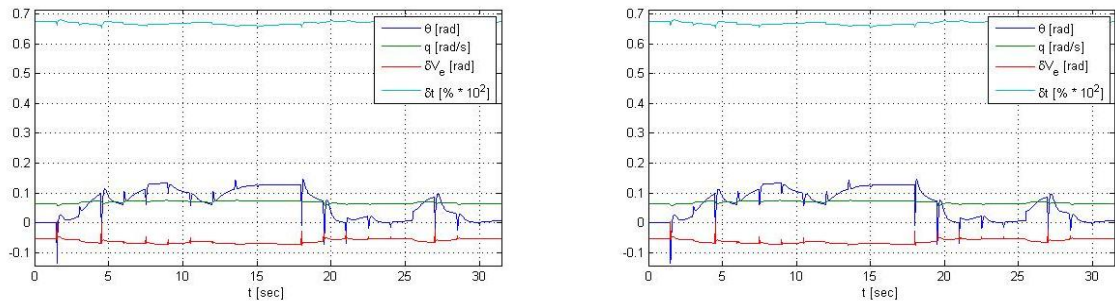


Figure 4.45 Detailed pitch control and state variables comparison between the two methods for a random variation of the pitch angle for y_2 .

LQR & Batz-Kleinman Random Variation of Theta Simulation Comparison for Longitudinal Flight Control

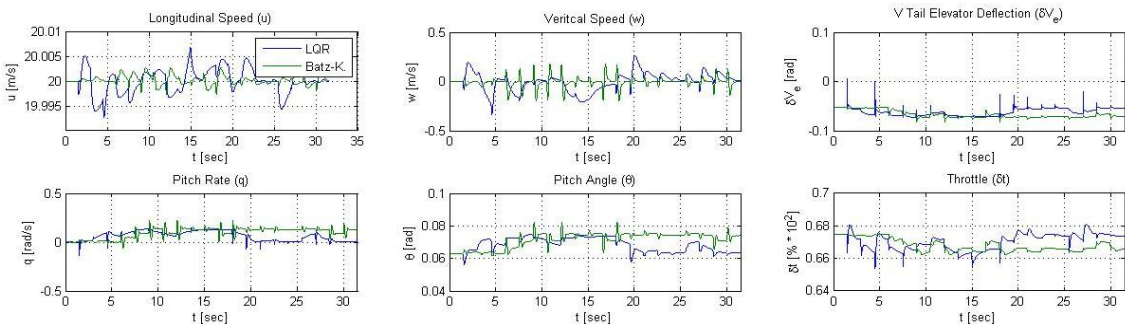


Figure 4.46 Single variable response comparison between LQR and *Batz-Kleinman* controller methods for a random variation of the pitch angle for y_2 .

LQR Random Simulation of Theta variation for Longitudinal Flight Control

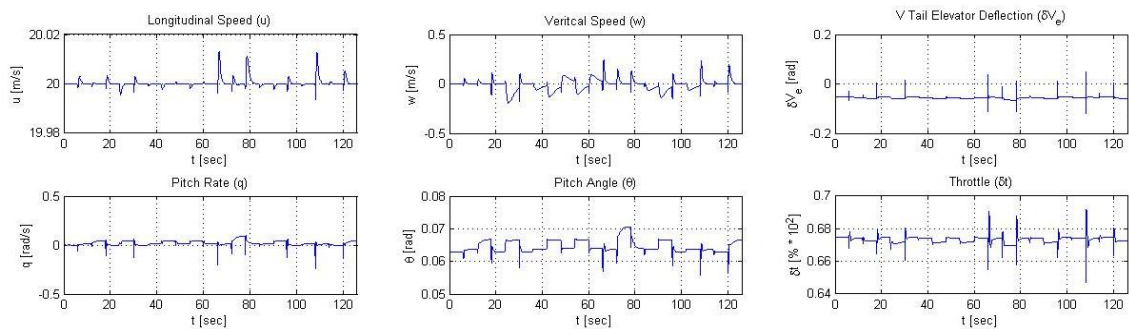


Figure 4.47 LQR simulation for a random variation of the pitch angle for y_1 .

Batz-Kleinman Random Variation of Theta for Longitudinal Flight Control

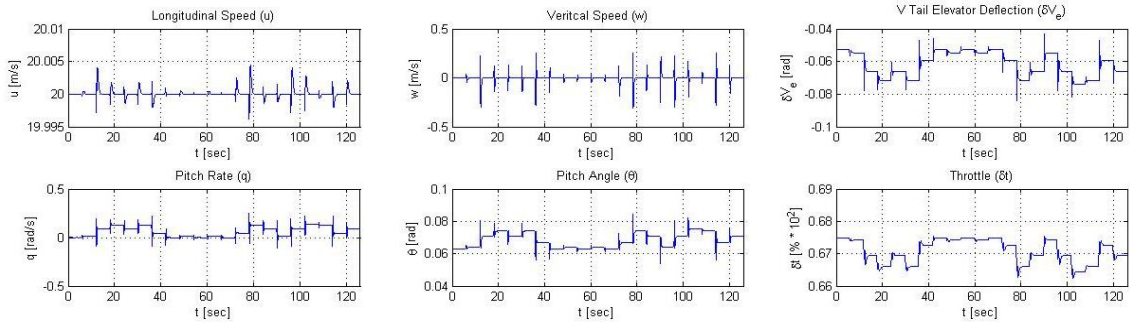


Figure 4.48 *Batz-Kleinman* simulation for a random variation of the pitch angle for y_1 .

LQR and Batz-Kleinman Methods Comparisson for Longitudinal Flight Control in a Random Variation of Theta

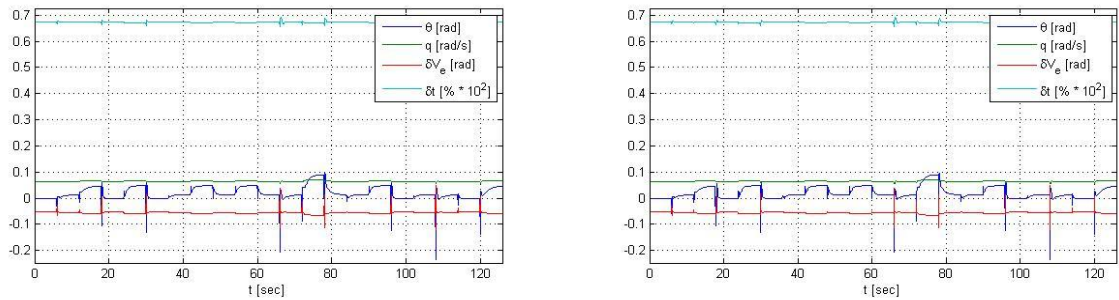


Figure 4.49 Detailed pitch control and state variables comparison between the two methods for a random variation of the pitch angle for y_1 .

LQR & Batz-Kleinman Random Variation of Theta Simulation Comparison for Longitudinal Flight Control

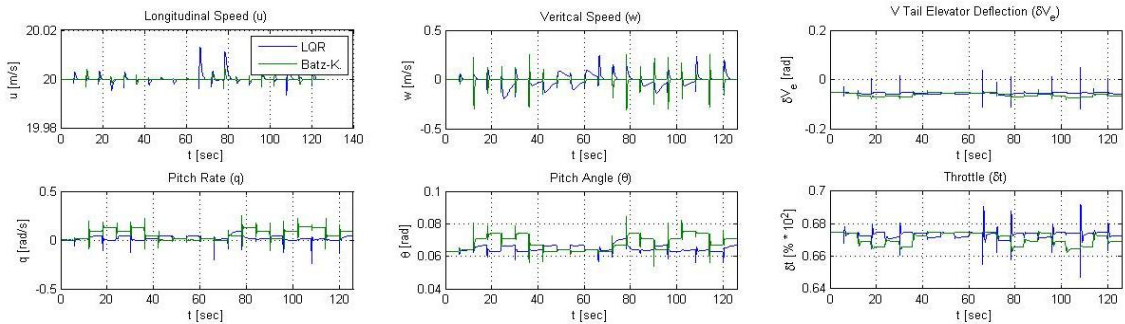


Figure 4.50 Single variable response comparison between LQR and *Batz-Kleinman* controller methods for a random variation of the pitch angle for y_1 .

As easily verifiable, a simulation of this kind is representative of a constant random change in pitch attitude, however the controller still retains the ability to stabilize the aircraft up to some degree for both methods (LQR and *Batz-Kleinman*) in both simulations (y_1 and y_2).

Blank Page

Chapter 5

Conclusions

After nearly 6 months of hard work, roughly six thousand lines of scripted MATLAB® files, and this 161 pages document containing nearly thirty thousand words, it's safe to say that this work represented a major challenge to the author's capabilities. It does not only involves a large set of fields (mathematics, physics, aerodynamics, electronics and informatics) required for the development of a flight controller system, as it also involves new experimental and untested technologies, not to mention weeks of study, research and planning. Therefore, the successful conclusion and presentation of this work is very rewarding for the author.

As demonstrated in Chapter 4, all the simulations and tests prove the working concept and reliability of the developed longitudinal flight controller system under different and even unusual flight conditions. Of course, the values obtained may not be, and probably aren't, entirely accurate as they are based in calculations and estimations of several variables. Thus they may not faithfully represent the true aircraft behaviour. However, it is the substantiation of the working concept that matters the most, as the program can later be easily updated and adjusted for the more accurate data retrieved from further flight tests or other methods of data acquisition. In fact, a lot of effort was put into making the controller's script structure very simple to modify, update or integrate with other programs by means of a modular structure. Thus, allowing its use with different aircraft configurations or even different aircraft, as well as permitting its further development into a fully functional 4D autopilot.

As already stated in this document, this work's purpose was to test two different control methods for longitudinal flight stabilization of a VSMW equipped UAV under different flight conditions, with the objective of ensure the feasibility of actually implement the controller on the aircraft for test flight purposes. However, as also stated, it is not a longitudinal autopilot and therefore, it will not really take the aircraft from point A to B as it happens with actual autopilot systems. It simply stabilizes the aircraft on its longitudinal axis given minor atmospheric disturbances such as turbulence, wind variations, or thermals. Nevertheless, initial steps were taken in that direction (autopilot development), i.e. some of the controller modes mentioned before such as the TFTA, although simulated by the controller program will be unusable in the actual aircraft control without further development of the controller into a full 4D autopilot system. Therefore, regardless of the fact that such complex and detailed programming requirements are far beyond the scope of

the present work, the bases for such flight modes were already implemented in the controller in advance for such development. Many other improvements to the controller were made in that direction, even though not described in this work as they require further development and/or lack necessary data. For instance, the TFTA mode depends of the utilization of a radar altimeter, and although an algorithm had been developed to integrate data provided by a barometric altimeter, a radar altimeter and a GPS altogether, the lack of information on the avionics to be used, if to be used at all, invalidates an accurate simulation of such flight mode, besides requiring further development of the controller as already mentioned. Also to be noted is the fact that at the time of this work, the engine type to be used in the aircraft and its location on the airframe were yet to be decided, and therefore, the engine parameters used in the controller have had to be assigned values that may differ from the actual ones. However, because the controller actively acts upon the aircraft's dynamics when they fall from the intended equilibrium state, such considerations such as the engine location, CG variation due to fuel consumption, weight variation due to fuel consumption or payload jettison, or pitch variation due to acceleration should not interfere with controller ability to maintain flight stability as it will interpret such variations as atmospheric disturbances and act accordingly.

Then, the main achievement of this work was, as it was its objective, to develop and provide a robust controller system that validates the UAV for test flight using a combination of controller techniques accordingly to the situation. It was demonstrated that, contrary to what some previous studies have indicated, the VSMW system is actually liable (or capable) of being actively controllable during flight by achieving the required longitudinal flight stability parameters providing that proper controller optimization is performed.

Despite the main goals of this work have been achieved, much further work can still be performed regarding both the controller algorithm and its evolving into a full autopilot system, as the UAV itself. And such is the topic discussed in the next paragraphs.

As hinted before, the next stage of works concerning the VSMW project involves a test flights trial for the system's operation concept approval and reliability check, as well as data gathering from such flights to update the controller with more accurate values. Meanwhile, there is still plenty of room (despite the best efforts of the author) for improvements in the present controller and its development/integration in a fully operational autopilot system. Such development would probably require the integration of both the present controller with the previous developed roll motion controller.

Regarding the *Olharapo's* project, there are also a few other development projects undergoing in parallel. They involve, for instance, the development of alternative and/or complementary morphing wings technologies and avionics integration. However the precise details and current state of such projects are unknown to the author.

Blank Page

Blank Page

Bibliography

- [1] The MathWorks Inc., et al. *MATLAB 7 Function Reference: Volume 1 (A-E)*. s.l.: The MathWorks, Inc.
- [2] *Getting Started with MATLAB 7*. s.l.: The MathWorks, Inc., 2007.
- [3] Tavares, F. *Roll Motion Control of a Dissymmetrical Wingspan Aircraft* MSc. Dissertation, Department of Aerospace Sciences. Covilhã, Portugal: University of Beira Interior, 2011.
- [4] Stevens, Brian L. and Lewis, Frank L. *Aircraft Control and Simulation*. New York, USA: John Wiley & Sons, Inc, 1992. ISBN 0-471-61397-5.
- [5] Sousa, Maria J. and Baptista, Cristina S. *Como Fazer Investigação, Dissertações, Teses e Relatórios segundo Bolonha*. Lousã, Portugal: PACTOR, 2011. 978-989-693-001-1.
- [6] Roskam, Jan. *Airplane Flight Dynamics and Automatic Flight Controls Part II*. Lawrence, Kansas, USA: DARcorporation, 1998. ISBN 1-884885-18-7.
- [7] Roskam, Jan. *Airplane Flight Dynamics and Automatic Flight Controls Part I*. Lawrence, Kansas, USA: DARcorporation, 2001. ISBN 1-884885-17-9.
- [8] Roskam, Dr. Jan. *Methods for Estimating Stability and Control Derivatives of Conventional Subsonic Airplanes*. Lawrence, Kansas, USA: The University of Kansas, 1971.
- [9] Roskam, Dr. Jan. *Airplane Design Part VII: Determination of Stability, Control and Performance Characteristics: Far and Military Requirements*. Lawrence, Kansas, USA: The University of Kansas, 1991.
- [10] Roskam, Dr. Jan and Lan, Dr. Chuan-Tau Edward. *Airplane Aerodynamics and Performance*. Lawrence, Kansas, USA: DARcorporation, 1997. ISBN 1-884885-44-6.
- [11] Perkins, Courtland D. and Hage, Robert E. *Airplane Performance Stability and Control*. New York, USA: John Wiley & Sons, 1949. ISBN 0-471-68046-X.
- [12] Pamadi, B. N. *Stability, Dynamics and Control of Airplanes*. Hampton, USA: AIAA: American Institute of Aeronautics and Astronautics, Inc. , 1998. ISBN 1-56347-222-8.
- [13] Nelson, Robert C. *Flight Stability and Automatic Control*. New York, USA: McGraw-Hill Book Company, 1989. ISBN 0-07-046218-6.

- [14] Mestrinho, J. *Design of a Variable-Span Morphing Wing* MSc. Dissertation, Department of Aerospace Sciences. Covilhã: University of Beira Interior, 2009.
- [15] McLean, Donald. *Automatic Flight Control Systems*. Hertfordshire, UK: Prentice Hall International Ltd, 1990. ISBN 0-13-054008-0.
- [16] Luo, Jia and Lan, C. Edward. Determination of Weighting Matrices of a Linear Quadratic Regulator: *Journal of Guidance, Control and Dynamics*, 1995. Vols. 18, no.6. pp. 1462-1463.
- [17] Lewis, F.L. *Linear Quadratic Regulator (LQR) State Feedback Design*. [Online] 2008. [Cited: April 19, 2012.] <http://arri.uta.edu/acs/Lectures/lqr.pdf>.
- [18] Abzug, M. J. and Larrabee, E.E. *Airplane Stability and Control*. Second Edition. Cambridge, UK: Cambridge University Press, 2002.
- [19] Kuncicky, David. *MATLAB Programming*, s.l.: E Source, 2003. ISBN-13: 978-0130351272.
- [20] Konstantinov, M.M., Petkov, P. Hr. and Gu, D. W. *Robust Control Design with MATLAB*. London, UK: Springer, 2005. ISBN 10-185233-983-7.
- [21] Hull, David G. *Fundamentals of Airplane Flight Mechanics*. New York, USA: Springer-Verlag Berlin Heidelberg, 2007. ISBN-10 3-540-46571-5.
- [22] Henry, Janisa J. and Pines, Ph.D. Dr. Darryl J. *Roll Control for UAVs by use of a Variable Span Morphing Wing*. Maryland, USA: University of Maryland, 2005.
- [23] Gamboa, Ph.D. Professor P. Projecto UAV01 Part II. [Online] [Cited: April 19, 2012.] http://webx.ubi.pt/~pgamboa/pessoal/2033/2001-2002/Projecto_UAV01_Parte_II.pdf.
- [24] Gamboa, Ph.D. Professor Pedro. [Online] [Cited: 19 April 2012.] <http://webx.ubi.pt/~pgamboa/pessoal/projecto2001/projecto2001.htm>.
- [25] Gamboa, P., et al. Design Optimisation of a Variable-Span Morphing Wing. In *52nd AIAA/ASME/ASCE/AHS/ASC Structures, Structural Dynamics and Materials Conference*, Lisbon, Portugal: s.n., April 2011. Denver, Colorado, USA, pp. Paper no. AIAA 2011-2025.
- [26] Felício, J. *Development and Testing of a Variable-Span Morphing Wing* MSc. Dissertation, Department of Aerospace Sciences. Covilhã: University of Beira Interior, 2010.
- [27] Etkin, B. and Reid, L. D. *Dynamics of Flight Stability and Control*. Third Edition. s.l.: John Wiley & Sons, Inc., 1996. ISBN 0-471-03418-5.
- [28] Deperrois, A. XFLR5 Stability and Analysis. *XFLR5*. [Online] November 2010. [Cited: April 19, 2012.] <http://www.xflr5.com/xflr5.htm>.

- [29] Boiffier, Jean-Luc. *The Dynamics of Flight: The Equations*. New York, USA: John Wiley & Sons, 1998. ISBN 0-471-94237-5.
- [30] Anderson, John D., Jr. *Aircraft Performance and Design*. New York, USA: McGraw-Hill. ISBN 0-07-00197-1.
- [31] Anderson, B. D. O. and Moore, J. B. *Linear Optimal Controler*. s.l.: Prentice-Hall, 1989.
- [32] Handling Qualities Rating Scale. [Online] [Cited: 20 June 2012.] <http://history.nasa.gov/SP-3300/fig66.htm>.
- [33] MATLAB. [Online] [Cited: June 20, 2012.] <http://www.mathworks.com/products/matlab/>.
- [34] Wing Configuration. [Online] [Cited: 20 June 2012.] http://en.wikipedia.org/wiki/Wing_configuration.
- [35] XFLR5. [Online] [Cited: 20 June 2012.] <http://xflr5.sourceforge.net/xflr5.html>.
- [36] The Norden Bomb Sight. *Plane-crazy*. [Online] [Cited: 06 25, 2012.] <http://www.plane-crazy.net/links/nord.htm>.
- [37] Searle, Loyd. The bombsight war: Norden vs. Sperry. *The value sell*. [Online] 09 2009. [Cited: 06 25, 2012.] http://thevaluesell.com/images/LSearle_bombsight.pdf. IEEE 0018-9223/89/0900-0060.
- [38] John, Philip A. St. *Bombardiers of WWII - Vol II (Limited)*. s.l.: Turner Publishing Company, 1998. ISBN 1563113384.
- [39] Sperry Corporation. *Wikipedia*. [Online] [Cited: 06 25, 2012.] http://en.wikipedia.org/wiki/Sperry_Corporation.
- [40] Norden bombsight. *Wikipedia*. [Online] [Cited: 06 25, 2012.] http://en.wikipedia.org/wiki/Norden_bombsight#Autopilot.2C_production_problems.
- [41] Consolidated B-24 Liberator. *Behind Barbed Wire*. [Online] [Cited: 06 25, 2012.] <http://www.behindbarbedwire.org/b-24.htm>.
- [42] Aircraft flight control system. *Wikipedia*. [Online] [Cited: 06 25, 2012.] http://en.wikipedia.org/wiki/Aircraft_flight_control_system.
- [43] Longitudinal Static Stability. [Online] [Cited: 06 25, 2012.] <http://adg.stanford.edu/aa241/stability/staticstability.html>.

- [44] *Aviacion Argentina*. [Online] [Cited: 06 25, 2012.] <http://www.aviacionargentina.net/foros/fuerza-aerea-argentina.4/2113-mirage-cual-es-el-mejor.html>.
- [45] STOVL . *Aviation Explorer*. [Online] [Cited: 06 25, 2012.] http://www.aviationexplorer.com/STOVL_How_Does_Standard_Takeoff_Vertical_Landing_Work.html.
- [46] Pugachev's Cobra. *All About Military*. [Online] [Cited: 06 25, 2012.] <http://all-about-military.blogspot.pt/2009/12/pugachevs-cobra.html>.
- [47] Roskam, Dr. Jan. *Airplane Design Part I: Preliminary Sizing of Airplanes*. Ottawa, USA: Roskam Aviation and Engineering Corporation, 1985.
- [48] Gamboa, P et al. Evaluation of a Variable-Span Morphing Wing for Small UAV. In *52nd AIAA/ASME/ASCE/AHS/ASC Structures, Structural Dynamics and Materials Conference*. Lisbon, Portugal: s.n., April 2011. Denever, Colorado, USA, pp. Paper no. AIAA 2011-2074.
- [49] Bishop, R.H. *Modern Control Systems Analysis & Design Using Matlab & Simulink*. s.l.: Addison Wesley Longman Inc., 1997.
- [50] Ang, K.H., Chong, G.C.Y. and Li, Y. PID Control system analysis, design and technology. *IEEE Transactions on Control Systems Technology*, vol. 13, no. 4, 2005, pp. 559-576.
- [51] Bousson, K. *Flight Mechanics II* lecture notes. Covilhã, Portugal: University of Beira Interior, 2011.
- [52] Bousson, K. *Flight Control Systems* lecture notes. Covilhã, Portugal: University of Beira Interior, 2011.
- [53] Autopilot. *Wikipedia*. [Online] [Cited: 06 25, 2012] <http://en.wikipedia.org/wiki/Autopilot>
- [54] Hillenbrand, L. *Invencível*. Alfragide, Portugal: Publicações Dom Quixote, 2011. ISBN: 978-972-20-4806-4

Blank Page

Blank Page

Appendix

A – UAV “*Olharapo*” Drawings

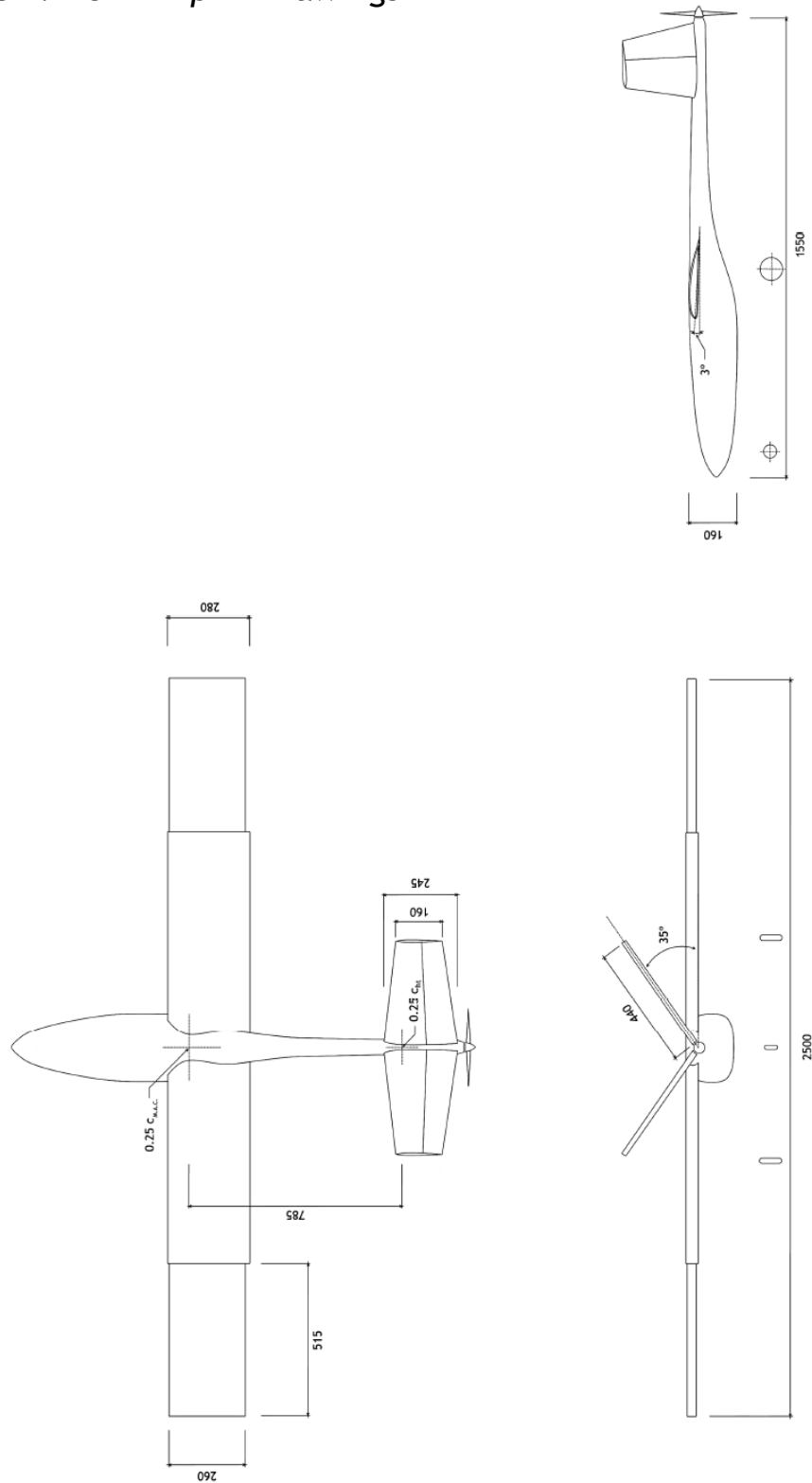


Figure A: UAV “*Olharapo*” 3 views drawings.

Blank Page

B – UAV “Olharapo” Specifications

Module	Parameter	Value	Units
Weight	Empty Weight	3.7000	[kg]
	Max. Take-Off Weight	6.7000	[kg]
Inertial Properties	Ixx	0.6175	[kg.m ²]
	Iyy	0.3410	[kg.m ²]
	Izz	0.9345	[kg.m ²]
	Ixy	0.0000	[kg.m ²]
	Ixz	0.0391	[kg.m ²]
VSMW Geometry	Fuselage Span (at wings intersection section)	0.2000	[m]
	IFW span	0.6250	[m]
	OMW span	0.6250	[m]
	IFW-OMW overlap span	0.1000	[m]
	Max. VSMW wingspan	2.5000	[m]
	Min. VSMW wingspan	1.4500	[m]
	IFW chord	0.2830	[m]
	OMW chord	0.2500	[m]
	VSMW mean chord	0.2665	[m]
	Max. VSMW Area	0.6663	[m ²]
	Min. VSMW Area	0.3864	[m ²]

Longitudinal Derivatives							
Stability Derivatives		Zero Angle of Attack	C_{L_0}	0.11	$[\text{rad}^{-1}]$		
			C_{D_0}	0.089	$[\text{rad}^{-1}]$		
			C_{m_0}	0.06	$[\text{rad}^{-1}]$		
			Aerodynamic Coefficients		C_L	0.61	$[\text{N}]$
					C_D	0.259	$[\text{N}]$
			Given an Angle of Attack		C_{L_α}	4.58	$[\text{rad}^{-1}]$
					C_{D_α}	0.17321	$[\text{rad}^{-1}]$
					C_{m_α}	-2.54	$[\text{rad}^{-1}]$
			Given a Pitch Rate		C_{L_q}	4.888	$[\text{rad}^{-1}]$
					C_{D_q}	0	$[\text{rad}^{-1}]$
					C_{m_q}	-7.995	$[\text{rad}^{-1}]$
			Given an Angle of Attack due to Pitch Rate		$C_{L_{\dot{\alpha}}}$	0	$[\text{rad}^{-1}]$
		$C_{D_{\dot{\alpha}}}$			0	$[\text{rad}^{-1}]$	
		$C_{m_{\dot{\alpha}}}$			0	$[\text{rad}^{-1}]$	
		Control Derivatives		V-Tail Elevator	$C_{L_{\delta v_e}}$	0.127	$[\text{rad}^{-1}]$
					$C_{D_{\delta v_e}}$	0.036361	$[\text{rad}^{-1}]$
					$C_{m_{\delta v_e}}$	-1.8844	$[\text{rad}^{-1}]$
		Engine			Maximum Thrust	25.000	$[\text{N}]$
Derivatives	Stability Derivatives	Given an Angle of Bank	C_{y_β}	-0.272	$[\text{rad}^{-1}]$		
			C_{l_β}	-0.9957	$[\text{rad}^{-1}]$		
			C_{n_β}	0.0036	$[\text{rad}^{-1}]$		
		Given a Roll Rate	C_{l_p}	-0.58	$[\text{rad}^{-1}]$		
			C_{n_p}	-0.0727	$[\text{rad}^{-1}]$		

Lateral-Directional		Given a Rudder Angle	C_{l_r}	0.162	$[\text{rad}^{-1}]$
			C_{n_r}	-0.092	$[\text{rad}^{-1}]$
	Control Derivatives	Dissymmetrical Wing Spans Deflection	$C_{l_{\delta y}}$	-0.183	$[\text{rad}^{-1}]$
			$C_{n_{\delta y}}$	0.028	$[\text{rad}^{-1}]$
			$C_{y_{\delta y}}$	0	$[\text{rad}^{-1}]$
		V-Tail Rudder	$C_{y_{\delta v_r}}$	-1.15	$[\text{rad}^{-1}]$
			$C_{l_{\delta v_r}}$	0.099	$[\text{rad}^{-1}]$
			$C_{n_{\delta v_r}}$	0.36	$[\text{rad}^{-1}]$

Table B: UAV's full stability and control derivatives data and aircraft's specifications.

Blank Page

C – Handling Qualities Data

Level 1	The flying qualities are completely adequate for the particular flight phase being considered.
Level 2	The flying qualities are adequate for the particular phase being considered, but there is either some loss in the effectiveness of the mission, or there is a corresponding increase in the workload imposed upon the pilot to achieve the mission, or both.
Level 3	The flying qualities are such that the aircraft can be controlled, but either the effectiveness of the mission is gravely impaired, or the total workload imposed upon the pilot to accomplish the mission is so great that it approaches the limit of his capacity.

Table C1: Flight Levels [3][15].

Class I	Small, light aircraft (max. weight = 5 000 kg)
Class II	Aircraft of medium weight and moderate manoeuvrability (weight between 5 000 and 30 000 kg).
Class III	Large, heavy aircraft with moderate manoeuvrability (weight above 30 000 kg).
Class IV	Aircraft with high manoeuvrability.

Table C2: Airplane Classes [3][15].

Non-terminal phase of flight	
Category A	Includes all the non-terminal phases of flight such as those involving rapid manoeuvring, precision tracking, or precise control of the flight path. Included in category A would be such flight phases as: Air-to-Air Combat (CO or ACM); Ground Attack (GA); Weapon Delivery (WD); Reconnaissance (RC); Air-to-Air Refuelling in which the aircraft acts as the receiver (RR); Terrain Following (TF), Maritime Search and Rescue (MS or MSAR), Close Formation Flying (FF), and Aerobatics (AB).
Category B	Involves the non-terminal phases of flight usually accomplished by gradual manoeuvres which do not require precise tracking. Accurate flight path control may be needed, however. Included this category would be: Climbing (CL); Cruising (CR); Loitering (LO); Descending (D); Aerial Delivery (AD) and Air-to-Air Refuelling in which the aircraft acts as the tanker (RT).
Terminal phase of flight	
Category C	Involves terminal flight phases, usually accomplished by gradual manoeuvres, but requiring accurate flight path control. This category would include: Take-Off (TO); Landing (L); Overshoot (OS) and powered approach (including instrument approach) (PA).

Table C3: Flight Categories [3][15].


Phugoid Mode		Level 1	$\zeta > 0.04$			
		Level 2	$\zeta > 0$			
		Level 3	T2 > 55 seconds			
Short-Period Mode		Categories A and C		Category B		
		minimum ζ	maximum ζ	minimum ζ	maximum ζ	
	Level 1	0.35	1.30	0.3	2.0	
	Level 2	0.25	2.00	0.2	2.0	
	Level 3	0.15	—	0.15	—	

Table C4: Longitudinal Phugoid and Short-Period Flight Qualities Parameters [3][15].

Spiral Mode				
Class	Category	Level 1	Level 2	Level 3
I and IV	A	12 seconds	12 seconds	4 seconds
	B and C	20 seconds	12 seconds	4 seconds
II and III	All	20 seconds	12 seconds	4 seconds

Table C5: Lateral-directional's Spiral Flight Qualities Parameters [3][15].

Roll Mode				
Class	Category	Level 1	Level 2	Level 3
I and IV	A	1.0 seconds	1.4 seconds	10 seconds
II and III	A	1.4 seconds	3.0 seconds	10 seconds
All	B	1.4 seconds	3.0 seconds	10 seconds
I and IV	C	1.0 seconds	1.4 seconds	10 seconds
II and III	C	1.4 seconds	3.0 seconds	10 seconds

Table C6: Lateral-directional's Roll Flight Qualities Parameters [3][15].

Dutch Roll Mode					
Level	Category	Class	minimum ξ	minimum ω_n [rad/s]	minimum $\xi \times \omega_n$ [rad/s]
Level 1	A	I and IV	0.19	1.0	0.35
	A	II and III	0.19	0.5	0.35
	B	All	0.08	0.5	0.15
	C	I and IV	0.08	1.0	0.15
	C	II and III	0.08	0.5	0.1
Level 2	A	I and IV	0.02	0.5	0.05
	A	II and III	0.02	0.5	0.05
	B	All	0.02	0.5	0.05
	C	I and IV	0.02	0.5	0.05
	C	II and III	0.02	0.5	0.05
Level 3	A	I and IV	0	0.4	—
	A	II and III	0	0.4	—
	B	All	0	0.4	—
	C	I and IV	0	0.4	—
	C	II and III	0	0.4	—

Table C7: Lateral-directional's Dutch Roll Flight Qualities Parameters [3][15].

Blank Page

Blank Page

D – Simulation's Full Output Data Example

Normal Simulation

Disturbances Case 2

Altitude Hold Mode Selected

Automatic Symmetrical Wingspan Variation with Flight Speed Mode Activated

b = 2.1500

Longitudinal Stability Achieved

X =

25.0000

0

-0.0000

0.0416

0

0.0000

-0.0000

0

U =

-0.0242

0.8476

-0.0000

0.0000

A =

-0.2204	0.0000	0.0352	0.5599	-0.0000	0	0	0
-0.7839	0	24.1527	-152.3447	-0.0000	0	0	0
0.0000	0	-7.2629	-432.9078	0	-0.0000	0.0000	0
0	0	1.0000	0	0	0	0	0.0000
-0.0000	0.0000	0	0	-0.4805	0	-25.0000	9.7982
0.0000	0	0.0000	0	-30.2762	-19.0869	5.1775	0
0.0000	0	0.0000	0	-0.5426	-2.3661	-1.7685	0
0	0	0	-0.0000	0	1.0000	0.0416	-0.0000

B =

1.3542	3.7313	0	0
-4.0810	0	0	0
-321.1699	0	0	0
0	0	0	0
0	0	0	-37.4319
0	0	-138.4317	86.8240
0	0	8.2641	184.2544
0	0	0	0

Vp_A =

-22.9552
 -3.6314 +20.4871i
 -3.6314 -20.4871i
 -0.2204
 0.0000
 0.9529 + 8.9034i
 0.9529 - 8.9034i
 -0.2864

C =

1	0	0	0	0	0	0	0
0	1	0	0	0	0	0	0
0	0	1	0	0	0	0	0
0	0	0	1	0	0	0	0
0	0	0	0	1	0	0	0
0	0	0	0	0	1	0	0
0	0	0	0	0	0	1	0
0	0	0	0	0	0	0	1

The System is Longitudinally Controllable

The System is Longitudinally Observable

Handling Qualities: Cruise Mode Selected (Level 1, Class I, Category B)

$\lambda =$

-2.2500 + 1.9843i

-2.2500 - 1.9843i

-0.0693 + 0.1588i

-0.0693 - 0.1588i

0

0

0

0

$R =$

0.0821 0 0 0

0 0.0100 0 0

0 0 0.0377 0

0 0 0 0.0821

$Q =$

0.0059 0 0 0 0 0 0 0

0 0.0001 0 0 0 0 0 0

0 0 0.0200 0 0 0 0 0

0 0 0 0.0137 0 0 0 0

0 0 0 0 0.0491 0 0 0

0 0 0 0 0 0.0006 0 0

0 0 0 0 0 0 0.1072 0

0 0 0 0 0 0 0 0.0161

$\xi =$

23.0000

2.0000

0.0300

0.0716

-2.0000

-0.0300

-0.0300

-0.0300

Longitudinal Flight Control With a Variable Span Morphing Wing
UBI – DCA

K =

-0.0001	0.0248	-0.4789	-1.7043	0.0000	0.0000	0.0000	0.0000
0.7115	-0.0043	0.0031	0.1096	-0.0000	-0.0000	-0.0000	-0.0000
0.0000	-0.0000	-0.0000	0.0000	0.0296	-0.0898	0.1599	-0.9866
0.0000	0.0000	-0.0000	-0.0000	-0.7496	-0.0042	1.0725	-0.2910

Velocity; Altitude, Pitch Angle, Wingspan, Bank Angle, Vertical Speed, Lateral Speed,
Angle of Attack, Trajectory Angle, Pitch Rate

ATTITUDE =

25.0000
60.0000
2.3809
2.1500
0
0
0
5.6429
-3.2620
-0.0000

Blank Page

Blank Page

E - Paper

Longitudinal Flight Control with a Variable Span Morphing Wing

KOUAMANA BOUSSON, PEDRO GAMBOA, TIAGO SANCHES

Department of Aerospace Sciences
University of Beira Interior
Convento de Sto. António 6201-001 Covilhã
PORTUGAL
k1bousson@yahoo.com, tiago_sanches@sapo.pt

Abstract: - The present study focuses on the design of a longitudinal flight controller for an unmanned aircraft equipped with dissymmetric variable-span system (VSMW or Variable-Span Morphing Wing). It's primary role consists in the longitudinal flight stabilization of the aeroplane while in levelled cruise flight, although, it was designed to offer longitudinal flight stabilization for other flight phases as well, such as e.g. take-off and landing. The stabilization algorithm relies on the most up-to-date developments in the state-of-the-art LQR and *Batz-Kleinman* controller techniques to stabilize the aircraft on its intended longitudinal attitude upon any small atmospheric disturbances inflicted. It was designed for the experimental UAV prototype “*Olharapo*” equipped with the VSMW, so it can automatically adjust the VSMW's overall wingspan in accordance with the flight speed and stabilize the aircraft in the desired attitude, although, its modular concept allows it to be used for different configurations of the aircraft or even for a different aircraft. The development, simulation and testing of the algorithm were done using the MATLAB[®] software and the aircraft's stability and control derivatives previously obtained using the XFLR[®] software. Minor adaptations of the flight dynamics equations were performed to allow the compatibilization with the VSMW. The required implementation of imposed flight qualities was also performed to ensure proper scaling the controller weight matrix for optimal values. Finally, the algorithm was tested using two different methods: Classic Disturbances Simulation and Sinusoidal Pitch Variation Response.

Key-Words: - Aircraft, Autopilot, *Batz-Kleinman* Controller, Flight Stabilization, Linear Quadratic Regulator, Longitudinal Flight Dynamics, LQR, Morphing Technology, Robust Controller, UAV, Variable-Span Wing..

1 Introduction

Since the very beginning of the aviation history that the need for stability and control had been acknowledged by both aircraft makers and aviators (pilots). Not only it was perceived as fundamental for flight safety as, as the military operators realized the enormous potential of aircraft for combat, it became mandatory. Indeed, the fast developments in aerodynamics

theory quickly led to improvements in aircraft design and its pilot-to-control-surfaces interaction, thus increasing flight stability and controllability which allowed for increased flight safety. However, as both military and civilian pilot's workload progressively increased with the need to operate an increasingly higher amount of complex systems on longer flights, the need to assist the pilot with automatic controls

for all kind of tasks, including the flight itself, became imperative. And so, in 1914 the *Sperry Corporation* showed its first gyroscopic stabilizer system in a demonstration flight over Paris. That was in fact, the first mechanical autopilot in history as it allowed the aircraft to fly straight and levelled in a given compass direction, and even allowed for a controlled take-off and landing [16].

The first all-electronic A-5 autopilot was developed in 1940, and marked the beginning of the digital era by surpassing the previous autopilot systems in almost every aspects [12][13][14].

However, even with the nowadays equipment, the optimization of such stabilization systems for a specific aircraft remains a critical factor. Especially if that aircraft incorporates new morphing technologies that alter the traditional control method by standard control surfaces.

This work is structured in the following way: section 2 describes the problem that originated the need for this work; section 3 presents the theory behind the solution to such problem; section 4 presents an analysis to the results of the application of such solution; and section 5 the conclusions to be obtained from this work.

2 Problem Statement

The VSMW is an experimental wing designed and developed at UBI (University of Beira Interior) that can both symmetrically or dissymmetrically change its overall wingspan in order reduce drag, increase lift, or perform a roll. As such, there was the need for an automatic system to control the wingspan variation in the various flight phases in accordance with the required flight criteria such as the airspeed or climb ratio. This work concerns only about the longitudinal flight stabilization of the, also experimental UAV, “*Olharapo*”, also developed at UBI, when equipped with the VSMW system. For roll control and

lateral-directional stability matters please refer to the previous work “*Roll Motion Control of a Dissymmetrical Wingspan Aircraft*” [2].

3 Solution Proposal

The solution consists in making full use of the fundamentals of Flight Dynamics Theory, Aircraft Stability and Control Theory, Aircraft Handling Theory and up-to-date Control Methods to develop and test a Longitudinal Flight Controller algorithm adjusted to the VSMW particularities. Therefore, both the algorithm and its respective testing simulations were performed using MATLAB[®] software [1] and two different control methods known as LQR and *Batz-Kleinman* methods. However, in order to fully understand the scope of this project and its results, a brief summary of theory involved is provided in the following sections.

3.1 Longitudinal Flight Dynamics

For longitudinal flight control only purposes, all the non-longitudinal parameters can be considered null, and it is thereby enough to solely use the longitudinal velocity (u), the vertical velocity (w), the pitch angle (θ), the pitch rate (q), the throttle percentage (δ_T), the elevators deflection (δ_e), the angle of attack (α), the path angle (γ) and the altitude (h) variables of an aircraft motion equations.

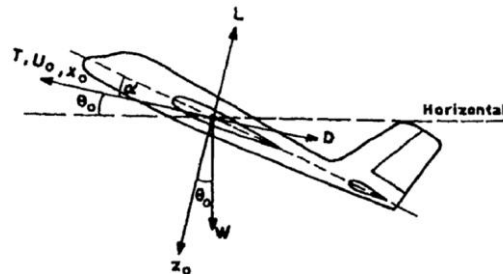


Fig. 1 Forces and Angles concerning the longitudinal flight plane analysis [2][4]

Figures 1 and 2 illustrate the relation between such variables, the body-axis system, and the four main forces that act

upon an in-flight aircraft, namely Lift (L), Drag (D), Thrust (T), and Weight (W).

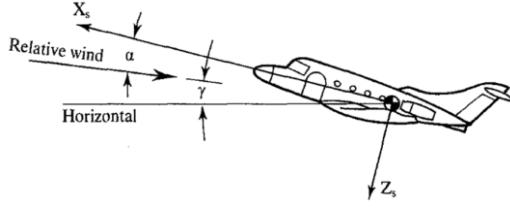


Fig. 2 Relation between α and γ [2][11]

Figure 3 shows the relation between the elevator deflection (δ_e or δ_{et} as shown in the figure) and the tail's angle of attack (α_t) associated to the pitch moment (M), and thus also to both pitch angle (θ) and pitch rate (q).

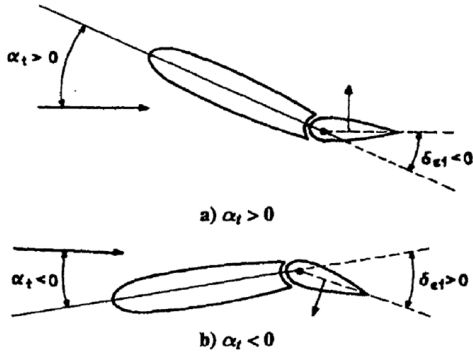


Fig. 3 Effect of the elevator's deflection (δ_e) on α_t [2][4]

Figure 4 illustrates how the tail's pitch moment (M_t) resultant from the variation in (α_t) adds to the wing's pitch moment (M_w) due to α to cause an overall pitch moment (M or M_f as depicted in Fig.4) acting upon the aircraft's Centre of Gravity (C.G.).

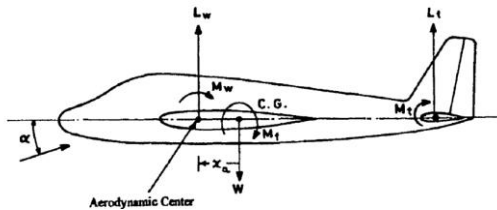


Fig. 4 Forces and Moments acting on a levelled-flight aircraft [2][4]

As the angle of attack (α) relates to the longitudinal and vertical velocities as [2][11]:

$$\alpha = \tan^{-1} \frac{w}{u} \quad (1)$$

with [2][11]:

$$u = V \cos \alpha \quad (2)$$

$$w = V \sin \alpha \quad (3)$$

And since [2][6][11]:

$$\theta = \alpha + \gamma \quad (4)$$

$$V = \sqrt{u^2 + w^2} \quad (5)$$

$$Q = \frac{1}{2} \rho V^2 \quad (6)$$

Where V represents the velocity vector resultant from the longitudinal and vertical velocities, and Q represents the dynamic pressure.

The only applied moment coefficients to this flight mode are the drag, lift and pitch related ones [2][3][11]:

$$C_D = C_{D_0} + C_{D_\alpha} \alpha + C_{D_{\delta_e}} |\delta_e| \quad (7)$$

$$C_L = C_{L_0} + C_{L_\alpha} \alpha + C_{L_{\delta_e}} \delta_e + C_{L_q} \frac{q \bar{c}}{2V} + C_{L_{\dot{\alpha}}} \frac{\dot{\alpha} \bar{c}}{2V} \quad (8)$$

$$C_m = C_{m_0} + C_{m_\alpha} \alpha + C_{m_{\delta_e}} \delta_e + C_{m_q} \frac{q \bar{c}}{2V} + C_{m_{\dot{\alpha}}} \frac{\dot{\alpha} \bar{c}}{2V} \quad (9)$$

Therefore, the general flight equations can be reduced to [2][11]:

$$\dot{u} = \frac{1}{m} \left(\frac{1}{2} \rho(h) S u^2 (1 + \tan^2 \alpha) (C_L \sin \alpha - C_D \cos \alpha) + T \cos \epsilon_T \right) - g \sin \theta - q w \quad (10)$$

$$\dot{w} = \frac{1}{m} \left(T \sin \epsilon_T - \frac{1}{2} \rho(h) S u^2 (1 + \tan^2 \alpha) (C_D \sin \alpha - C_L \cos \alpha) \right) + g \cos \theta + q u \quad (11)$$

$$\dot{\gamma} = \frac{T \sin(\alpha + \varepsilon_T) + \frac{1}{2} \rho(h) V^2 S C_D}{mV} - \frac{g}{V} \cos \gamma \quad (12)$$

$$\dot{h} = u \sin \theta - w \cos \theta \quad (13)$$

$$\dot{q} = \frac{\rho(h) u^2 (1 + \tan^2 \alpha) S \bar{C}_m}{2 I_{yy}} \quad (14)$$

$$\dot{\theta} = q \quad (15)$$

With both thrust and its coefficient variables given by:

$$T = \frac{1}{2} \rho(h) S u^2 (1 + \tan^2 \alpha) C_T \quad (16)$$

$$\text{and } C_T = C_{T\delta_T} \delta_T. \quad (17)$$

3.2 Handling Qualities and Flight Stability

The handling qualities of an aircraft are the quality characteristics that determine the ease and precision with which the pilot controls that aircraft. The stability augmentation systems are means by which the appropriate handling qualities can be properly attributed to an aircraft. Such systems are based on the concepts of state feedback control that allow the improvement of the control and stability of an aircraft that does not comply with the desirable handling qualities. When a trimmed aircraft meets the required/desirable handling qualities, it performs a natural frequency motion if disturbed from its equilibrium state [2].

According to the *Cooper-Harper* Scale, there are certain limits to the natural frequency, damping and period for each mode that define the respective flying characteristics of the aeroplane. And each mode's respective Eigen value is obtained from the characteristic equation of the state

matrix A . It is important to notice that negative eigenvalues refer to converging motions, which represent dynamically stable flying modes [2].

The equilibrium state of an aeroplane is defined by the absence of resultant forces or moments applied to its C.G.. The static stability consists on the tendency of the aircraft to return to its previous equilibrium state after a disturbance of flight. This will happen only if the aeroplane has restoring moments or forces to counter the disturbance.

The dynamic stability however, focuses on what happens to the motion of the aeroplane for the duration of the disturbance. For that matter, dynamic stability can be achieved by either oscillatory (damped or undamped) or non-oscillatory motions [2][5][6]. However, it is important to notice that although an aeroplane may be statically stable but dynamically unstable, if the aeroplane is dynamically stable, then it must be statically stable as well.

The oscillatory modes can be described by a second-order equation, based on the principle of a rigid body attached to a spring and a damping device [2][5]. The spring has a natural frequency of ω_n and the damping device a damping rate of ξ . The characteristic equation for this system is therefore as follows:

$$\lambda^2 + 2\xi\omega_n\lambda + \omega_n^2 = 0 \quad (18)$$

Where the two roots, in the complex form of $\lambda = a \pm bi$, are given by:

$$\lambda_{1,2} = -\xi\omega_n \pm \omega_n\sqrt{1 - \xi^2}i \quad (19)$$

In longitudinal flight (which includes level-flight, climbing, and descending flight attitudes), two modes can be acknowledged: phugoid (long-period) and short-period oscillations.

The phugoid motion is created when, locking the angle of attack (α), there is a natural long-period oscillatory motion with variations of speed, altitude and attitude. In other words, the phugoid oscillation occurs as an exchange of kinetic and potential energy when there is a variation in both pitch angle (θ) and longitudinal speed (u) with almost no variation of α , that later returns to its equilibrium point [2]. This flight mode is dependant only of the equilibrium speed of a given airplane as stated by *Lanchester* in 1908 [15].

The short-period oscillation consists of a rotation around the yy axis of the vehicle when affected by a vertical disturbance such as an air blast in a thermal column updraft or a downdraft on an air-pocket. During this mode the longitudinal airspeed remains constant as the vertical draft disturbance causes a variation of the angle of attack (α) which in turn leads to a variation in lift causing a pitch moment that disrupts attitude equilibrium. In the short-period mode the aircraft may not have the ability to return to its initial attitude equilibrium depending on the severity of the disturbance and on the fact of the aeroplane being either dynamically stable or unstable. By other words, the short-period mode is a usually heavily damped oscillation with a period of only a few seconds where the fast pitching of the aircraft about its C.G. generates a variation of the angle-of-attack (α). As the name suggests, the short-period has a shorter oscillation period than the phugoid, which prevents a promptly response of the pilot to correct aircraft's attitude, and thereby requiring a proper damping by the aircraft itself in order to sustain longitudinal dynamic stability. In fact, the period is so short that that the speed does not have time to change. However, this allows the identification of each conjugated eigenvalue, obtained from the state-matrix A of the linear mode, where the period is determined by [2][15]:

$$T_p = \frac{2\pi}{\omega_n \sqrt{1 - \xi^2}} \quad (20)$$

With $\omega_n = |\lambda|$ and:

$$\xi = -\frac{a}{\omega_n} \quad (21)$$

Finally, by defining the longitudinal flight modes of the aeroplane in accordance with the *Cooper-Harper* Scale system, it's now possible to define the parameters of the controller's algorithm.

3.2.1 Imposed Flying Qualities

The imposition of the eigenvalues, in accordance with the *Copper-Harper* Scale system, to the controller allows the optimization of the Q matrix, resulting in an optimal longitudinal controller for any flight phase. It was concluded that the values to be used in the controller could be the same for all the three different flight categories as presented in table 1:

Longitudinal Motion Theory values for a Level 1, Class I Aeroplane			
Motion Theory	ω_n	ξ	T_2
Short-Period	3	0.75	—
Long-Period	—	0.40	10 s

Table 1 Chosen values for eigenvalue calculation

The eigenvalues vector (or eigenvector) composed by these calculated values to be used in control optimization is then given by:

$$\lambda = [\lambda_{SP} \ \lambda_{LP}] = [-2.25 \pm 19843i \ -0.0693 \pm 0.1588i] \quad (22)$$

3.3 Block Diagram of a Control System

The amount of energy required to operate an aeroplane (specially an unstable intended one (generally for improved manoeuvrability purposes)) is indeed one of main reasons that justifies the need for an optimal control system as it minimizes the energy loss in the stabilization process. Therefore it is crucial to understand the concept of a full system block diagram when designing a full state regulator that is later intended for actual physical implementation. The scheme is composed by the controller itself and all the systems and subsystems that influence the aircraft's attitude. However, most aircraft's control systems are still based on the more elementary scheme of a general AFCS (Automatic Flight Control System) as depicted on Figure 5:

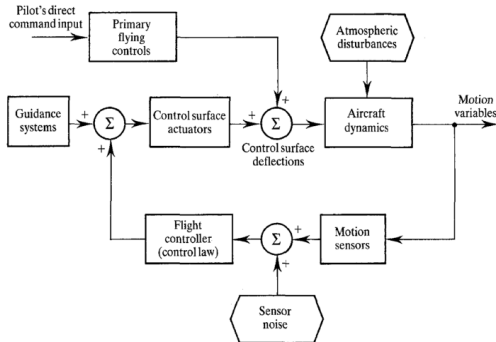


Fig. 5 General block diagram of an AFCS [2][6]

Therefore, a Longitudinal Flight Controller may be perceived as a component of an AFCS, that generally is part of a larger system known as FMS (Flight Management System) and it is responsible for the monitoring and control of the aircraft's longitudinal speed and attitude (climb, dive, or levelled-flight attitudes) via elevators, throttle, flaps and airbrakes actuators and can be represented by the block diagram of Figure 6:

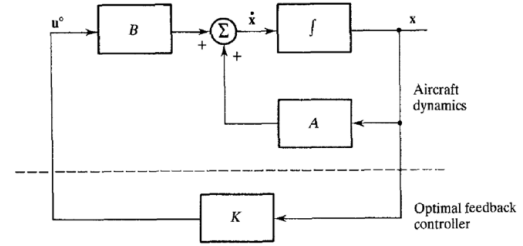


Fig. 6 Closed loop state regulator with optimal feedback [2][6]

Figure 5 exemplifies how the control variables (u) obtained from the system linearization for a given equilibrium state are iterated to allow the stabilization of the state variables (x) by means of the control surface's actuators in a LQR controller. Blocks A , B and K represent respectively the state, control and gain matrices explained later in the next Section. Whereas the integral block (f) represents the solution of the differential equation $\dot{x} = Ax + Bu$ achieved by using K in the LQR's control law. Analogously, Figure 6 would also represent a *Batz-Kleinman* controller if the K block was replaced by an L block indicating the use of an L matrix instead of the K matrix in the control law.

3.3.1 LQR Controller

In a LQR controller, the time-continuous linear system is described by [2][4][6][8][10][11]:

$$\begin{cases} \dot{x} = Ax + Bu \\ \dot{y} = Cx + Du \end{cases}, x \in \mathbb{R}^n \text{ and } u \in \mathbb{R}^m$$

The cost function is defined as:

$$J = \int_0^{+\infty} F(x, u) dt \quad (23)$$

$$\text{With } F(x, u) = x^T Q x + u^T R u. \quad (24)$$

As for longitudinal flight, A is the *Jacobian* matrix of F concerning the aircraft's state vector x and B the *Jacobian* matrix concerning the aircraft's control vector u obtained from linearization.

$$A = \begin{bmatrix} (\nabla_x f_V(x_0, u_0))^T \\ (\nabla_x f_Y(x_0, u_0))^T \\ (\nabla_x f_q(x_0, u_0))^T \\ (\nabla_x f_\theta(x_0, u_0))^T \end{bmatrix}; B = \begin{bmatrix} (\nabla_u f_V(x_0, u_0))^T \\ (\nabla_u f_Y(x_0, u_0))^T \\ (\nabla_u f_q(x_0, u_0))^T \\ (\nabla_u f_\theta(x_0, u_0))^T \end{bmatrix}$$

$$x = [V \ Y \ q \ \theta]^T; \ u = [\delta_e \ \delta_T]^T$$

Where u must be such that it minimizes the cost function on the following way:

$$u: \rightarrow u(x): J(u) = \int_0^{+\infty} (x^T Q x + u^T R u) dt$$

The feedback control law that minimizes the cost function in eq. 23 is described by:

$$u = -Kx \quad (25)$$

Where $K \in \mathbb{R}^{m \times n}$ is the system's gain matrix determined by:

$$K = R^{-1} B^T P \quad (26)$$

This cost function (eq. 23) is often defined as a sum of the deviations of key measurements from their desired values.. However, the main problem while properly scaling a LQR controller, i.e. fine-tuning the controller for optimal performance, resides in finding the adequate weighting factor's Q and R matrices. In general LQR design, Q and R are simply determined by *Bryson's method* [2][11], where each state (Q matrix) and control (R matrix) parameter (diagonal element) is calculated in relation to its maximum amplitude:

$$Q_{ii} = \frac{1}{x_{i,\max}^2} \quad R_{ii} = \frac{1}{u_{i,\max}^2} \quad (27)$$

Although this method being a good starting point for trial-and-error iterations on the search for the intended controller results, it is somehow limited by its maximum state values as, even though the control values are limited only by their control surface's maximum physical

properties, they lack a more proper optimization algorithm.

However, is available since 1995 a better alternative method for the Q and R matrices estimation proposed by *Jia Luo* and *C. Edward Lan* [7]. The R matrix is still determined using Bryson's method [2][11] (eq. 27), as the problem lies, as noted before, in the determination of the optimal state values of the Q matrix. In this method, the cost function J (eq. 23) is minimized by a Hamiltonian matrix H , which is used to determine P .

Q and R are, as stated before, weighting matrices for, respectively, the state and control variables, and must be respectively defined as positive-semidefinite and positive-definite. Considering the Theorem whereby a symmetrical matrix has only real eigenvalues, it can be deduced that when $Q = Q^T, Q \geq 0$, all its eigenvalues are $\lambda_i(Q) \geq 0$ and, when $R = R^T, R > 0$, then all its eigenvalues are $\lambda_i(R) > 0$.

The R matrix is therefore a Penalization (or Ponderation) matrix of the control vector, which allows a certain flexibility upon its generation, and is therefore calculated by *Bryson's method* (eq. 27). However the Q matrix must be such that its eigenvalues match the eigenvalues from a group I Hamiltonian matrix H . Accordingly to the principle of the *Pontriagin's Maximum*, the Hamiltonian matrix is associated to the LQR's "P Problem" in the following way:

$$P \left\{ \begin{array}{l} \dot{x} = Ax + Bu \\ J(u) = \int_0^{+\infty} (x^T Q x + u^T R u) dt \Rightarrow \\ \Rightarrow H = \begin{bmatrix} A & -BR^{-1}B^T \\ -Q & -A^T \end{bmatrix} \end{array} \right. \quad (28)$$

The eigenvalues of H are thereby symmetrically distributed in relation to the imaginary axis, thus having positive and negative symmetrical real parts only. And as the "P Problem" is part of the \hat{A} matrix

of the LQR's feedback system described as follows:

$$\hat{A} = A - BR^{-1}B^TP \quad (29)$$

P is found by solving the continuous time algebraic *Riccati*'s equation [2][7] [11] in eq. 30:

$$A^TP + PA - PBR^{-1}B^TP + Q = 0 \quad (30)$$

As the eigenvalues of \hat{A} are the same of those of the Group I of the Hamiltonian matrix H, they can be specified as:

$$\begin{cases} \lambda_1 = \mu_1 + i\omega_1; \\ \vdots \\ \lambda_n = \mu_n + i\omega_n; \end{cases} \quad (31)$$

With $\text{Re}(\lambda_n) = \mu_n < 0$; $\text{Im}(\lambda_n) = \omega_n = 0$. Therefore, the state matrix Q must be determined such that:

$$\forall i: \det(\lambda_i I - H) = 0 \quad (32)$$

Where I is an Identity matrix.

For simplified calculations it is enough to use the state matrix A's eigenvalues, but in order to minimize the cost function J (eq. 23) under certain imposed flight qualities, and therefore, these eigenvalues must be subjected to such impositions. The Q matrix is thereby defined as a diagonal matrix composed by a single vector $q_i = [q_1 \ q_2 \ \dots \ q_n]^T$. To satisfy the prior condition (eq. 32), q_i must be such that:

$$\begin{aligned} \forall i: f_i(q_i) = \det(\lambda_i I - H(q_i)) = 0 \Rightarrow \\ \xrightarrow{\text{in order to minimize}} J(q) = \sum_{i=1}^n (f_i(q))^2 \end{aligned} \quad (33)$$

As Q is positive-semidefinite with Group I eigenvalues, the "diagonal vector" is rather defined as $q_i = [q_1^2 \ q_2^2 \ \dots \ q_n^2]^T$ to prevent the case of any of the determined q_i values being negative. A new control law comes as:

$$u = u_{\text{ref}} - K(x - x_{\text{ref}}) \quad (34)$$

This allows the LQR controller to fully stabilize an aircraft state and control variables for optimized R and Q weighting matrices.

3.3.2 Batz-Kleinman Controller

This method is in all identical to the LQR method, except by the gain matrix, now defined by the following L matrix [2]:

$$L = B^T(P(\tau))^{-1} \quad (35)$$

Where P is now defined by the *Gramian* as [2]:

$$P(\tau) = \int_0^\tau e^{-At} B B^T e^{-A^T t} dt \quad (36)$$

Where an always positive assumed variable τ appears to limit the integration interval for optimization purposes. The smaller the variable τ , the smaller the control amplitude, and the faster the convergence for optimal values [2].

The control law is, therefore the same as that of the LQR but with the gain matrix L instead of the previous K one:

$$u = u_{\text{ref}} - L(x - x_{\text{ref}}) \quad (37)$$

It must be mentioned that although several other control methods are available. These ones are the most efficient ones, and therefore the most appropriated to use in this work.

3.4 VSMW equipped "Olharapo"

The "Olharapo" is an UAV designed and developed by students at the University of Beira Interior, as is its new telescopic wing, designated VSMW. The main goal of this wing is to allow a performance optimization by reducing its wingspan, and thus also reducing its drag. Due to its small size, the wing must also allow roll control through dissymmetrical wings "deflection". And, because it is an UAV, the entire process must be fully automated, which primarily justifies the requirement for the

development of Roll-Motion [2] and Longitudinal Flight Controllers.

Based in a study presented back in 2011 by *Gamboa et all* [9], it was possible to deduce the equations that relate velocity (V), overall symmetric wingspan (b), and the angle of attack (α).

$$\alpha(V) = \frac{2}{(V - 11)/15} - 3,5 \quad (38)$$

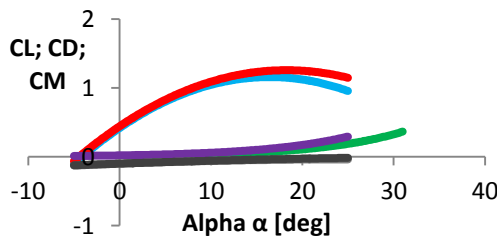
The angle of attack (α) assumes therefore, a maximum amplitude (α_{\max}) of 15 degrees at minimum flight speed ($V_{\min} = 10\text{m/s}$) and then decreases according to eq. 38 until it stabilizes at approximately 3.5 negative degrees (α_{\min}) for flight speeds above 40 m/s.

$$b(V) = -\frac{(V - 20)}{14.2858} + 2.5 \quad (39)$$

Equation 39 shows how the wingspan is at its maximum extension of 2.5m for airspeeds lower than 20m/s, and gradually decreases until it reaches the minimal wingspan of 1.45m at speeds greater than 35m/s.

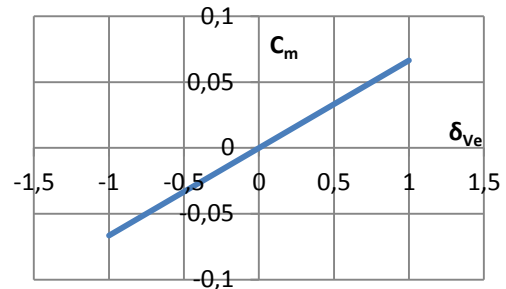
These equations (eq. 38 and eq. 39) are of the utmost importance for this work as are they that mostly define the particularities of the application of the VSMW.

One important thing to be noticed is the capability of the UAV to increase its lift in order to climb by extending its wings without the necessity of an increase in pitch or power. Such capability is even more evident at angles of attack (α) higher than 10 degrees, as seen in graph 1.

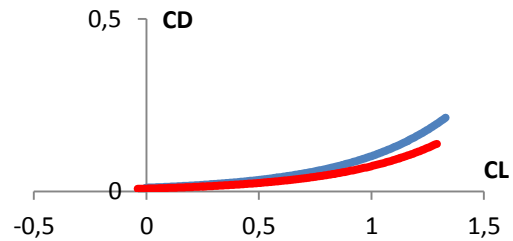


Graphic 1 VSMW Polars for b_{\max} and b_{\min}

Graphic 1 was obtained through a detailed analysis to the provided data for a flight condition of 20m/s MSL. The red and blue lines are respective to the Lift Coefficient (C_L) for respectively b_{\max} and b_{\min} , and analogously purple and green lines are respective to the Drag Coefficient (C_D). Graphics 2 and 3 provide an overview on the expected Pitch Moment Coefficient (C_m [rad $^{-1}$]) distribution due to the elevator deflection (δ_{V_e} [%]) and drag reduction ratio respectively.



Graphic 2 Expected C_m distribution due to δ_{V_e} percentage



Graphic 3 Effective drag reduction from maximum (red) wingspan to fully retracted (blue) OMWs

Another particularity of this aircraft is its V-Tail, which means, δ_e had to be replaced by an δ_{V_e} given by the software XFLR5[®] taking into account the tail's geometry. All the aircraft parameters are specified in the table below:

Parameter	Value
Empty Weight	3.7000
Max. Take-Off Weight	6.7000
Ixx	0.6175
Iyy	0.3410
Izz	0.9345
Ixy	0.0000

I_{xz}	0.0391
Fuselage Span	0.2000
IFW span	0.6250
OMW span	0.6250
IFW-OMW overlap span	0.1000
Max. VSMW wingspan	2.5000
Min. VSMW wingspan	1.4500
IFW chord	0.2830
OMW chord	0.2500
VSMW mean chord	0.2665
Max. VSMW Area	0.6663
Min. VSMW Area	0.3864
C_{L_0}	0.11
C_{D_0}	0.089
C_{m_0}	0.06
C_L	0.61
C_D	0.259
C_{L_α}	4.58
C_{D_α}	0.17321
C_{m_α}	-2.54
C_{L_q}	4.888
C_{D_q}	0
C_{m_q}	-7.995
$C_{L_{\dot{\alpha}}}$	0
$C_{D_{\dot{\alpha}}}$	0
$C_{m_{\dot{\alpha}}}$	0
$C_{L_{\delta v_e}}$	0.127
$C_{D_{\delta v_e}}$	0.036361
$C_{m_{\delta v_e}}$	-1.8844
Maximum Thrust	25.000

Table 2 *Olharapo*'s Specifications

4 Applications

Using the stability and control derivatives provided by XFLR5[®] and MATLAB[®] software analysis, and theories described in the previous section, it was possible to develop, test and simulate an algorithm for longitudinal flight control of the experimental UAV "*Olharapo*" when equipped with the also experimental VSMW system. However it is important to refer that, a prior compatibilization of the flight equations system with both the controller methods (LQR and *Batz-Kleinman*), through a linearization of that

system, was performed as a requirement of such methods.

Three simulation types were then performed to completely prove the working concept and reliability of this Longitudinal Controller System: Classical Disturbances Simulation; Sinusoidal Pitch Variation Test; and Random Pitch Variation Test.

The time domain method, offers an easy concept where the control variables are described by first-order differential equations easily solved with computational software like the MATLAB[®] and applied to the controller using the most efficient and up-to-date controller methods available on modern control theory of LQR and *Batz-Kleinman* described in Section 2 [2].

The most classic method of analyzing a controller design is by simulating the state variable response of the trimmed aircraft to an atmospheric disturbance [2]. Therefore, the code script for the digital longitudinal controller follows the diagram scheme of Figure 7.

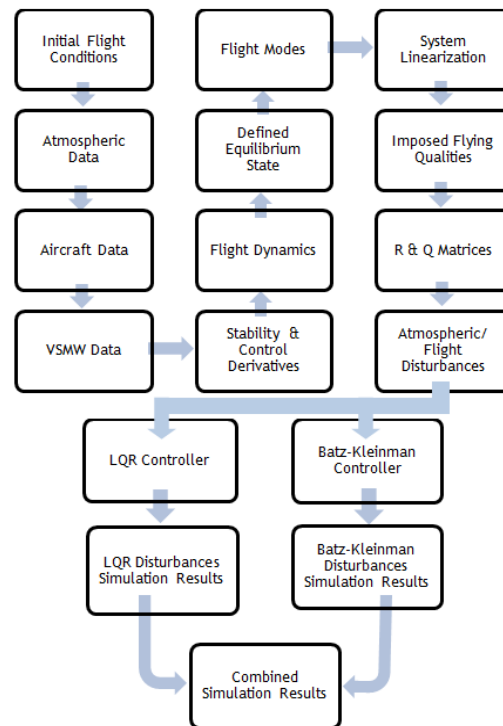


Fig. 7 Diagram of the general path scheme of the simulation code

The disturbance suffered by the aeroplane can be defined as a uniform fractional divergence from the pre-established variables for equilibrium state vector $x = [u \ w \ q \ \theta]^T$, obtained by linearization of the flight equation systems. In the simulation however, the atmospheric disturbances are inputted values defined by the user and imposed to the controller by means of a new vector designated x_1 or disturbances vector.

In fact, two symmetrical disturbances vectors (x_1 and x_2) were created to provide enough prove of work to each controller module.

$$x_1 = \begin{bmatrix} +2 \\ -2 \\ -0.03 \\ -0.03 \end{bmatrix} \text{ and } x_2 = \begin{bmatrix} -2 \\ +2 \\ +0.03 \\ +0.03 \end{bmatrix}$$

Therefore, when applying Disturbances Case 1 (x_1 disturbances vector), the UAV is deviated from its equilibrium state, by suffering an increase in forward longitudinal airspeed of 2 m/s, as well as an increase of 2 m/s in vertical speed (the vertical axis w points in direction to Earth as opposed to what happens with the more easily perceived concept of an altitude axis pointing in the opposite direction. Refer to Chapter 2), a decrease of 0.03 rad/s on pitch rate (meaning the nose is pitching up by the same reason of w being positive when pointing down to Earth) and the same reduction in pitch angle. That results in a new after-disturbances state vector (x_i) that the controller will have to return to the original equilibrium state values of vector x by applying the appropriate controls in control surfaces and throttle. In this case, a given vector x , e.g. $x = [30 \ 1 \ -0.2 \ 0.2]^T$ would become, after suffering the disturbances of case 1, $x_i = x + x_1 = [32 \ -1 \ -0.23 \ 0.17]^T$. The equilibrium state and control vectors are calculated to each flight mode specific simulation prior to any disturbances by solving

$f(x_{eq}, u_{eq}) = f(x_0, u_0) = 0$. Note that the x vector replaces the theoretical variables of V , γ and α by the longitudinal and vertical components of the velocity vector (V) and the pitch rate (q). That happens because, as seen in the previous Chapters, the angle of attack (α) depends directly of longitudinal velocity of the aircraft, while the path angle (γ) is, by definition dependent of both α and θ angles. For that reason this two variables are the direct result of longitudinal velocity (u), pitch angle (θ) and pitch rate (q) and are therefore calculated separately.

The controller was designed to operate in seven different modes for different flight phases: Altitude Hold Mode; Pitch Hold Mode; Climb or Descent/Dive Mode; Landing Mode; Take-Off Mode; TFTA (Terrain Following Terrain Avoidance); and Dissymmetrical Wing Mode. It also features (although yet untested) several safety algorithms such as an Automatic Stall Recovery system or a Minimum Altitude Safety based in the correlation of data provided by GPS and barometric and radar altimeters. However, for the purpose of this paper, only one example of each of the three different test simulations is presented.

4.1 Classical Disturbances Simulation

For the case of the Classical Disturbances Simulation Test, the chosen mode was the first one, Altitude Hold Mode (AHM) as it is the most important mode. Since $U = [\delta_{V_e} \ \delta_T]^T$, the test results for altitude stabilization at 60m ASL levelled flight of the UAV *Olharapo* when fully loaded and at an airspeed of 25m/s, the controller response to a simulated disturbance is as follows:

$$x = \begin{bmatrix} 25.000 \\ 0.0000 \\ 0.0000 \\ 0.0416 \end{bmatrix} \text{ and } U = \begin{bmatrix} -0.0242 \\ 0.8676 \end{bmatrix}$$

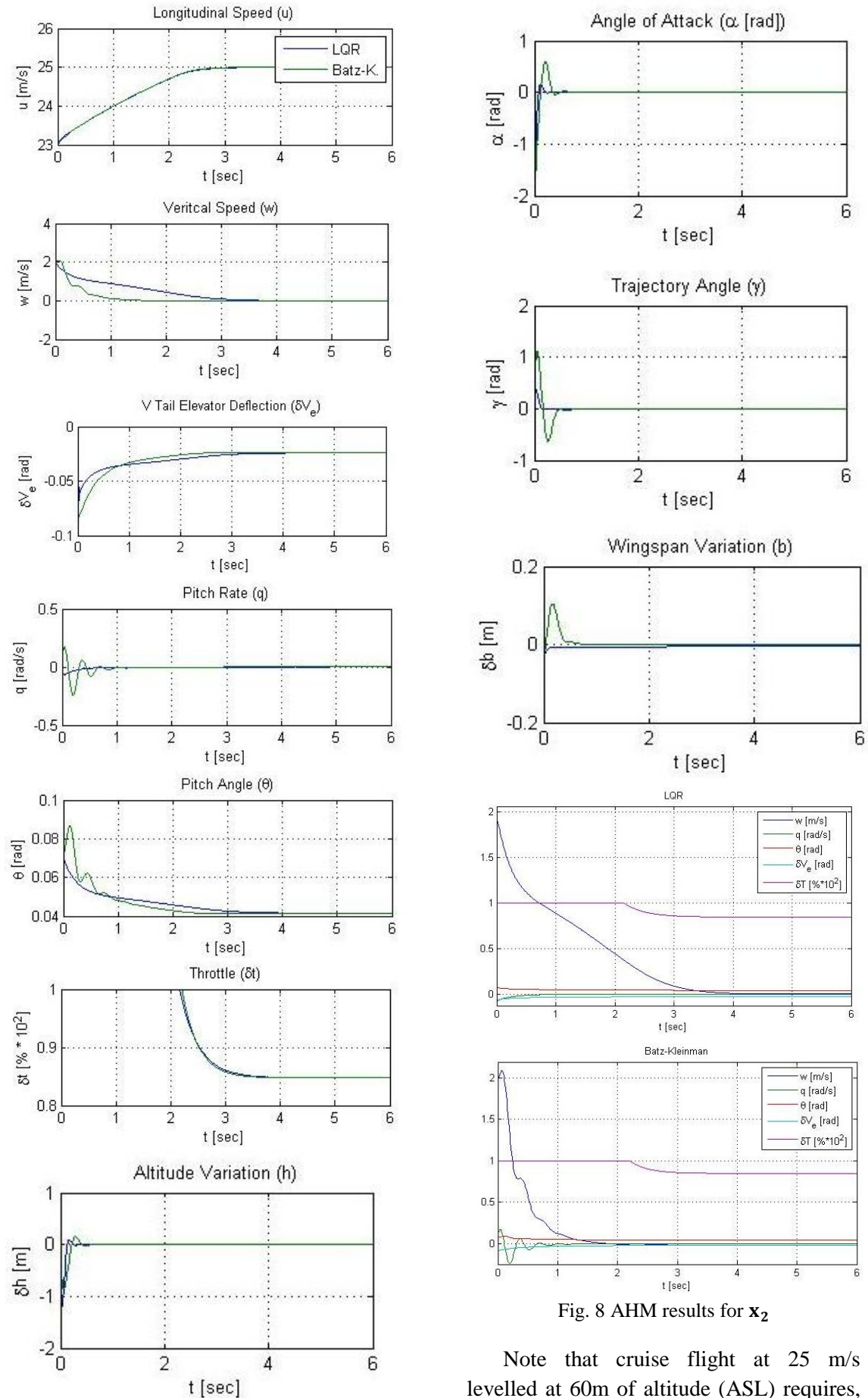


Fig. 8 AHM results for x_2

Note that cruise flight at 25 m/s levelled at 60m of altitude (ASL) requires,

in accordance with the ISA (International Standard Atmosphere) model for STP (Standard Temperature and Pressure) conditions, about 87% of power (i.e. Throttle settled for 87% of full power meaning $\delta_T = 0.87$) and an elevator trim of $\delta_{V_e} = -0.02 \text{ rad}^{-1}$, meaning a slight upwards deflection of the elevator (i.e. as in a nose up attitude).

The objective of the simulated controller is to stabilize the aircraft after small atmospheric disturbances within six seconds. As seen from Figures 4.3 to 4.7, all values converge to their equilibrium values within the established time limit on this simulation. Therefore after the simulation the aircraft is returned to stable flight levelled ($\gamma = \arctan(w/u) = 0$) at 60m of altitude, 25 m/s of indicated airspeed, nose slightly down ($\theta = 0.74$ degrees), and an angle of attack of 3.26 degrees.

4.2 Sinusoidal Pitch Variation Test

The simulation works by systematically forcing the UAV to change its pitch angle every fixed amount of time (a few seconds), and then calculating the associated equilibrium state and control vectors. The objective of such simulation is to analyze the reactions of the state and control variables to a dynamic variation of the pitch attitude as it is prone to happen during actual flight, proving that both the concept mechanism behind the controller and the controller itself work properly and are thus, theoretically viable to be implemented in the actual aircraft prototype for test flight purposes.

Although the classical simulation results allow a clear observation of the aircraft's state response to an atmospheric disturbance, it somehow lacks such observation clarity when it comes to the direct relationship between the induced control inputs and the consequent reaction in state variables. Therefore, there was the need to perform a more complex analysis

regarding such relationship. In this simulation, a larger number of equilibrium states had to be calculated, in order to simulate the aircraft's response to a sinusoidal variation of the pitch angle (θ) up to a maximum of 7 degrees. The simulation's code script is mostly the same as the one used in previous simulations regarding the classical disturbances method. It is set to simulate the aircraft's control surfaces (elevators) and engine's power while attempting to maintain a levelled flight at 20 m/s at sea level and with the wings extended to its maximum wingspan.

To induce a smooth fully symmetrical amplitude variation in pitch, a sinusoidal (more precisely, a cosine) variation of the pitch angle (θ) using the following equation:

$$\theta = \frac{|\theta_{\max} - \theta_{\min}|}{2} \left[\left(\frac{2\pi}{(t_{\max} - t_{\min})} \right) \left(t + \frac{3}{4}(t_{\max} - t_{\min}) \right) \right] \quad (40)$$

With $-\theta_{\min} = \theta_{\max} = 7$ degrees for either of two different time spans ($y_1 = 6\text{s}$ or $y_2 = 3\text{s}$).

The controller creates a total of 20 equilibrium points for each simulation independently of the time span chosen, which means that, for the time span of 6 seconds of y_1 , the total simulation time is of $t_{\max} = 20 \times 6 = 120 \text{ sec}$. However, in order to enable the graphic visualization of the variables returning to their initial values, the simulation was extended by a time factor of $t_{\max}/20$, which means that the actual simulation duration is of $t_{\max} + t_{\max}/20$, meaning a total time of 126 sec to y_1 .

The results for y_1 are as follows:

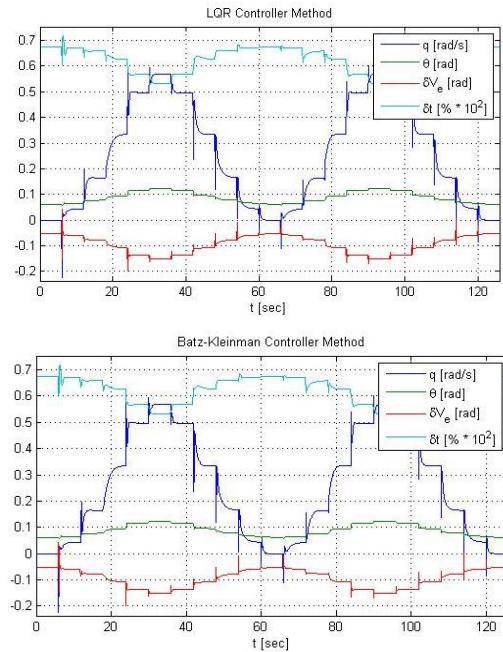
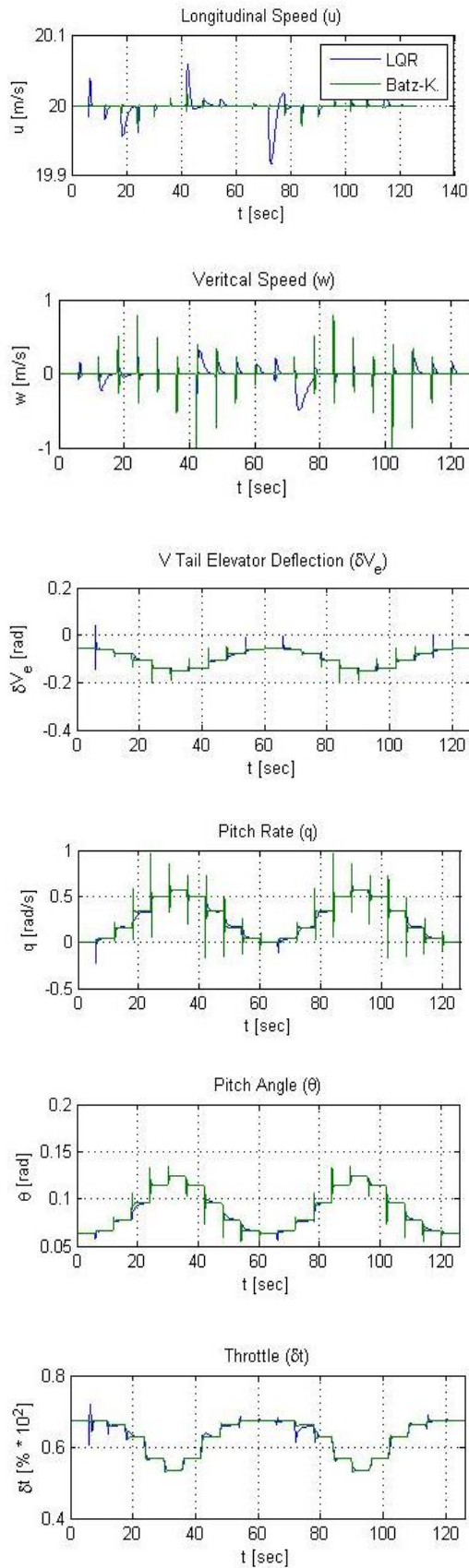


Fig. 9 Graphical results of the sinusoidal simulation for y_1

With this test response simulation, the main longitudinal variables responses can now be fully observed in detail, revealing the actual aircraft motion parameters and their relationship. It is now clear that, as expected, a sinusoidal variation on pitch angle leads to a similar sinusoidal response of both the elevators and engine power controls that in turn results in an also sinusoidal pitch rate variation in order to maintain the aircraft stable at levelled flight and at the intended velocity.

4.3 Random Pitch Variation Simulation

The previous Classical Disturbances and Sinusoidal Pitch Variation simulations already describe and validate the working concept of this flight controller. However, to validate the controller for actual use, a more complex simulation had to be performed. For that effect, a random simulation of the pitch angle was created in order to evaluate the controller's ability to stabilize the aircraft under such harsh and unpredictable conditions.

This random simulation uses the same base code script and equilibrium states as the ones used in the previous sinusoidal simulation. However, in this simulation, the program chooses a random point every t seconds no more than 10 steps above or below the previous equilibrium point. That means that, since the same equilibrium points of the sinusoidal simulation are being used, the program will always chose the equilibrium point immediately after, the equilibrium point immediately before, the second equilibrium point immediately after, or the second equilibrium point immediately before the current equilibrium point. Because the equilibrium points are the same as those of the sinusoidal simulation, it will always mean an increase or decrease in pitch angle accordingly to the current equilibrium point. By that same reason, the variation in pitch will be smaller if the random chosen point is closer to the current equilibrium point and vice-versa.

The results for y_1 are presented in the following graphics:

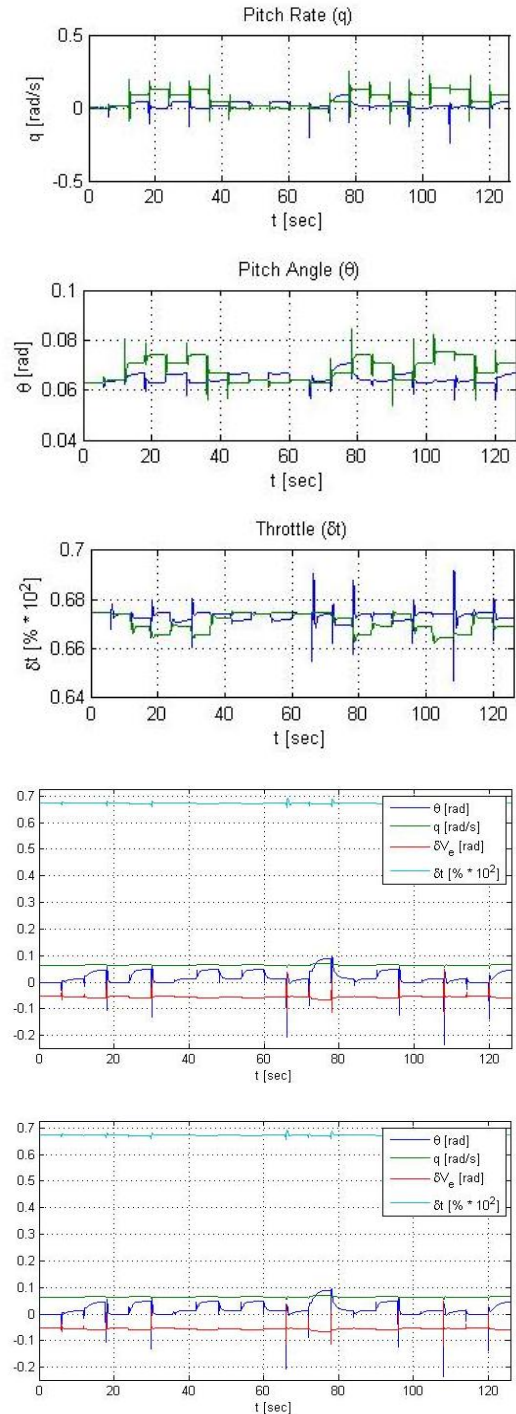
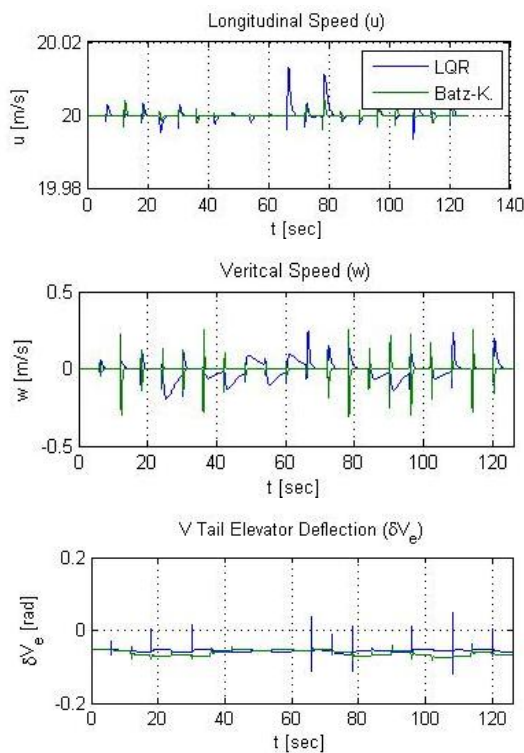


Fig. 10 Graphical results of the random simulation for x_2

5 Conclusions

After nearly 6 months of hard work and roughly six thousand lines of scripted MATLAB® files, involving, not only, a large set of fields (mathematics, physics, aerodynamics, electronics and informatics) required for the development of a flight controller system, as also new experimental

and untested technologies, this work presented itself as a major challenge. However, as briefly described in this paper, all the simulations and tests prove the working concept and reliability of the developed longitudinal flight controller system under different and even unusual flight conditions. Of course, the values obtained may not be, and probably aren't, entirely accurate as they are based in calculations and estimations of several variables. Thus they may not faithfully represent the true aircraft behaviour. However, it is the substantiation of the working concept that matters the most, as the program can later be easily updated and adjusted for the more accurate data retrieved from further flight tests or other methods of data acquisition. In fact, a lot of effort was put into making the controller's script structure very simple to modify, update or integrate with other programs by means of a modular structure. Thus, allowing its use with different aircraft configurations or even different aircraft, as well as permitting its further development into a fully functional 4D autopilot.

This work's purpose was to test two different control methods for longitudinal flight stabilization of a VSMW equipped UAV under different flight conditions, with the objective of ensure the feasibility of actually implement the controller on the aircraft for test flight purposes. However, as also stated, it is not a longitudinal autopilot and therefore, it will not really take the aircraft from point A to B as it happens with actual autopilot systems. It simply stabilizes the aircraft on its longitudinal axis given minor atmospheric disturbances such as turbulence, wind variations, or thermals. Nevertheless, initial steps were taken in that direction (autopilot development), i.e. some of the controller modes mentioned before such as the TFTA, although simulated by the controller program will be unusable in the actual aircraft control without further development

of the controller into a full 4D autopilot system. Therefore, regardless of the fact that such complex and detailed programming requirements are far beyond the scope of the present work, the bases for such flight modes were already implemented in the controller in advance for such development. Many other improvements to the controller were made in that direction, even though not described in this work as they require further development and/or lack necessary data. For instance, the TFTA mode depends of the utilization of a radar altimeter, and although an algorithm had been developed to integrate data provided by a barometric altimeter, a radar altimeter and a GPS altogether, the lack of information on the avionics to be used, if to be used at all, invalidates an accurate simulation of such flight mode, besides requiring further development of the controller as already mentioned. Also to be noted is the fact that at the time of this work, the engine type to be used in the aircraft and its location on the airframe were yet to be decided, and therefore, the engine parameters used in the controller have had to be assigned values that may differ from the actual ones. However, because the controller actively acts upon the aircraft's dynamics when they fall from the intended equilibrium state, such considerations such as the engine location, CG variation due to fuel consumption, weight variation due to fuel consumption or payload jettison, or pitch variation due to acceleration should not interfere with controller ability to maintain flight stability as it will interpret such variations as atmospheric disturbances and act accordingly.

Then, the main achievement of this work was, as it was its objective, to develop and provide a robust controller system that validates the UAV for test flight using a combination of controller techniques accordingly to the situation. It was demonstrated that, contrary to what some

previous studies have indicated, the VSMW system is actually liable (or capable) of being actively controllable during flight by achieving the required longitudinal flight stability parameters providing that proper controller optimization is performed.

References:

- [1] **The MathWorks Inc., et al.** *MATLAB 7 Function Reference: Volume 1 (A-E)*. s.l.: The MathWorks, Inc.
- [2] **Tavares, F.** *Roll Motion Control of a Dissymmetrical Wingspan Aircraft* MSc. Dissertation, Department of Aerospace Sciences. Covilhã, Portugal: University of Beira Interior, 2011.
- [3] **Stevens, Brian L. and Lewis, Frank L.** *Aircraft Control and Simulation*. New York, USA: John Wiley & Sons, Inc, 1992. ISBN 0-471-61397-5.
- [4] **Pamadi, B. N.** *Stability, Dynamics and Control of Airplanes*. Hampton, USA: AIAA: American Institute of Aeronautics and Astronautics, Inc. , 1998. ISBN 1-56347-222-8.
- [5] **Nelson, Robert C.** *Flight Stability and Automatic Control*. New York, USA: McGraw-Hill Book Company, 1989. ISBN 0-07-046218-6.
- [6] **McLean, Donald.** *Automatic Flight Control Systems*. Hertfordshire, UK: Prentice Hall International Ltd, 1990. ISBN 0-13-054008-0.
- [7] **Luo, Jia and Lan, C. Edward.** Determination of Weighting Matrices of a Linear Quadratic Regulator: *Journal of Guidance, Control and Dynamics*, 1995. Vols. 18, no.6. pp. 1462-1463.
- [8] **Abzug, M. J. and Larrabee, E.E.** *Airplane Stability and Control*. Second Edition. Cambridge, UK: Cambridge University Press, 2002.
- [9] **Gamboa, P., et al.** Design Optimisation of a Variable-Span Morphing Wing. In *52nd AIAA/ ASME/ ASCE/ AHS/ ASC Structures, Structural Dynamics and Materials Conference*, Lisbon, Portugal: s.n., April 2011. Denver, Colorado, USA, pp. Paper no. AIAA 2011-2025.
- [10] **Etkin, B. and Reid, L. D.** *Dynamics of Flight Stability and Control*. Third Edition. s.l.: John Wiley & Sons, Inc., 1996. ISBN 0-471-03418-5.
- [11] **Anderson, B. D. O. and Moore, J. B.** *Linear Optimal Controler*. s.l.: Prentice-Hall, 1989.
- [12] **Searle, Loyd.** The bombsight war: Norden vs. Sperry. *The value sell*. [Online] 09 2009. [Cited: 06 25, 2012.] http://thevaluesell.com/images/LSearle_bombsight.pdf. IEEE 0018-9223/89/0900 0060.
- [13] **John, Philip A. St.** *Bombardiers of WWII - Vol II (Limited)*. s.l.: Turner Publishing Company, 1998. ISBN 1563113384.
- [14] **Sperry Corporation.** *Wikipedia*. [Online] [Cited: 06 25, 2012.] http://en.wikipedia.org/wiki/Sperry_Corporation.
- [15] **Bousson, K.** *Flight Mechanics II* lecture notes. Covilhã, Portugal: University of Beira Interior, 2011.
- [16] **Autopilot.** *Wikipedia*. [Online] [Cited: 06 25, 2012] <http://en.wikipedia.org/wiki/Autopilot>